A STUDY OF POROUS TRANSITIONS OF LAYER-BY-LAYER THIN FILMS AND PATTERNING MULTILAYERS

A Dissertation

by

CHUNGYEON CHO

Submitted to the Office of Graduate Studies of
Texas A&M University
in partial fulfillment of the requirements for the degree of

DOCTOR OF PHILOSOPHY

Chair of Committee,	Nicole S. Zacharia
Committee Members,	Jodie L. Lutkenhaus
	Mustafa Akbulut
	Sreeram Vaddiraju
Head of Department,	Ibrahim Karaman

August 2013

Major Subject: Materials Science and Engineering

ABSTRACT

This thesis research focuses on fundamental understanding regarding the morphological transitions of weak polyelectrolyte multilayers (PEMs) formed by the layer-by-layer (LbL) electrostatic assembly of oppositely charged polymers.

The first part of this thesis focuses on patterning polyelectrolyte multilayers that are able to undergo transitions from continuous films to porous materials by using hydrogel stamps. The stamping process is able to locally etch and pattern the porous transition in the LbL films by using reactive wet stamping (r-WETS). It was found that r-WETS of PEMs can also enable the modification of chemical functionality.

The second part is an investigation about morphological changes of weak polyelectrolyte multilayers assembled with PAH and PAA using r-WETS in which hydrogel stamp material was soaked into various salt solutions and then applied to the LbL films. Also, in this study we presented a novel strategy to create a continuous gradient structure in thickness or porosity along the lateral direction of the thin films using concentration gradient salt stamping.

The third part is an investigation regarding the mechanism of the transition from a continuous morphology to a porous morphology within weak polyelectrolyte multilayers. These morphological changes were able to be created by both acidic and basic post-assembly treatments, showing various morphological transitions from the introduction of porosity to the collapse of these porous structures and the eventual dissolution of the films.

A similar observation of morphological transitions in weak polyelectrolyte multilayers was obtained by applying an electric field to the films in the fourth part of this thesis. Exposure to an electric field resulted in the creation of a porous structure, which can be ascribed to local changes in pH and subsequent structural rearrangements of the weak polyelectrolyte constituents.

The final part of this thesis is to make PEMs into nanostructured matrices for inorganic synthesis. Multilayers possessing ion-exchangeable carboxylic acid groups were used for binding metal catalysts such as platinum (Pt) nanoparticles (NPs) within the film. Therefore, polyelectrolyte multilayers were able to stabilize catalytic Pt NPs in order to increase the useful time of catalyst materials suitable for use in proton exchange membrane fuel cells.

사랑하는 은미,

가족, 그리고

천국에 계시는 부모님께

- 조충연

To

my beloved wife, Eunmi Yoo,

my family, and

my parents in heaven

- Chungyeon Cho

ACKNOWLEDGEMENTS

First of all, I would like to especially thank my advisor, Prof. Nicole S. Zacharia, for her constant support, encouragement, and constant supply of helpful advice during my course of study at Texas A&M University. It was a great opportunity for me to conduct the researches under her guidance. I really appreciate all the time she has spent teaching me and helping me come up with experimental plans. Not to mention her ability to solve basic problems and practical knowledge in dealing with the experimental research, her warmth and friendliness always motivated and guided me throughout my research activities.

I would also like to thank my thesis committee members Prof. Jodie L. Lutkenhaus, Prof. Mustafa Akbulut, and Prof. Sreeram Vaddiraju for their interest and valuable guidance during the research.

I am thankful to have worked with my past and current lab mates: Nina Ivanova, Okan Ala, Hsiu-Chin Huang, Xiayun Huang, Yusuf Kar, Lauren Link, and Ryan Davis. Without their cooperation and friendship throughout my research, I would not have been able to complete this thesis. From the Prof. Lutkenhaus group, I also would like to thank Ju-Won Jeon for helping me work on a research about an electric field. In addition, I would like to thank the undergraduates for their tremendous experimental assistance that I worked with: Lauralee Valverde, Jeremy Kaiser, Dan Gessner, Drew Parks, and Mandy Schubert.

Special thanks go to my family; my sister, brother-in-law, father-in-law, late mother-in-law. I would have never come this far without their love, patience and support. I would especially like to thank my wife, Eunmi Yoo, for her love and constant support over the years; I could not have made it through without her encouragement and assistance.

Finally, I dedicate this thesis to my parents in heaven.

TABLE OF CONTENTS

Page

LIST OF FIGURES

Page

LIST OF TABLES

Page

CHAPTER I

INTRODUCTION

1.1 INTRODUCTORY REMARKS

The layer-by-layer (LbL) deposition to prepare polyelectrolyte multilayers (PEMs) has been extensively studied over the past decade as a highly successful and versatile technique for producing ultrathin films with surface tunable properties.[1-3] With increasing interest in this method, understanding the principle mechanism of multilayers formation by the adsorption of polyelectrolytes has become more and more important. This chapter gives basic definitions and important concepts regarding polyelectrolyte multilayer thin films assembled by the LbL method. The first part of this introduction presents a definition of polyelectrolytes along with polyelectrolyte complexes. The second part presents an overview about LbL self-assembly technique for the assembly of PEMs, suggesting that this method is suitable for multi-functional thin film fabrication because of its simplicity, robustness, and versatility. In the third part, the effect of assembly pH on the thickness and morphology of weak PEMs is examined. Finally, the objectives and outline of the topics covered in this thesis are presented.

1.2 GENERAL INTRODUCTION

1.2.1 Polyelectrolyte

Polyelectrolytes (PEs) have received vast attention due to their broad variability, unique molecular structure, and the chemical functional groups inherently present as part

of their structure that facilitate different functionality and derivatization. [4] A polyelectrolyte (PE) is a macromolecule carrying covalently bound anionic or cationic groups as well as low molecular weight counterions on the main chain or in pendent groups. [5] Examples of naturally occurring PEs are proteins, DNA and polysaccharides. When exposed to water or any other ionizing solvent, PEs dissociate into a highly charged polymeric molecule. After dissociation the polymer is typically accompanied by smaller oppositely charged counterions that tend to neutralize the charge on the repeating units of the macromolecule preserving electroneutrality, either by loosely binding to the polyelectrolyte chain or condensing to it.[6] In terms of their charges, PEs can be classified into three categories: polycations, polyanions and polyampholytes. Polyampholytes are ionic polymers having both positively and negatively charged groups, which makes them have compact conformations due to the attractive forces between the opposite charges. On the other hand, polycations and polyanions have positively and negatively charged groups, respectively, making them take on extended chain conformations owing to repulsive forces among charged groups. [7] Depending on the charge density and the degree of dissociation, they are categorized as strong or weak PEs. This classification refers to the pH sensitivity of the PEs. Strong PEs are not pH sensitive, so they have permanent charges and they are fully ionized over the whole pH range in solution, whereas the degree of dissociation of the ionizable groups on weak PEs is highly dependent on a change of pH (similar to strong or weak acids and base).

The conformation of PE in a solution is characterized by a wide range of interaction lengths varying from molecular distances (counterion-chain condensation) to

almost micrometer length scales. [8] The degree of charge density or repulsive forces between charge groups in PEs is dependent upon the ionic strength of the solution as well as the pH of the solution. [9, 10] The degree of dissociation of weak PEs is highly dependent on the pH of the solutions, as mentioned above. At pH values below the pKa (specific pH value at which half of functional groups of polyelectrolytes are ionized) of the polymer, the low degree of dissociation of charge groups in negatively charged weak PEs (such as poly(acrylic acid), PAA) takes on a coiled conformation. In contrast, at pH values above the pKa, these negatively charged weak PEs take on an extended chain conformation due to the repulsive forces between charges. In this system, the PE solubility in water is also increased as a result of the ionization of charge groups on the polymer. [11]

Depending on the ionic strength, both weak and strong PEs can have different molecular conformation, leading to fine control over the thickness of each deposited polymer layer. In low ionic strength solutions, PEs tend to be in more extended and uncoiled form (large radius of gyration) due to the intramolecular repulsion of the unscreened charges on each monomeric unit of the macromolecule. On the other hand, with increasing ionic strength the charges along the PE chain are screened by the excessive presence of smaller salt counterions, and as a consequence the PEs tend to become more flexible and coiled, as shown in Figure 1.1.[12] These special physical properties of PEs in response to pH variation or salt concentrations are of experimental importance in controlling film the stability, [13] morphology, [14] swelling, [15] and thickness [16] for PEMs fabricated by sequential deposition steps.

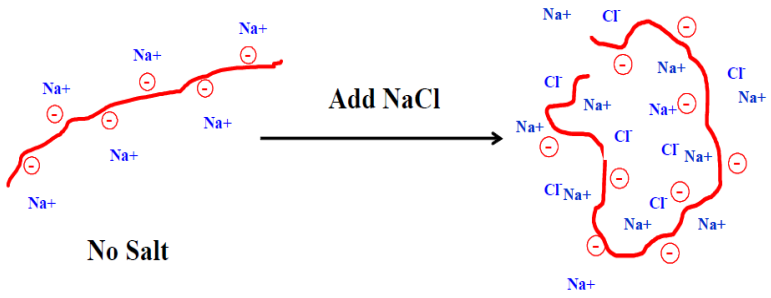

Figure 1.1 Scheme showing the effect of ionic strength on the conformational changes of a PE in solution. [12]

Recently, PEs have found extensive applications both in academic and industrial research fields. They have been widely studied in all of the major fields of chemical science and engineering such as chemistry and biology, especially in colloids, surface and interface of polymer. They also play a major role in nature and find widespread application in many industrial processes and in numerous products of our daily life, as illustrated in table 1.1. Thickening reagents, [17] water treatment, [18] waste treatment [19] and sludge dewatering [20] as well as flocculation and coagulation agents for solid-liquid separations [21] are amongst the most common examples. Additionally, some PEs are used as additives to alter the physical properties of aqueous products, and other PEs are also used in the biochemical and medical engineering fields such as implant coatings and for drug delivery. [22]

Table 1.1 Some areas of PEs Application[4]

Industrial area	Product or process example
Film and textile industry	Viscose process, Textile sizes
Paper industry	Retention aids
Water and effluent processing	Flocculants, Sludge dewatering
Chemical Industry	Supporting materials, Membranes
Mining Industry	Flocculants
Petrol Industry	Oilwell drillling aids
Building Industry	Pigment dispergants
Cosmetics Industry	Antistatic agents, Gelling agents
Medicine and pharmacy	Tablet coating

One of the most important physical properties of PEs is their ability to form complexes when oppositely charged PEs are mixed together in solution. [23] This is an electrostatic- and entropy-driven self-assembly process. The opposite charges are attracted to each other but more importantly the release of counter ions that are not restricted to the polymer backbone chain creates entropic gain for the system. [24] The process is very fast and mainly controlled by counterion diffusion. When PEs with weak ionic groups and large differences in molar mass are used and mixed in a non-stoichiometric ratio, water soluble PECs can be formed (homogenous one phase system).[25] Non-stoichiometric PECs are usually in two categories; (i) highly aggregated PECs made up of several PE chains that are stabilized by the polyion in excess, which charges the PEC surface and prevents macroscopic precipitation; (ii) water-soluble molecular PECs that form under special conditions.[8] When PEs with strong ionic groups and similar molar mass are mixed together near 1:1 stoichiometry in dilute aqueous solution, a precipitate is formed which contains phase-separated solids of the component

polyions. In this system, all the charged units of the polymer chains are internally compensated by oppositely charged units from the other PE. In the presence of additional salt ion, ions tend to enter the bulk of the complex and transform it into an extrinsically compensated state. [12, 26] The formation of PECs is dependent on the electrostatic interactions of oppositely charged groups. Increase of the ionic strength of the solution leads to a decrease of the ionic interactions between the PEs due to screening of the charges. A further increase of salt concentration can even result in complex dissolution.

1.2.2 Layer-by-Layer Assembly of Polyelectrolyte Multilayers

Consecutive deposition of multivalent particles dates back to Iler, who demonstrated [27] that films of alternating positively charged alumina and negatively charged silica colloids could be built up on hydrophilic glass in the 1966. Decher first described an electrostatic directed self-assembly method to make multilayer thin films with nanoscopic order and macroscopic orientation using electrostatic interaction between two oppositely charged PEs, which is called the LbL (layer-by-layer) method. [28] Since then, research about this self-assembly technique has attracted increasing amounts of attention in both academic and industrial fields. Fabrication of functional thin films is still studied by several deposition techniques including chemical vapor deposition (CVD), [29] Langmuir-Blodgett (LB), [30] LbL assembly, and other methods. Among all the techniques mentioned above, LbL has several significant advantages that make this method very useful for fabrication of ultrathin multifunctional thin films with precise control of film's composition and structures.

Polyelectrolyte multilayers (PEMs) are polymer thin films simply prepared by alternatively dipping a substrate into solutions containing negative or positive polyelectrolytes (a technique known as Layer-by-Layer or LbL[28, 31], essentially directing the complexation of polyelectrolytes onto a substrate. Each adsorption step is accompanied by the charge reversal of the film's surface, enabling the next deposition as well as self-limiting each deposition step (Figure 1.2). This direction of polyelectrolyte complexation onto a substrate allows for the highly reproducible fabrication of thin polymer films.

The primary driving force for the fabrication of films by the LbL method is mainly entropic effects as opposed to enthalpic ones. [32-35] When oppositely charged polyelectrolytes come close enough to bind to previously absorbed polymer on a surface, the complexation of the polyions to that charged surface liberates previously undissociated low molar mass counterions, increasing entropy and minimizing the free energy of the system. Additional contributions to entropic gain may derive from the liberation of structured water molecules (solvation shell) around hydrophobic portions of the PEs and by the formation of short-ranged van der Waals interactions between hydrophobic regions. [36] The other forces driving the fabrication of polyelectrolyte multilayers can include as electrostatic interactions, hydrogen bonding, [37, 38] charge transfer, [39, 40] and hydrophobic interactions.[41, 42]

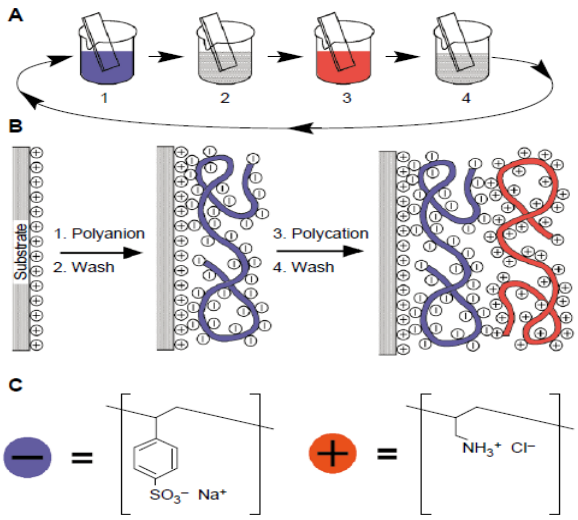

Figure 1.2. (a) Schematic of the film deposition process of layer-by-layer assembly method, (b) simplified molecular picture of the adsorption steps, and (c) chemical structure of two typical polyions, the sodium salt of poly(styrene sulfonate) and poly(allylamine hydrochloride).[31]

With PEMs it is possible both to create ultra-thin coatings of tens of nanometers, but also films that are many microns thick, and they can be made as free-standing assemblies if desired. Another strong point about the LbL method is the ability to incorporate many different types of building blocks (and therefore functionalities) as long as they are multivalent, and subsequently PEMs have been proposed as being potentially useful in very diverse areas, such as separation membranes, light-emitting diodes, anti-reflection coatings and other biomaterials.[43 - 47]

The LbL deposition technique has the advantage that it can conformally coat nearly any type and geometry of substrate, but the greatest limitation in commercializing this technique has been the long deposition times and many steps required to create the films. Recent studies have developed faster and more versatile methods such as spin

coating or spraying. As one of the variations, spin-coating LbL method was demonstrated by Hong [48] and also by Wang [49]. This spin self-assembly method as an alternative for making well-organized PEMs has the advantage that only small amounts of liquids are needed to coat large surface area in a very short process time. The main difference between the conventional dipping method and the spin coating method arises from the adsorption mechanism; in the solution-dipping method polymer chains diffuse to the substrate and subsequently rearrange themselves on the surface. However, in the spin method the adsorption and rearrangement of adsorbed chains on the surface and the elimination of weakly bound polymer chains from the substrate are almost simultaneously achieved by using high spinning speeds for short periods of time (Figure 1.3 (a)). [50] This technique also produces a highly ordered internal structure with precisely controlled the thickness of the multilayer thin films.

Schlenoff first demonstrated multilayers deposited by a sequential spraying method, yielding thin films of equivalent structures, composition, and morphology to those prepared by classical solution-dipping LbL assembly method. [51] In his work, PE solutions were sprayed on the substrate and a spray of D.I water was used to remove physically bound excess polymer chains (Figure 1.3 (b)). This method typically takes only a few seconds for each layer before the adsorption becomes homogeneous over the whole surface area, while dipping method normally requires the several minutes between each exposure step. The flow rate and mass transfer of spray play an important role in reducing the process time while retaining good quality of PEMs. Spray-coating of PEMs is a feasible and promising method, and yields conformal coatings, opening up new

possibilities for reactive porous membranes in separation fields such as gas separation and desalination. [52, 53]

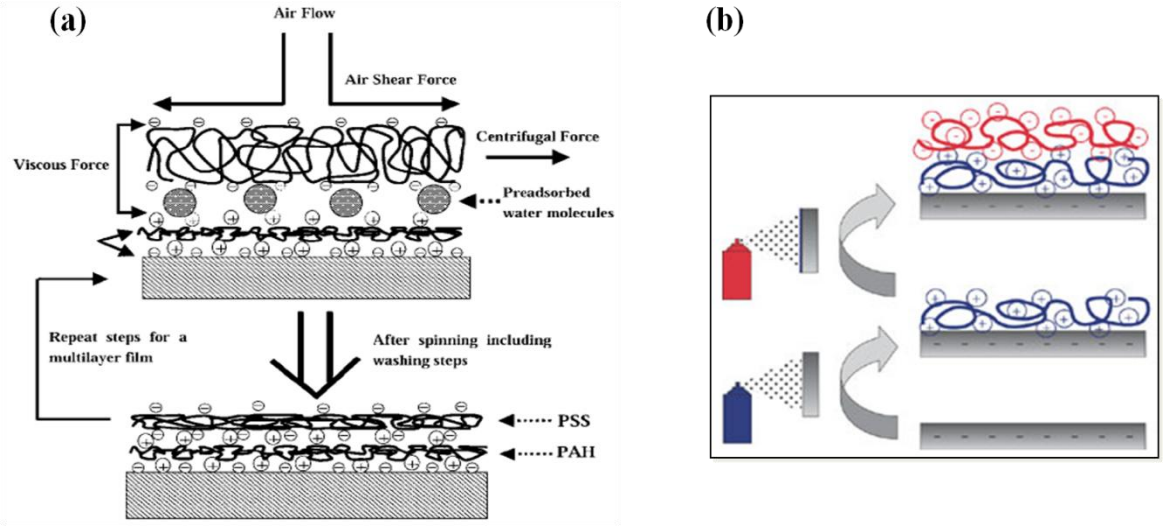

Figure 1.3. (a) A side view schematic depicting the buildup of PEMs by consecutive spinning processes of anionic and cationic PEs. [50] (b) Schematic drawing of LbL deposition by alternating spray-coating of polyanions (red) and polycations (blue). The rinsing between deposition steps is not shown. [52]

1.2.3 pH Controlled Weak Polyelectrolyte Multilayers

The properties of LbL thin films are controlled by several parameters other than the chemical nature of the polyelectrolytes used in the assemblies such as temperature, pH values of bath solution, and molecular weight of polymers used.[54 - 56] The thickness of adsorbed PE layers (hence, conformation of the polyelectrolyte chains) can be finely controlled on a nanometer level by adjusting pH of polyelectrolyte solutions relative to polyelectrolyte pKa.[57 - 60] For instance, using weak polyelectrolytes, such as PAH and PAA, enables the creation of a wide variety of multilayer structures simply by adjusting

the pH-sensitive linear charge density of the assembling polymers. PAA (pKa ~ 5) and PAH (pKa ~ 9) contain ionizable carboxylic acids and amines, respectively.[61] The actual pKa of a weak PE is very sensitive to its local ionic environment and may shift significantly from the solution value when in the multilayer. [62] Thus, depending on the deposition pH conditions, the degree of ionization of these weak polyelectrolytes (COO^- vs. COOH groups for PAA and NH_3^+ vs. NH_2 groups for PAH) and the number of ionic bonds may be tuned as desired. As seen in Figure 1.4,[63] when PAH and PAA are each deposited from solutions at pH 6.5, both PAH and PAA are essentially fully charged. At this pH condition, these polymers assemble into a highly ionically cross-linked multilayer comprised of molecularly thin (as shown in Figure. 1.5) [64] and highly crosslinked layers in which the polymer chains adopt flattened conformations. In this scenario most of the functional groups are used in crosslinks in this case they are therefore not available for subsequent chemistry.

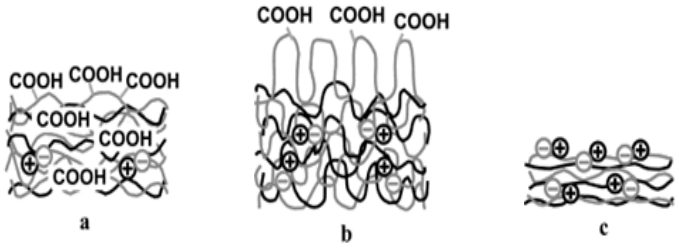

Figure 1.4. Schematic of the (a) 2.0/2.0, (b) 7.5/3.5, and (c) 6.5/6.5 PAH/PAA LbL thin films. [63]

If the pH of the dipping solutions used to fabricate a multilayer film is either increased or decreased, dramatic increases in the layer thickness of both PAA and PAH

are observed. When PAH and PAA chains are assembled from pH 7.5 and 3.5 dipping solutions, respectively, the PAA chains adsorb at a low pH with a low degree of ionizations onto fully charged chains of PAH, resulting in loop-rich conformations and a PAA surface layer with a high density of free acid groups. For the adsorption of the PAH chains, however, the pH is increased and the remaining acid groups of PAA become fully ionized. The PAH chains penetrate into the PAA surface layer and neutralize this extra charge, thereby forming thick layers with a high degree of internal charge pairing.

Multilayers assembled at pH 2.0 for each polyelectrolyte exhibit little ionic cross-linking because the degree of ionization of the PAA chains is kept low during each polymer adsorption step. The PAH chains, on the other hand, are fully ionized at this low pH. This results in a non-stoichiometric pairing of repeat unit units and a bilayer composition that is rich in PAA groups with their uncharged, protonated COOH state.

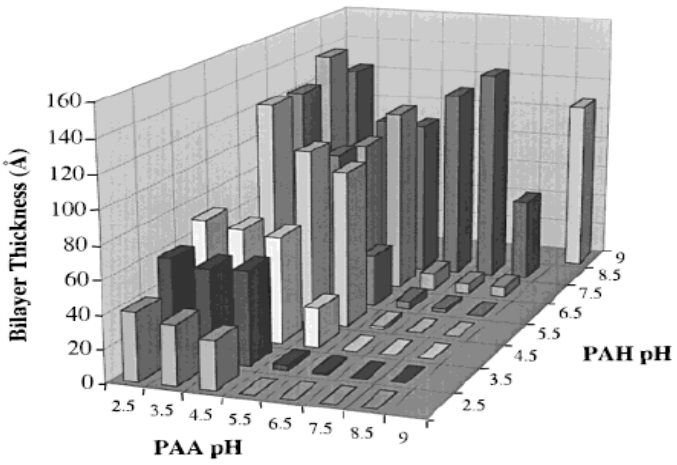

Figure 1.5. Complete pH matrix showing the average incremental thickness contributed by a PAH/PAA bilayer as a function of dipping solution pH. [64]

1.3 THESIS OBJECTIVE AND OUTLINE

The major objective of this thesis is to exploit the versatility of weak PEMs to gain insight into the fundamental origin about morphological transformation. Particular interest will be paid to the porous transition of LbL thin films caused by an external stimulus such as post-acid/base treatment, high ionic strength and electric field. Chapter 2 presents patterning PEMs by using the novel method of reactive wet stamping (r-WETS) with a hydrogel stamp material. This technique has the potential to locally control the porous transition, physical properties such as pore size and swelling. In chapter 3, the use of r-WETS of varying the concentrations with various salt solutions is explored. Depending on salt concentrations, it was possible to control the swelling ratio of thin films and morphology changes, and also lateral gradient thickness / porosity structures of LbL thin films were formed. Chapter 4 describes the mechanism regarding film stability during post-assembly changes in weak PEMs due to acid and base exposure. We present new information about the structural rearrangements in multilayers, indicating that weak polyelectrolytes are selectively or partially released from the PEMs in response to the post-assembly treatment. Chapter 5 describes another way to control the creation of porous structures within weak PEMs using electric field. The application of an electric field creates protons at the electrode-LbL film interface, which was used as a driving force for morphology changes in the multilayers. Finally, in Chapter 6, the application of PEMs to proton exchange membrane fuel cells was explored. PEMs containing carboxylic acid groups were used as a nanoreactor where polyelectrolyte chains can bind metal nanoparticles and also prevent the mobility their mobility.

CHAPTER II

REACTIVE WET STAMPING FOR PATTERNING OF POLYELECTROLYTE MULTILAYERS*

2.1 INTRODUCTION

Spatial control over a surface's physical and chemical properties is important for various applications such as the fabrication of electrical devices or in order to control cell adhesion and migration. Not just control over surface chemistry, but swelling and stiffness of a surface are important for these and other applications. Different patterning techniques have been developed to do just this, such as photolithography,[65] various microfluidic patterning methods,[66] microcontact printing,[67] and nanoimprint lithography.[68,69] Each of these fabrication techniques has its own advantages and drawbacks; photolithography is extremely good at accurately patterning surfaces but requires expensive equipment and toxic chemicals. Fabricating microfluidic devices requires a clean environment and specialized equipment. Microcontact printing is a very simple method for transferring various small molecules and polymers onto a surface but is limited in that it is a technique only for surface modification. Nanoimprint lithography can create new topographies, but not chemistries. Polyelectrolyte multilayers (PEM) [70] are one type of thin film potentially interesting for different applications and coatings such as ion transport, self-cleaning surfaces, drug delivery, and different biomedical

* Reprinted with permission frohm "Reactive Wet Stamping for Patterning of Polyelectrolyte Multilayers" by Chungyeon Cho, Lauralee Valverde, Geoffrey A. Ozin, and Nicole S. Zacharia., 2010. Langmuir, 26, 13637-13643, © 2010 ACS.

applications such as tissue scaffolds.[71] They are fabricated by the layer-by-layer (LbL) method, which is a process to direct the complexation of polyelectrolytes onto a surface by alternately exposing a charged substrate to oppositely charged polyelectrolyte solutions. This process results in a film deposition that can be controlled to the nanoscale in terms of placement of its components in the direction of deposition.[72] Electrostatic interactions are most commonly used, but other complementary interactions such as hydrogen bonding,[73] metal ion/ligand interactions,[74] or even covalent bonding [75] can be used to form films. There are a number of reports in the literature on the patterning of PEM using the various methods described above. Soft lithography especially has been used to pattern the surface of multilayers, and a variation on it, multilayer transfer printing, has been used to transfer patterned regions of entire mutlilayers.[12] Another method is to pattern the substrate and then selectively deposit PEM onto charged regions.[76-80] Growing multilayers in patterned areas generally has an upper thickness limit, however, and most of the other methods for patterning PEM are generally limited to surface modifications. Hydrophobic stamps made out of polydimethylsiloxane (PDMS) may be used to deliver "inks" such as organic small molecules or polymers but cannot be used to deliver aqueous reagents such as acid or basic solutions, or salt solutions, which have all been shown to be able to modify the structure of PEM postassembly.[81, 82]

Here we present the use of hydrogel stamps to pattern PEM films. Using a hydrogel stamp soaked in a chemical reagent of interest is called reactive wet stamping (r-WETS) or just wet stamping (WETS) and has been demonstrated by Grzybowski and

co-workers to be an effective way to etch substrates such as glass when soaked in HF or to locally do chemistry in thin hydrogel films.[83-85] The use of a hydrogel material for the stamp differs from PDMS in that the body of the stamp itself takes up aqueous solutions, which diffuse out of the stamp into the substrate when the two are placed in contact. Microcontact printing with PDMS generally transfers a single layer of molecules or "ink" whereas wet stamping continues to deliver the aqueous solution as long as there is a concentration gradient present. The r-WETS technique has some limitation in precision when compared to the single-layer transfer of more traditional microcontact printing methods, as after some time the aqueous solution begins to diffuse laterally through the substrate that is being stamped. WETS, to the best of our knowledge, has never previously been applied to LbL films. We demonstrate here that r-WETS can be an effective way to locally pattern porosity into PEM, change swelling and film thicknesses, pattern regions of different chemical functionalities, and etch them in a patterned fashion using high ionic strength solutions.

2.2 EXPERIMENTAL METHODS

2.2.1 Materials

Poly(acrylic acid) (PAA,MW=50 000 g/mol) and linear poly(ethylene imine) (LPEI, MW=25 000 g/mol) were purchased from Polysciences. Poly(allylamine hydrochloride) (PAH, MW = 70 000 g/mol), sulfonated poly(styrene) (SPS, MW = 70 000 g/mol), poly(methyldiallyl ammonium chloride) (PDAC), sodium hydroxide, and sodium chloride were purchased from Sigma-Aldrich. EMD high gel strength agarose,

hydrogen peroxide, sulfuric acid, and hydrochloric acid were purchased from VWR. All materials were used as received. For all solutions Milli-Q 18.2 MΩ deionized (DI) water was used. Polyelectrolyte solutions were 20 mM with respect to the repeat unit molar weight, and the pH of these solutions was adjusted using 0.1 and 1M HCl or NaOH solutions as needed. Glass slides and silicon wafers used as substrates were cleaned using piranha solution (~70% HCl and 30% H_2O_2).

2.2.2 Film Assembly

LbL films were formed by alternately dipping substrates in polyelectrolyte solutions using either a Zeiss HMS series programmable slide stainer or a NanoStrata StrataSequence 6. Cleaned substrates were submerged first in polycation solution for 10 min and then in a series of three rinse baths of deionized water. This was followed by polyanion solution for 10 min and three rinse baths again. This process was repeated until the desired number of bilayers was deposited. Unless otherwise stated, the outermost layer of the PEM used in this experiment was the polyanion.

2.2.3 WETs Stamping

A 7-10 wt % aqueous solution of high strength agarose (EMD OmniPur, VWR) was cast against Si-wafer master having an array of microscopic features. After agarose was cured thermally, the agarose layer was peeled away from the master and cut into rectangular blocks (ca. 1 cm × 3 cm × 5 mm). Next, micropatterned agarose stamps were soaked in a low pH for 2 h or salt ion solution for 1 h, respectively, to be used in LbL films patterning. Immediately prior to use, agarose stamps were dried by blowing dry nitrogen gas and then applied onto the LbL films. The stamps were then lightly pressed

against the LbL film and left in contact for the desired amount of time (Fig. 2.1). All films presented here were examined after stamping with no further rinsing or other treatment steps.

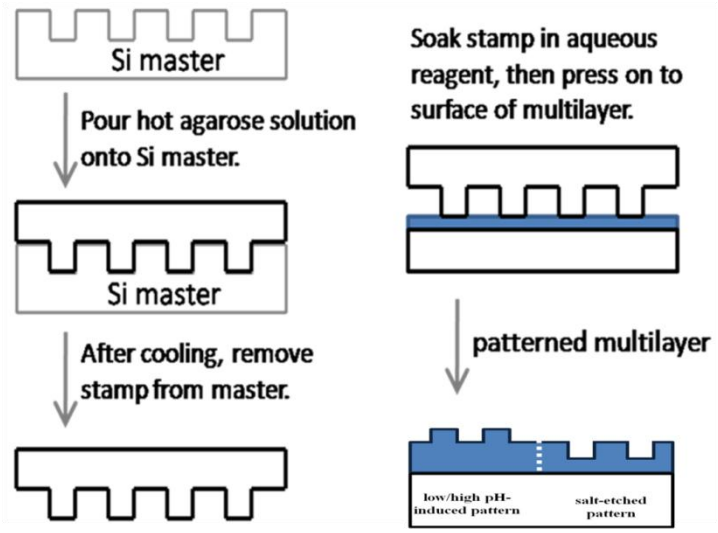

Figure 2.1. Schematic representation of the process of agarose stamp formation and stamping LbL films.

2.2.4 Film Characterization

The physical properties of the stamped LbL films were confirmed by using a profilometer (KLA - Tencor Instruments P-6), and values reported represent an average of at least 10 separate measurements on each film. AFM images were taken with a Digital Instruments Nanoscope using the tapping mode (scan rate 1 Hz) under ambient conditions. Fluorescence microscopy was performed with a Carl Zeiss equipped with an Axiocam imaging system. Bandpass filters with an excitation wavelength of 450-490 nm and emission wavelength of 515-565 nm were used for fluorescein detection.

2.3 RESULTS AND DISCUSSION

2.3.1 Pattern Formation with Agarose Stamp

Stamping with agarose soaked in either acidic or basic water or salt solutions was performed on the surface of various PEM films. After stamping no other treatment was performed (i.e., the films are not further rinsed in water). The r-WETS process was seen to create micrometer scale line patterns. Figure 2.2 shows (a) the featureless surface of a 12-bilayer-thick PAH/PAA (or a $(PAH/PAA)_{12}$ film) multilayer assembled with polyelectrolyte pH values of 8.5/3.5 respectively,(b) stamping on that same film with an agarose line pattern soaked in neutral water, (c) stamping the PEM for 10 min with a stamp soaked in pH 2.3 water, and (d) stamping the multilayer with a line pattern stamp soaked in 5MNaCl for 10 min. Images (a) and (b) show both that the films are featureless as assembled and that the line patterns seen in later experiments are formed as a result of the various reagents (acid, salt) being delivered by the stamp, and not just pressure from the application of a line pattern. Figure 2.2 (c) clearly shows the development of a porous morphology in every other stripe; presumably the regions that were in contact with the agarose stamp. Porous morphologies are known to develop in certain weak polyelectrolyte films with a sharp change in pH post film assembly.[17] The reason for this is that as certain groups (amines in this case) become charged and others (carboxylic acid) are protonated and become neutral, ionic bonds are broken in the film and charge repulsion causes a phase separation in the film. Figure 2.2 (d) demonstrates that application of high ionic strength solutions locally will create an etching of the PEM

film. Exposure to high ionic strength solutions can cause charge screening of the ionic cross-links within the films, disrupting them and dissolving the PEM films.[82]

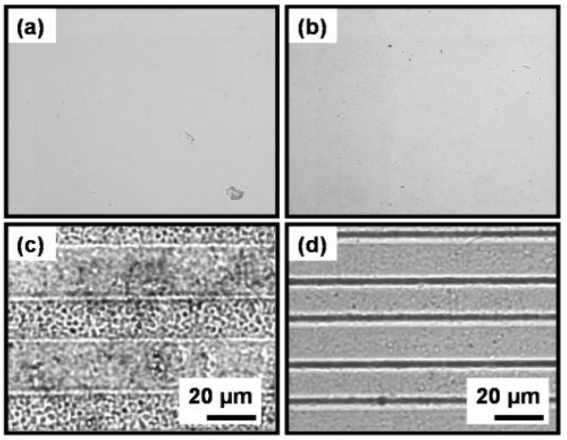

Figure 2.2. Optical micrographs of a $(PAH/PAA)_{12}$ 8.5/3.5 film surface (a) as assembled, featureless PEM film (b) film after stamping with agarose line pattern soaked in neutral water, (c) $(PAH/PAA)_{12}$ 8.5/3.5 film after stamping with agarose line pattern soaked in pH 2.3 water, and (d) $(PAH/PAA)_{12}$ 8.5/3.5 film after stamping with line pattern soaked in 5M NaCl. Stamping PEM films with hydrogel stamps can etch the films as well as locally change film morphology.

2.3.2 Patterning Chemical Functionality

When PEM films are assembled with chains that are not fully charged (such as in the case of PAH/PAA at 8.5/3.5 or 9.5/3.5) or in the presence of salt ions screening the polymers' charge, there will be some number of functional groups not participating in the ionic cross-links. These groups are therefore available for chemistry postassembly. Protonation or deprotonating these groups, for example, can alter the charge density within the film. These types of chemical modifications can be performed with agarose stamps. To visualize the control of functional group charge induced by an agarose stamp

soaked in pH 2.3 water, stamped $(PAH/PAA)_{12}$ films were exposed to 5 mM fluorescein solution for 1-2 min at room temperature, followed by rinsing for 1-2 min in deionized water. Figure 2.3 (a) shows the patterned Si wafer used to form the agarose stamp and Figure 2.3 (b) the corresponding line pattern in the LbL film resulting from the application of that stamp. Figure 2.3 (c) demonstrates that r-WETS of PEM films can enable the modification of chemical functionality. After immersing stamped $(PAH/PAA)_{12}$ films into fluorescein solution, green fluorescence was localized in the regions where the agarose stamp had been in contact with the films. This fluorescence is a manifestation of the strong electrostatic interaction between the negatively charged fluorescein molecules and the stamped regions where the density of positively charged NH_3^+ groups is high (exposure to low-pH solution protonating the available amine groups of the PAH chains). When an agarose stamp soaked in acidic water is brought into contact with a PAH/PAA film, the pH 2.3 solution is readily and constantly delivered from the agarose stamp to the film via diffusion along the concentration gradient.[19] Consequently, the supplied low-pH water modifies the PAH/PAA films, cleaving the ionic linkage between positively charged amine groups of PAH layer and carboxylate groups of the PAA chains. After stamping, the newly protonated amine groups of the PAH/PAA films in the stamped regions are reacted with negatively charged fluorescein molecules in solution to form ionic bonds. As a result, by using agarose stamps soaked in a variety of chemical reagents as well as the low pH, we demonstrate here the nature of patterned PEM films can be further modified and utilized for applications such as tissue engineering and biosensors.[86] Aqueous-based covalent

reactions should be possible, or embedding the PEMs with different kinds of ions, perhaps to locally synthesize metal nanoparticles. Furthermore, this technique offers the possibility of utilizing chemical functionality within the bulk and on the surface of the film, as opposed to just the surface as with many soft lithographic techniques.

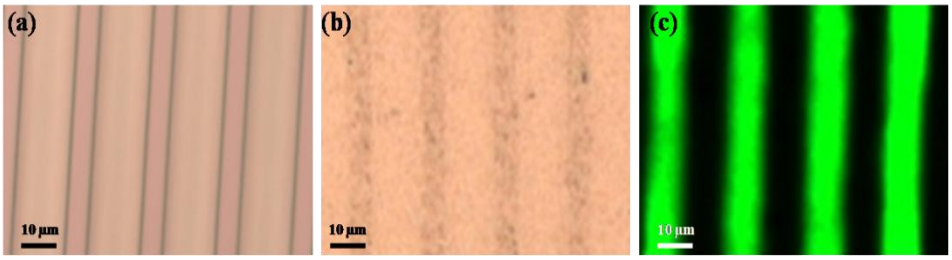

Figure 2.3. Optical microscopy (a) of master Si-wafer (b) LbL film (PAH/PAA) 9.5/3.5 that had been stamped with agarose line pattern soaked in pH 2.3 solution, and (c) after immersing the patterned films into aqueous fluorescein solution. The thinner lines indicate the stamped regions.

2.3.3 Measurement of Swelling from the Agarose Stamp

Because of the introduction of pores, PEM are expected to expand as they are swollen by the low pH. We have employed profilometer and AFM to determine the swelling in the patterned lines. The degree of swelling was obtained by comparing the thickness of an as-assembled film with that of the patterned line created by agarose stamping. Figure 2.4 (a) shows the smooth and continuous surface morphology of a pH 9.5/pH 3.5 12-bilayer PAH/PA film with a thickness of 300 nm. This is similar to growth reported on 7.5/3.5 multilayers.[87] As can be seen directly from the AFM images in Figure 2.4 (b) - (d), the height of the patterned line proportionally increases with stamping time. Precise measurements regarding the change of thickness of the patterned

regions were obtained by profilometer. The measured values were obtained by analyzing 10 regions on at least 10 separate samples and present an average of these. After averaging over all measurements, it was observed that the feature heights differed by only approximately ±10%, showing that this technique results in reproducibly uniform features. One would expect that eventually lateral diffusion of the acidic solution would cause a blurring of the line pattern, but within the time frame of the stamping experiments (less than 15 min), lateral diffusion was not observed to be an issue.

The thickness profiles measured for each stamping time was 38 nm above the original film surface for 0.5 min, 63 nm for 1 min, and 110 nm for 2 min of stamping time. The degree of swelling was calculated by the ratio of the film thickness of the as assembled LbL film to that of the patterned line, ranging from 13% for 0.5 min, 21% for 1 min, to 37% for 2 min of stamping time. Increased film swelling agrees well with the AFM images of the developing line patterns, suggesting that the increased degree of swelling with stamping time reflects the relative degree of interaction between polyelectrolytes and low pH solution during the contact of the stamp with the PEM. Ionic crosslinks between positively charged amine groups of PAH and negatively charged carboxyl groups of PAA are expected to dissociate in contact with low pH water, increase the film's thickness to compensate for the volume of the voids introduced, and thus swell more and more with stamping time. More detailed information regarding competitive interactions between PAH and PAA caused by diffusion of pH 2.3 water from the agarose stamp is shown in time evolution experiments below.

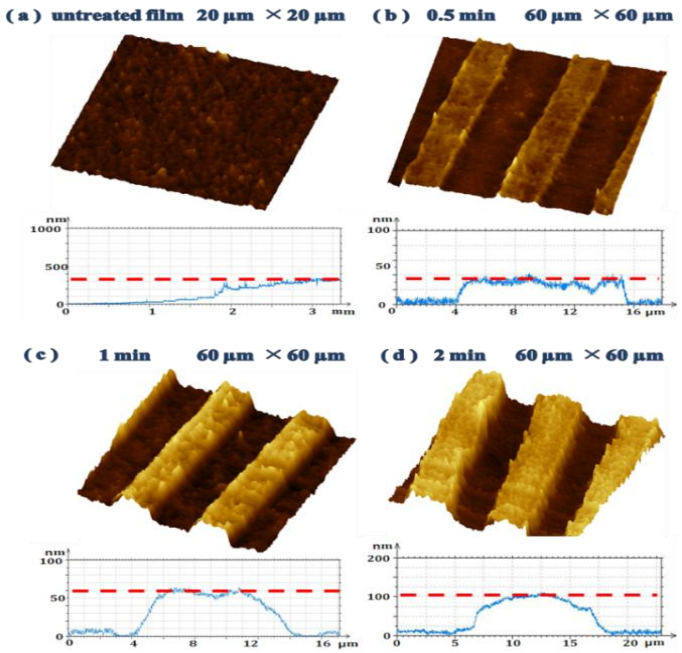

Figure 2.4. AFM images and profilometer scans (a) $(PAH/PAA)_{12}$ of unstamped LbL films (b) LbL films that had been stamped with agarose stamp for 30 sec, (c) 1min, and (d) 2 min.

2.3.4 Time Evolution Studies

High surface area porous materials have become excellent candidates for many applications such as electrode separators, sequestration of molecules, or change of refractive index. The porosity transitions and creation of nano- and micro-sized pores from PEM films by immersing into low pH [88] or high pH solution,[89-91] referred to as "post-assembly treatment", have been reported, but there are still questions regarding the origin and mechanism of these porous transitions. This transition is thought to be caused by a rearrangement of the polymer chains within the PEMs along with rejection of water from the films.[92] Deposition conditions and post-assembly treatments can create either nano or microscale pores, and what causes these different morphologies is not fully

explained. To the best of the authors' knowledge, reactive wet stamping of PEM films with hydrogel stamps does not exist in the literature. Here, the research presented is the use soft lithographic techniques both to pattern porosity transition and also to qualitatively study the time evolution of the porous transformation and gain information about its mechanism as well as to create previously unreported structures in PEM films. The stamp presents acid to the film surface at a much lower rate than if the films were immersed in acidic solution, allowing for direct observation of the evolution of the phase transformation.

To achieve this, agarose stamps were immersed in pH 2.3 water for 2 hr and blown dry with nitrogen gas for 30 sec. Finally, the stamp was brought into contact with a pH 9.5/pH 3.5 $(PAH/PAA)_{12}$ film with PAA as the outermost layer as a function of stamping time ranging from 30 sec, 1 ~ 10 min. Following stamping, the patterned PEM films were characterized by AFM, as can be seen in Figure 2.5, which shows 60 by 60 micron regions of films (a) as assembled and (b) – (f) over a range of stamping times. The insets in Figure 2.5 (b) – 4(f) are 10 by 10 micron enlargements of the patterned regions. In order to evaluate the physical properties such as height of patterned line, pore depth and pore width, profilometer was used and presented in Figure. 2.6. As mentioned above, the morphology of (pH 9.5 PAH/pH3.5 PAA) PEM films was characterized by a featureless surface (Figure. 2.5 (a)). However, in as short of a stamping time as 30 sec as shown in Figure 2.5 (b), line patterns appeared to be formed on the PEM films in AFM images and the height of patterned line on the stamped regions increased from approximately 38 nm (~13% of original film thickness) to 110 nm (~37% of original

film thickness) through profilometric analysis as the stamping time was increased from 30 sec to 2 min.

An AFM image (Figure. 2.5 (c)) of 3 min of stamping time shows the onset of new features. At this stamping time, rearrangement of the polyelectrolytes within the film is visible in the line pattern, including a decrease of patterned line height (from 110 to ~80 nm). At 4 min of stamping time, the micro-sized porosity first appears on the line pattern, where pore depth was about 88 nm and pore width ranged from 2.0 to 2.7 μm. Both pore depth and pore width on the stamped regions increased from approximately 95 to 110 nm and 2.0 to 3.8 μm, respectively, at 5 min of stamping time, showing similar pore structure (Figure. 2.5 (d)). However, when the agarose stamp was in contact with the $(PAH/PAA)_{12}$ film for 6 min, the resultant pore structure is different from that of 4 or 5 min. Similar observations were made with 7, 8, and 9 min of stamping time. As can be seen directly from the AFM images in Figure 2.5 (e), the morphology in these four cases has a more organized and "honeycomb"-like structure in which stamped height of patterned line, pore depth and pore width reached a similar height of patterned line of about 52 nm, pore depth of 60 nm, and pore width of 4.0 μm, as determined from profilometric analysis. After these honeycomb-like pores were observed during 6 to 9 min of stamping time, collapsed structures were seen for times greater than 10 min (Figure 2.5 (f)).

On the basis of AFM images and profilometer data (Figure 2.6), it can be seen that the time evolution of pore formation undergoes different stages yielding different heights of patterned lines, pore sizes, pore size distribution and pore morphologies in the

PEM films. During the first stage of 30 sec to 2 min of stamping time, stamping of the $(PAH/PAA)_{12}$ pH 9.5/3.5 PEM quickly results in formation of line patterns with no pores, at least none that are observable by AFM. The swelling observed in this initial stage is due to a combination of water uptake and increased charge repulsion from the charging of unbound amine groups. At these pH conditions film formation produces thick layers since both polyelectrolytes are only partially ionized. PAH (pKa of PAH $\approx$ 9.5) and PAA (pKa of PAA $\approx$ 6.5) [93] chains both adsorb in loop-rich conformations with an ion-paired internal structure. When PAA is the outermost layer, there are essentially free, unpaired acid groups [94] at the film surface but also unpaired functional groups throughout the film's structure. Therefore, when the agarose stamp is applied to the $(PAH/PAA)_{12}$ pH 9.5/3.5 LbL film, some of the ionic linkages between COO^- of PAA layer and NH_3^+ groups of PAH layer are cleaved, and there is an increase in charged amine groups and an increase in neutral acid groups throughout the film. The PAA chains with their newly reduced charge density become more coiled, increasing the film thickness.

During the 2nd stage of pore formation during the third minute of stamping, rearrangements of both PAH and PAA leads to pH-induced phase separation, showing the decrease of height of patterned line and a morphology resembling spinodal decomposition. At the 3rd stage, which ranges from 4 to 5 min of stamping time, the repulsion of protonated amine groups of PAH resulted in the micro-size porosity, showing the gradual decrease of patterned line in height accompanied by thicker pore walls and larger pore widths. The same structure was observed for the 5 min stamping;

however, the distribution of porosity was denser and pore depth and pore width increased. In our stamping process, the films were not immersed into water of any pH after stamping. A notable point is that the microporous transition appears after only acidic treatment whereas the creation of nanoporosity requires a low pH treatment followed by a higher pH treatment. The underlying mechanism of molecular rearrangements have been thought to be caused by a combination of phase separation from charge repulsion and expulsion of water due to the formation of new ionic crosslinks. In this respect, our finding that microscale porosity was formed from the application of an agarose stamp soaked in low pH (2.3) water, without any further rinsing treatment, supports recent results by other groups. Also, rinsing in higher pH (~5.5) water does not completely reverse the swelling back to the original state. As can be seen in Figure S5, the line patterns caused by stamping with agarose stamp soaked in pH 2.3 water are still present after rinsing for 1 minute in pH 5.5 DI water.

From 6 min to 9 min, the 4th stage, rearrangement of polymer chains within the PAH/PAA have caused the pores structure to have become more organized, and honeycomb like. Also in this stage, the porosity transition induced by r-WETs stamping has reached a plateau where the values of the physical properties such as height of patterned line, pore depth and pore width are no longer changing. We assume this is because the protonation is complete by this stage and there is no longer any driving force for rearrangement. With further exposure of agarose stamp into LbL films, during the 5th stage of the porous transformation (10 and 11 min stamping), the structure appears to collapse at some points.

In our system, the time evolution of pore formation is closely related to the reaction of PAH and PAA functional groups with agarose stamp. After initial exposure to low pH via agarose stamping, the newly protonated acid and base groups within the LbL films induce phase separation. After chain rearrangement begins within the PEM films, strong repulsion of the protonated amine groups of PAH result in spinodal decomposition,[95] as well as ejection of water from the PEM structure, resulting in different morphologies and pore structures according to stamping time. Finally, stamping times beyond 10 min lead to a collapse of the porous structure. The above results suggest that by stamping LbL films with the agarose stamp, the porous transition and properties such as pore size, pore morphologies, and pore distribution can be controlled as a function of stamping time.

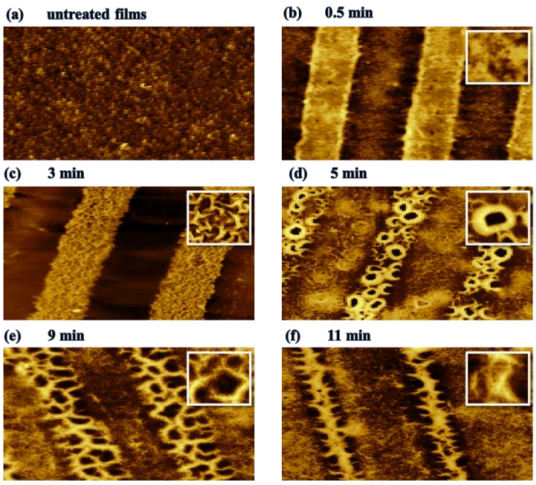

Figure 2.5. Time evolution of 60µm × 60µm AFM height images of (pH9.5 PAH/pH3.5 PAA)$_{12}$ PEM films in contact with agarose stamp for different times. The inset in (b) to (f) is the 10µm × 10µm AFM images corresponding to the stamped region.

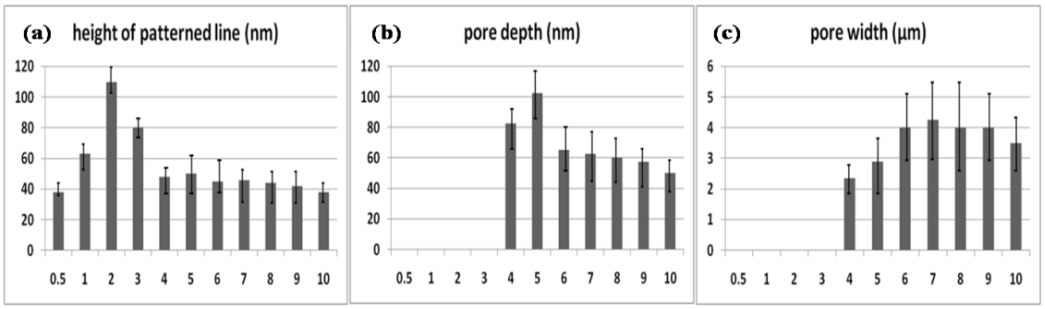

Figure 2.6. Histograms of physical properties (a) height of patterned line (b) pore depth (c) pore width. Heights of the patterned lines, pore depth, and width were measured in at least ten different areas for each of 10 samples of the stamped PEM films.

2.4 CONCLUSIONS

We demonstrate here the patterning and etching of polyelectrolyte multilayers using hydrogel stamps. Stamps soaked in acidic water used to pattern porosity into the films and stamps soaked in 5 M NaCl were used for etching. The salt etching can be done with both weak and strong polyelectrolyte multilayer systems. It is demonstrated that this wet stamping technique gives both lateral control of surface properties as well as depth control over the film's properties. This technique seems to be a promising way to pattern chemical reactions within PEM, phase transformation and physical properties such as film thickness and swelling. Novel pore structures, including the honeycomb-like structure were observed. While there are a few other reported patterning techniques for PEM films, we believe that r-WETS stamping has unique advantages. Especially for the patterning of porous regions, this technique is extremely versatile. Previously, such patterning has only been achieved with photo-crosslinkable polymers and masking.[96] Our method uses commercially available materials and is much simpler. In addition to patterning regions of porosity, we demonstrate the creation of patterned regions of

functional groups and of film swelling and thickness. Differently swollen PEM films have been shown to have different mechanical or cell adhesion properties. [97, 98] Inherent to LbL film assembly is a high degree of control of the film composition in the direction of growth, but this method could represent a powerful way to control PEM properties in the remaining two dimensions.

CHAPTER III

STRUCTURAL CHANGES IN POLYELECTROLYTE MULTILAYERS BY SALT STAMPING

3.1 INTRODUCTION

Polyelectrolyte multilayers (PEMs) are polymer thin films simply prepared by alternatively dipping a substrate into solutions containing the negative and the positive polyelectrolytes (a technique known as Layer-by-Layer (LbL))[99], essentially directing the complexation of polyelectrolytes onto a substrate. Each adsorption step is accompanied by a charge reversal of the film's surface, enabling the next deposition as well as self-limiting each deposition step. This direction of polyelectrolyte complexation onto a substrate allows for the highly reproducible fabrication of polymer thin films. The LbL deposition technique has the advantage that it can conformally coat nearly any type and geometry of substrate, but the greatest limitation in commercializing this technique is the long deposition times and many steps required to create the films. Recent studies have developed faster and more versatile methods such as spraying [100] or spin coating [101], but multiple, sequential steps are still required. With PEMs it is possible both to create ultra-thin coatings of tens of nanometers, but also films that are many microns thick, and they can be made as free-standing assemblies. Other strong point about LbL method is the use of incorporation of different types of building blocks (and therefore functionalities) and subsequently, PEMs fabricated by the LbL technique have been proposed as being useful in very diverse areas, such as separation membranes, light-

emitting diodes, anti-reflection and other biomaterials.[102, 103]

Although the electrostatic interactions holding PEMs together are strong, PEMS are nonetheless dynamic systems capable of response to a number of external stimuli; temperature, humidity, pH, ionic strong, solvent.[104-106] They are capable of reorganization during or their formation. Especially, by exposing PEMs assembled with weak polyelectrolytes into low pH[107, 108] or high pH solution[109-111], referred to as "post-assembly treatment",[81]weak polyelectrolyte films have shown phase separation induced porosity transitions with a significant increase in film thickness and roughness, and in other cases to exchange chains that are part of the electrostatic assembly for other chains in solution.[112] In our previous studies,[113] we have developed a new method about the phase separation induced porosity transitions within PEMs by post-assembly treatment to low/high pH solutions using reactive wet stamping (r-WETS) technique.[114,115] By using hydrogel stamps soaked in a chemical reagent of interest, (e.g. acid or base), the aqueous solutions can be delivered locally at controlled rates, giving the stamping technique a lot more control than other methods reported in the literature. Structural rearrangements of multilayers under the influence of environmental salt solutions have been reported;[116-118] by exposing thin films to salt solutions, salt ions screen the electrostatic charges of polyelectrolytes, disrupt the ionic crosslinks, dissolve the film, and consequently result in dramatic changes in the physicochemical properties of the multilayers. The deconstruction process of the PEMs through salt-induced structural changes is not a uniform top down process, creating a porous structure. However, more detailed information about the effect of salt solutions on the creation of pores as well as

changes of physical / mechanical properties is not known.

In this work, we paid special attention to the effect of the concentration of a salt solution on the morphological transitions as well as physical properties (degree of swelling by swollen thickness) and mechanical properties such as Young's modulus and hardness. We employed reactive wet stamping method in which hydrogel stamp materials were soaked into various concentrations of salt (NaCl and $CaCl_2$) solutions and then, applied onto PEMs. In addition to investigating the morphological transitions and the changes of physical/mechanical properties from the application of salt stamping, our work aims to design the gradient structures with either swelling or porous transitions along the lateral direction of the thin films to establish guidelines for introducing functionality into the materials. The application of differently concentrated salt solutions could provide a significant control over the structure formation in the multilayers. Motivated by these results, we applied a gradient in salt solutions to the polyelectrolyte multilayers using a stamp soaked in a gradient of salt concentration. Depending on different concentrations of combinations in salt stamping, either of the gradient structures in thickness or porosity could be created.

3.2 EXPERIMENTAL METHODS

3.2.1 Materials

Poly(acrylic acid) (PAA, MW=50 000 g/mol, 25% aqueous solution) was obtained from Polysciences. Poly(allyl amine hydrochloride) (PAH, MW = 70 000 g/mol), sodium hydroxide and sodium chloride were purchased from Sigma Aldrich.

Calcium chloride dihydrate and sodium chloride were obtained from EMD and Mallinckrodt, respectively. EMD high gel strength agarose, hydrogen peroxide, sulfuric acid, and hydrochloric acid were purchased from VWR. All the products of commercial origin were used as received without further purification. Ultra-pure water (Milli-Q system, Millipore Co.) with the specific resistance better than 18 MΩ was used.

3.2.2 Assembly of LbL Thin Films

Polyelectrolyte dipping solutions of 0.02 M PAH and PAA were prepared from received materials without further purification (based on the repeat unit molecular weight) in Milli-Q water. Polymer solution pH values were adjusted using 0.1 M or 1 M HCl and NaOH solutions as needed prior to multilayers assembly. Glass slides used as a substrate were cleaned using piranha solution (1:3 mixture of 30 % H_2O_2 and 98% H_2SO_4) and heated until no bubbles are released. The layer-by-layer deposition of PAH and PAA was done by alternately dipping substrates in polyelectrolyte solutions using a Nano Strata Sequence VI at room temperature. Cleaned glass slides were first immersed in the polycation (PAH) for 10 min and rinsed in three fresh water baths for 2, 1, and 1 min. The samples were then immersed in the polyanion (PAA) for 10 min, followed again by three rinsing steps. The deposition of one bilayer is defined as an adsorption step of polycation, followed by polyanion adsorption. Unless otherwise stated, the outermost layer of the multilayers used in this experiment was the polyanion (PAA), and the deposition process was repeated for 12 bilayers. PEMs notation of $(XPAH/YPAA)_Z$ is used, where X and Y are the assembly pH values of the polycation and polyanion, respectively, and Z is the total number of bilayers. All polyelectrolyte multilayers were

dried by nitrogen gas for 2 min and further dried in ambient air for several hours before patterning of thin films or additional characterizations.

3.2.3 Reactive Wet Stamping

Agarose stamp was prepared by mixing the agarose and D.I water in a 1: 10w/w ratio and then aqueous solution of high strength agarose was cast against the master Si-wafer having an array of microscopic features.[119] After cooling to room temperature, the agarose stamp was peeled off from the master Si-wafer, and cut into pieces of 1 cm X 1 cm X 0.5 cm size. Micro-patterned agarose stamps were soaked into salt solution for 1.5 h, dried under nitrogen stream, and stamped atop of the PAH/PAA multilayer for the desired amount of time, followed by brief rinsing with D.I water.

3.2.4 Gradient Salt Stamping

The patterning of 7.5PAH/3.PAA LbL films with gradient concentration of salt solutions was performed as followed ways; first, agarose stamp having line patterns was vertically placed in the glass vial, followed by injecting salt solutions in the order of less to dense concentration from the bottom of the vial. After soaking the agarose stamp into a gradient salt column for 1 h, the agarose stamp was taken out, gently blown out with a compressed nitrogen gas, and finally stamped onto the 7.5PAH/3.5PAA LbL films for a variety of times, followed by brief rinsing steps with distilled water.

3.2.5 Multilayer Film Characterization

Atomic Force Microscopy (AFM) was conducted by using Digital Instruments Nanoscope in the tapping mode (scan rate 1 Hz) under ambient conditions. Optical microscopy was performed with a Carl Zeiss optical microscope (model no. 430014-

9902) equipped with an Axiocam imaging system (AXIO M2m). The hardness and Young's elastic modulus were calculated by nanoindenter (Hysitron Triboindenter Nanoindenter (341-F)). At least 10 nanoindentation experiments were performed on each sample throughout the whole stamped area of the multilayers. The thickness of multilayer films was determined using a Profilometer (KNA–Tencor Instruments P-6), and values reported represent at least 10 separate measurements on 5 separate samples. All Quartz Crystal Microbalance with Dissipation (QCM-D) measurements were performed by using Q-sense E4 system.

3.3 RESULTS AND DISCUSSION

3.3.1 Morphological Transitions in PAH/PAA Films

Morphological changes in 7.5PAH/3.5PAA LbL films were investigated by patterning them with various concentrations of salt solutions and different stamping times. Figure 3.1 and 3.2 show AFM images at patterned regions where LbL films were stamped for 10 min by using agarose stamps that had been soaked in NaCl and $CaCl_2$ solutions, respectively, for 2 h. When the agarose stamp was applied onto the multilayers, no distinct surface features were observed at less than certain concentrations (1 M for NaCl stamping and 0.3 M for $CaCl_2$ stamping), as in the case of untreated PAH/PAA LbL film (Figure 3.3). However, significant differences in morphology were found for the multilayers patterned with agarose stamp having the concentrations of 1 M for NaCl and 0.3 M for $CaCl_2$ solutions, as shown Figure 3.1 and 3. 2. Pores with typical diameters of 300 ~ 400 nm and depths of 70 ~ 100 nm were created on the surface of

multilayers from the application of agarose stamping for both NaCl and $CaCl_2$ solutions. At a denser concentration of salt solutions (2 ~ 3 M for NaCl and 0.7 ~ 1.0 M for $CaCl_2$ solution), the pores of PAH/PAA LbL films became spinodal. When the agarose stamp soaked in more than 3 M of NaCl or 1 M of $CaCl_2$ solution was brought into contact with PAH/PAA LbL films, the thin films were partially detached or dissolved. AFM images showed that the surface of multilayers was nonporous (Figure 3.4). The salt ions-induced morphological changes, including pores, pitting, and spinodal are closely related to the structural rearrangements in polyelectrolyte multilayers upon an exposure to salt solutions.

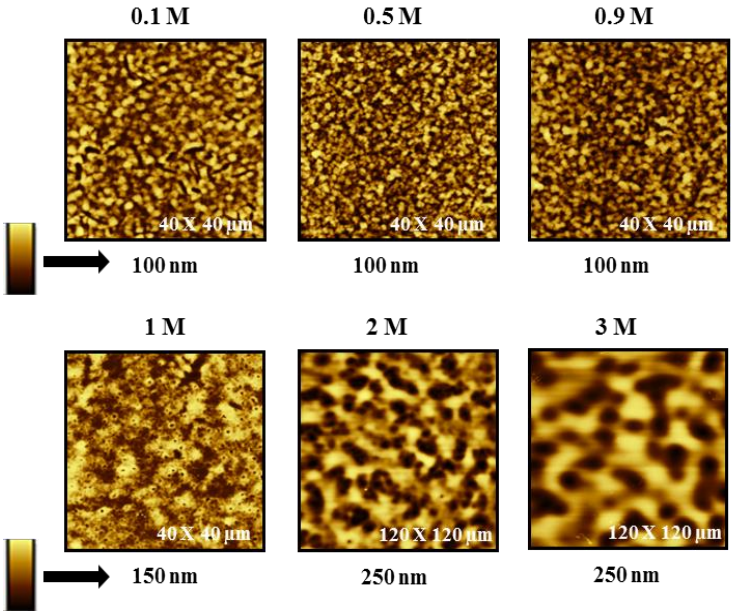

Figure 3.1: AFM images of 7.5PAH/3.5PAA LbL films that were taken from patterned regions under a variety of NaCl solutions. Agarose stamp was first soaked into various concentrations of salt solutions for 2h, and subsequently dried with compressed N_2 gas gently and then applied on the LbL films. After the thin films were patterned with agarose stamp, multilayers were rinsed with D.I water for 15 ~ 30 sec.

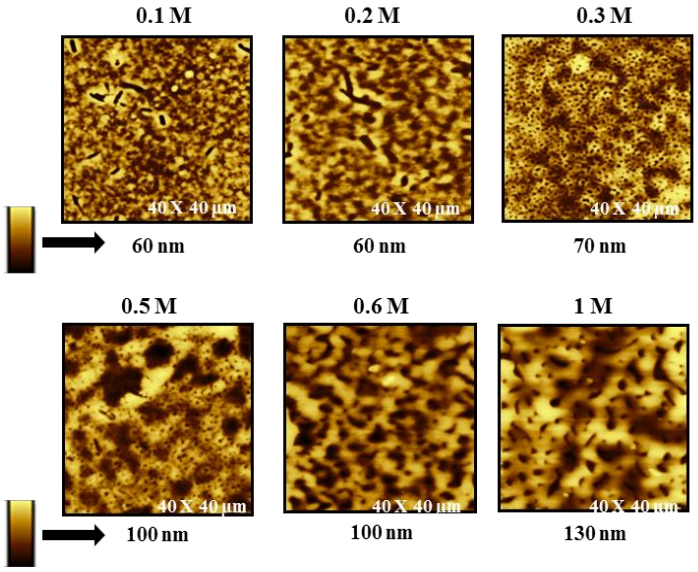

Figure 3.2: AFM images of 7.5PAH/3.5PAA LbL films that were taken from patterned regions under a variety of $CaCl_2$ solutions. Agarose stamp was first soaked into various concentrations of salt solutions for 2h, and subsequently dried with compressed N_2 gas gently and then applied on the LbL films. After the thin films were patterned with agarose stamp, multilayers were rinsed with D.I water for 15 ~ 30 sec.

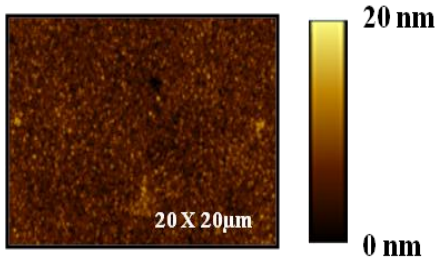

Figure 3.3: AFM image of an untreted 7.5PAH/3.5PAA LbL film.

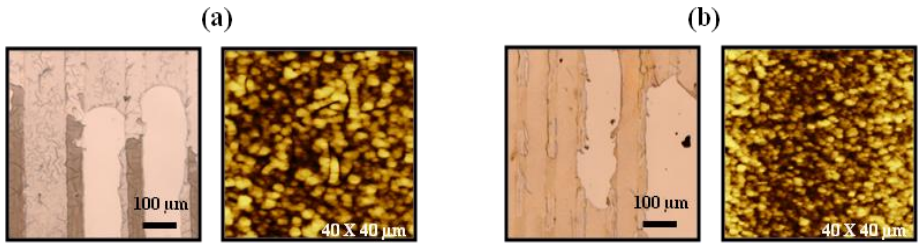

Figure 3.4: Optical Microscopy (left) and AFM (right) images of 7.5PAH/3.5PAA LbL films that were stamped with 4 M of NaCl solution (a) and 1.1 M of $CaCl_2$ solution (b). Both LbL films were stmaped for 1 min. AFM images were obtained from the regions where multilayers were remained after an application of agarose stamping.

3.3.2 Swelling and Mechanical Properties from Salt Stamping

To study the structural rearrangements of the multilayers under salt stamping in more detail, the profilometer was employed to measure the thickness changes and hence, degree of swelling in the patterned lines from the application of agarose stamp. Table 3.1 shows physical (swollen thickness and swelling ratio) and mechanical (modulus and hardness) property changes in response to 10 min of the agarose stamping. The degree of swelling was calculated by comparing the thickness of an as-assembled film (300 nm) with that of the patterned line created by agarose stamping. Optical microscopy images of the patterned thin films and the profilometer scans between stamped and unstamped regions are presented in Figure 3.5 and 3.6. The measured values were obtained by analyzing 10 regions on 5 separate samples.

It was expected that PAH/PAA LbL films would expand and be swollen because of the introduction of pores upon an exposure of PEMs to salt solutions. As expected, the thickness of the multilayers in patterned regions was increased as the salt concentration of agarose stamp increased up to 0.9 M of NaCl and 0.2 M of $CaCl_2$ solution. The height

of the patterned line proportionally increased with stamping time at each concentration. The maximum thickness profile for 10 min of stamping time was about 110 nm at 0.9 M of NaCl and 150 nm at 0.2 M of $CaCl_2$ solution. The corresponding maximum degree of swelling was 37 % for NaCl and 53 % for $CaCl_2$ stamping. The swollen thickness of the original film surface and the degree of swelling were decreased from 1 M of NaCl and 0.3 M of $CaCl_2$ solution. Then, they significantly dropped at 10 min of stamping time, where porous transitions were formed. At a higher salt concentration of agarose stamping (NaCl $\geq$ 1 M and $CaCl_2 \geq$ 0.3 M), the swollen thickness continuously decreased, showing deswelling behavior.

Mechanical properties such as hardness and Young's modulus at patterned lines of 7.5PAH/3.5PAA LbL films were investigated by nano-indentation analysis (right two columns in Table 3.1). The measured values were obtained by analyzing 10 different regions on 5 separate samples and presented an average of these. It was observed that both the thin films patterned with NaCl and $CaCl_2$ solution exhibited a lower Young's modulus and hardness than those of an untreated thin film. Those values of mechanical properties decreased with salt concentration. Minimum values of both modulus and hardness were obtained at 0.9 M for NaCl and 0.2 M for $CaCl_2$ solution stamping. Beyond this salt concentration, however, mechanical properties of patterned thin films increased. The interrelationship between the swelling / deswelling behavior and the mechanical property was discussed in detail in the subsequent section.

Table 3.1: Swollen thickness changes and swelling ratio of 7.5PAH/3.5PAA LbL films with various concentrations of salt solution. The thickness of pure 7.5PAH/3.5PAA LbL films of 12 bilayers employed in this experiment was 300 nm. Mechanical properties (Young's modulus and hardness) at stamped areas with different concentrations of salt solution were shown in right two columns, respectively, for NaCl and $CaCl_2$ stamping. An untreated PAH/PAA LbL film had 16.0 GPa in Young's modulus and 510 MPa in hardness.

NaCl	Swollen Thickness (nm)	Swelling Ratio (%)	Modulus (GPa)	Hardness (MPa)
0.1 M	5 ± 3	1 ~ 3	15.7	480
0.5 M	25 ± 5	7 ~ 10	13.1	380
0.9 M	100 ± 10	30 ~ 37	9.1	240
1.0 M	25 ± 3	7 ~ 9	13.5	400

$CaCl_2$	Swollen Thickness (nm)	Swelling Ratio (%)	Modulus (GPa)	Hardness (MPa)
0.1 M	50 ± 5	15 ~ 18	11.8	330
0.2 M	140 ± 10	43 ~ 53	7.8	180
0.3 M	30 ± 5	8 ~ 12	12.6	350

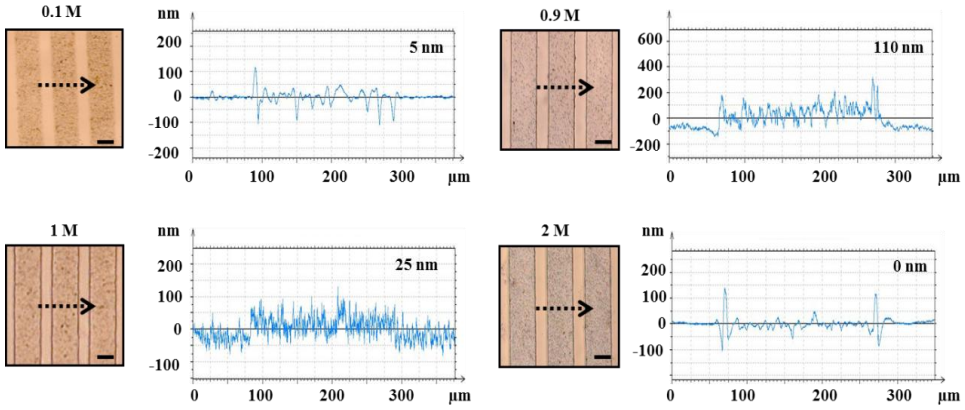

Figure 3.5: Optical Microscopy (left) and profilometer (right) images of 7.5PAH/3.5PAA LbL films patterned by a varios of concentrations of NaCl stamping. Stamping time was 10 min for every sample. Each arrow on the Optical Microscopy image indicates that the profilometer is scanned through the direction of arrow for a analysis of the degree of swelling. Scale bar in each optical microscopy imge indicates 150 µm.

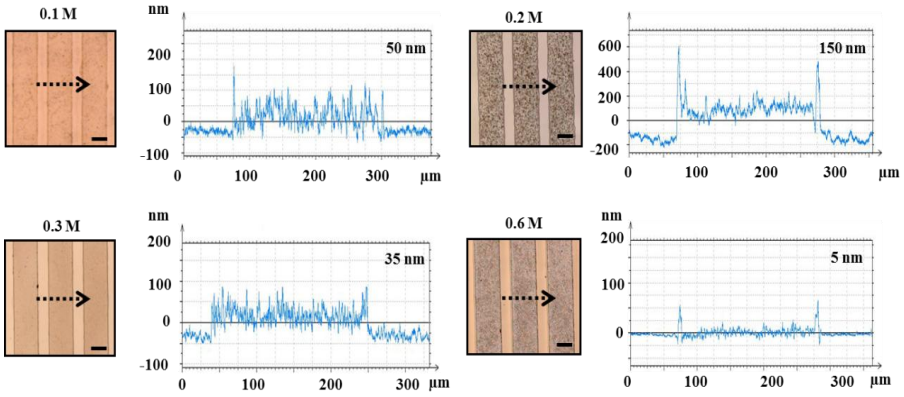

Figure 3.6: Optical Microscopy (left) and profilometer (right) images of 7.5PAH/3.5PAA LbL films patterned by a varios of concentrations of $CaCl_2$ stamping. Stamping time was 10 min for every sample. Each arrow on the Optical Microscopy image indicates that the profilometer is scanned through the direction of arrow for an analysis of the degree of swelling. Scale bar in each optical microscopy imge indicates 150 µm.

3.3.3 Structural Transitions of Multilayers by Salt Stamping

It is known that polyelectrolyte multilayers may be reorganized post-assembly by the exposure to high ionic strength solutions which can create morphology changes or partially dissolve the multilayers by charge screening of the ionic crosslink's in the film.[120-122] However, to the best of our knowledge, morphological transformations as well as physical and mechanical property changes due to the film's swelling / deswelling from different high ionic strength solutions have not been reported in the literature and still remain elusive. The usual technique [123-125] like completely immersing films at once in the solution or other techniques [76-80] reported in the literature creates a rapid rate of transformation, preventing certain structures from being readily viewed. Instead, by using hydrogel stamps soaked in salt solutions and then applying to the film's surface, salt solutions can be delivered locally at controlled rates, giving more detailed

information regarding physical property such as the degree of swelling as well as surface morphology transitions including pores, swelling, and spinodal.

On the basis of AFM analysis, profilometer data, and nano-indentation results, it can be seen that 7.5PAH/3.5PAA LbL films undergo various morphology changes including localized swelling, pores, and spinodal, yielding different swelling / deswelling behavior and mechanical properties. When the salt solution of NaCl or $CaCl_2$ was released from the agarose stamp to the thin film, the presence of salt ions delivered breaks contact between polymer chains in multilayers through competitive binding with free salt ions and allows the movement of the polyelectrolytes. Therefore, in this stage, an introduction of salt solutions swells the film locally with no pores by changing the interaction of the polymer chains, raising the film in regions where the stamp makes contact with the film surface. For both NaCl and $CaCl_2$ stamping, the film's thickness (hence, degree of swelling) increased up to 110 nm at 0.9 M of NaCl and 150 nm at 0.2 M $CaCl_2$, respectively. In addition to the film's swelling, the salt stamping changes mechanical properties. Basically, mechanical properties such as Young's modulus and hardness in the patterned film were lower than those of an untreated film or the regions of the film that had not come into contact with the stamp. Nano-indentation analysis indicated that the more swollen regions had a lower modulus and hardness, suggesting that the degree of swelling reflects the degree of interactions between polyelectrolytes.

The only difference between NaCl and $CaCl_2$ salt stamping was that the thin film patterned with $CaCl_2$ solution had more quick swelling / deswelling rates and mechanical properties, as well as the morphology variations in response to the

concentration changes than NaCl stamping throughout the paper. One possible explanation includes that divalent salt ($CaCl_2$) may have more interaction with polymer chains than monovalent salt (NaCl) at the same concentration, causing any morphological or physical changes to appear at the less concentrated of $CaCl_2$ salt solution. With increasing the concentration of salt solutions, the regions of the thin film onto which agarose stamp was applied showed porous transitions with about 300 ~ 500 nm pores in size. At this concentration of NaCl (1 M) or $CaCl_2$ (0.3 M) stamping, the denser concentration of salt ions free up more polymer segments, allowing them to form new polymer – polymer contacts, resulting in a new film morphology such as porosity structure. The creation of porous transition may be attributed to a change in the polyelectrolyte interlayer interactions; salt ions delivered from the stamp to multilayers result in charge shielding which disrupts the ionic crosslinks of thin films. Consequently, salt ions compensate charges in the multilayer, thereby inducing structural rearrangements within the thin films and showing the decrease of the height of patterned line (25 nm at 1 M of NaCl and 30 nm at 0.3 M of $CaCl_2$) and a morphology resembling porous structures. Upon the application of higher ionic strength solutions of NaCl ($1\ M < C_{NaCl} \leq 3\ M$) and $CaCl_2$ ($0.5\ M < C_{CaCl_2} \leq 1\ M$) stamping, the morphology of the thin film became spinodal. Both physical (swollen thickness) and mechanical properties (moduli and hardness) at this stage dramatically dropped and became almost as the same with those of an untreated film for NaCl stamping. Extremely high concentration of salt ions ($C_{NaCl} > 3\ M$ and $C_{CaCl_2} > 1\ M$) resulted in the deconstruction of multilayers due to a

significant disruption of the ionic crosslinks of polymer chains, and therefore locally dissolved the film.

To investigate in more detail the influence of the salt solutions on the physical and mechanical properties, we used QCM-D to study changes of the thickness and viscoelasticity upon the salt treatment under real time control. In all QCM-D experiments, each polyelectrolyte (10 mmol) was pumped into the chamber for 5 min and rinsing water was passed through the chamber for 1 min in between polyelectrolyte solutions at a flow rate of 0.15 g/min. The changes of frequency and dissipation occurring upon the injection of salt solutions were shown in Figure 3.7. When 0.1 M of either NaCl or $CaCl_2$ salt solutions were pumped into the QCM-D chamber, the resonant frequencies dropped and the dissipation values rose. When 0.9 M of NaCl or 0.2 M of $CaCl_2$ salt solution were passed over the PAH/PAA film, the frequency went down substantially and the dissipation went up dramatically. Upon the addition of 1 M of NaCl or 0.3 M of $CaCl_2$ salt solution, however, the frequency increased whereas the dissipation decreased significantly as compared to 0.9 M of NaCl or 0.2M $CaCl_2$ salt treatment. From the changes in frequency and dissipation, QCM-D can allow for obtaining the information regarding the changes in the physical and mechanical properties of the film. For example, a decrease of frequency indicates that polyelectrolyte chains or water molecules are adsorbed on the surface to form a thick film. An increase in dissipation is usually interpreted as a decrease in stiffness, which could indicate film's swelling and flexibility.

Our QCM-D data showed that when the salt concentration increased in the range of $C_{NaCl} \leq 0.9$ M and $C_{CaCl_2} \leq 0.2$ M, frequency decreased and dissipation increased. This indicates that a higher salt concentration causes the multilayers to swell more and become less rigid. This is most likely due to a combination of the uptake of water into the films by osmotic pressure and the screening of the polymer chains by salt ions. When the multilayers are exposed to ionic strength solutions, some of the ionic linkages between NH_3^+ of PAH and COO^- of PAA groups are broken because of the screen effect by salt ions. Therefore, both polymer chains become more coiled, increasing the film thickness. This observation is in good agreement with the results from profilometer and nanoindentation (Table 3.1); the height of patterned lines increased and hence, mechanical properties decreased at this range of concentration of both NaCl and $CaCl_2$ salt stamping. Thus, the strong swelling and more compliant films observed in QCM-D, profilometer, and nanoindentation experiments are a signature of water uptake, and these results can be taken as an indication for the conformational changes of polymer chains with ionic strength.

At the concentration of 1 M of NaCl and 0.3 M of $CaCl_2$ solution, where porous transitions were created on the surface, the frequency increased and the dissipation decreased as compared with less concentrated salt treatment. This indicates that the multilayers become deswelling and less soft. This result obtained from QCM-D also coincides with the observation from profilometer and nanoindentation data. Qualitatively, the QCM-D showed the same film swelling (low modulus and hardness) / deswelling

(high modulus and hardness) behavior depending on the ionic strength solutions, as was observed with profilometer and nanoindentation analysis.

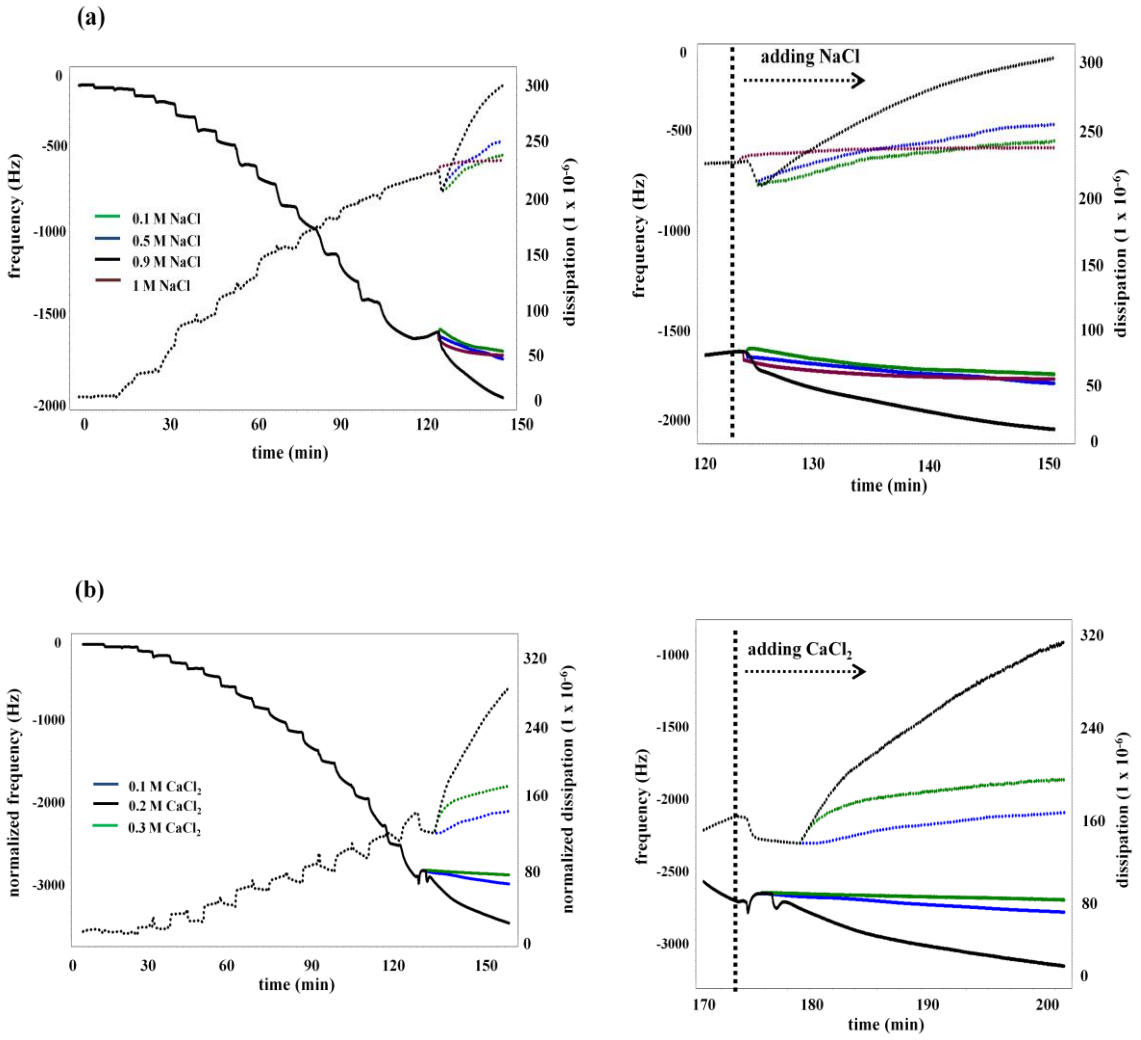

Figure 3.7: Influence of the ionic strength on the structural swelling of PAH/PAA multilayers. The QCM-D results showed normalized change in frequency (solid line) and dissipation (dotted line) upon the addition of salt solutions ((a) NaCl and (b) $CaCl_2$ solutions) after the build-up of a PAH/PAA LbL thin film. Right figures were taken from each left data, enlarging the changes of viscoelastic property after adding the salt solutions. All the change of frequency and dissipation were obtained from the measurements at the third overtone and all the experiments were conducted at 25°C.

3.3.4 Lateral Gradient Structures

Considerable effort has been focused on producing gradient materials with a gradient of properties such as roughness, composition, reactivity, and porosity in materials chemistry because of their superior mechanical and biological properties to uniform or homogeneous materials.[126- 128] However, in creating gradients of surface chemistry, mechanical properties (via crosslinking) and thickness are all problems that can be tackled with current methods to varying degrees of success. Here we present a novel approach to the fabrication of gradient structures by using r-WETS with salt solutions. On the basis of the above results, a gradient structure with continuous changes in thickness or porosity along the lateral direction was created in the following ways; an agarose stamp was first placed in the small glass vial and then salt solutions were injected from less to more concentrated salt solutions in the glass vial. After placing the agarose stamp for 1 h, the stamp having gradient salt solutions was applied onto the 7.5PAH/3.5PAA LbL films, consequently delivering different salt concentrations from the stamp to the film depending on the vertical position where the stamp was placed in the gradient concentration salt column.

The polyelectrolyte multilayers had two distinct surface features depending on the concentration of salt solutions; swelling behavior without pore structures at relatively less concentrations and porous transitions with deswelling behavior at denser concentrations. Based on this observation, we employed two different combinations of the concentration gradient salt column to make either lateral thickness or porosity gradient structures. First, to control the thickness changes at a specific location and make

a continuous gradient structure in film thickness, 7.5PAH/3.5PAA LbL films were patterned for 10 min with agarose stamp that had been soaked in 0 – 0.6 – 0.9 M gradients of NaCl solution or 0 – 0.1 - 0.2 M gradients of $CaCl_2$ solution. With this combination of the salt gradient column, stamped regions were easily observed, as shown in Figure 3.8 (a) and (b). AFM images in each patterned area showed nonporous structures on the surface of thin film. To see how much the thin films swelled at each stamped region, the profilometer scanned to the direction of dotted arrow. As expected, the thickness (100 nm for NaCl and 140 nm for $CaCl_2$ solution) above the original film at bottom region was more swollen than that of middle or top region.

Secondly, to create lateral gradient porous structures on the surface of thin films, we made different combination of salt gradient column in which 0 - 1 - 2 M of NaCl solutions and 0 - 0.5 - 1 M of $CaCl_2$ solutions were used to pattern multilayers. After stamping the films for 10 min, patterned lines were easily observed in Figure 3.9. The AFM was used to find out the variations in surface feature in more detail. The results showed that the structural rearrangements of polymer chains occurred due to an introduction of salt solutions into polyelectrolyte multilayers. This caused the thin films to have different morphological transformations depending on stamped areas. That is, no morphology change was observed at the top region, where multilayers were patterned with D.I water. On the contrary, porous transitions were formed at the middle of the thin film with several hundreds of pore size. Spinodal decomposition or larger size of pore structures was created at the bottom of patterned films, where the most concentrated salt solutions were released to PAH/PAA films. With this combination of gradient salt

solutions, we were able to create lateral gradient porous structures in which morphological transitions changed along the lateral direction of thin films. Also, the pore size and porosity in each region can be controlled simply by adjusting the concentration of salt solutions.

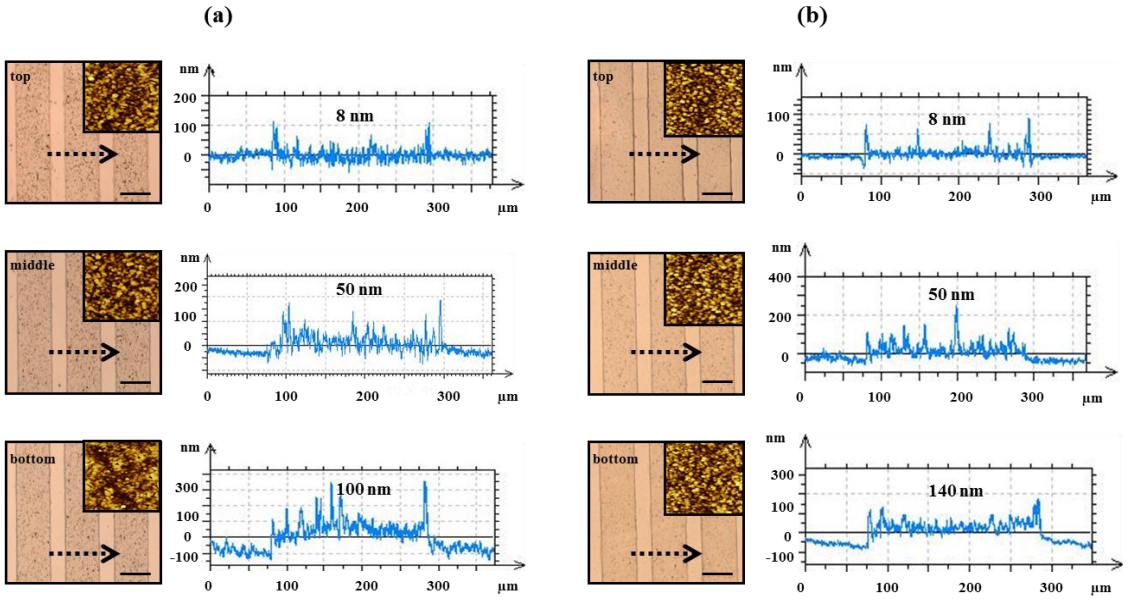

Figure 3.8: Lateral thickness (swelling) gradient structures of 7.5PAH/3.5PAA LbL films. Agarose stamp was soaked into 0 - 0.6 - 0.9M of NaCl gradient column (a) and 0 - 0.1 - 0.2 M of $CaCl_2$ gradient column (b) for 1 h, and then applied onto thin films for 10 min. The height of stamped regions was obtained by a profilometer scan with the direction of an arrow. A scale bar in optical microscopy images is 200 µm and scan size of insert AFM images is 40 X 40 μm^2.

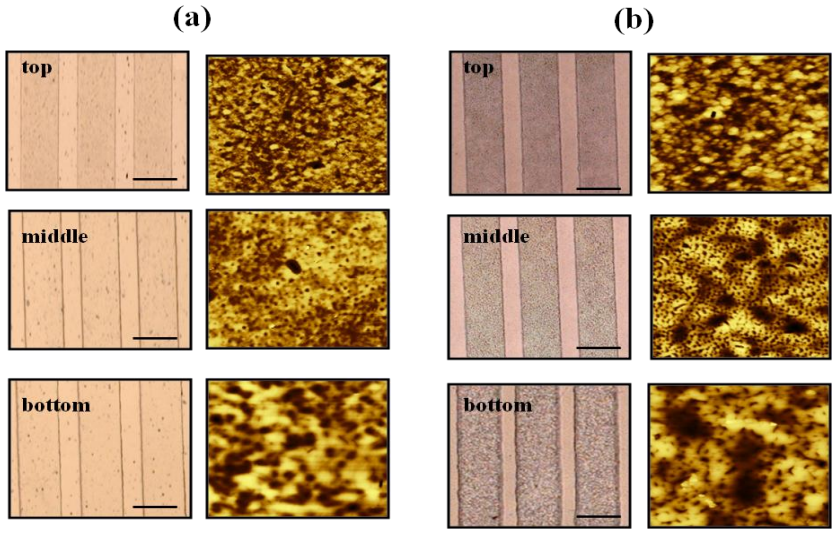

Figure 3.9: Lateral porosity gradient structures of 7.5PAH/3.5PAA LbL films. Agarose stamp was soaked into 0 - 1 - 2 M of NaCl gradient column (a) and 0 - 0.5 - 1 M of $CaCl_2$ gradient column (b) for 1 h, and then applied onto thin films for 10 min. A scale bar in optical microscopy images is 200 μm and scan size of AFM images is 60 × 60 μm^2 for (a) and 40 × 40 μm^2 for (b).

3.4 CONCLUSIONS

The main focus of this paper is to investigate the morphology transitions, physical, and mechanical changes of PAH/PAA LbL thin films by using the ionic strength solutions that are delivered from hydrogel stamp materials. It is apparent that salt-induced structural rearrangements in PAH/PAA LbL films can be controlled with different concentrations of salt solutions delivered from agarose stamp. The observations by AFM, profilometer, nano-indentation, and QCM-D analysis revealed that at specific salt concentrations morphological, physical, or mechanical properties of the thin film can be varied due to the change of the polyelectrolyte interlayer interactions. This resulted in swelling / deswelling behavior and porous transitions, and finally deconstructed

structures. This study also demonstrated the feasibility of producing multilayers with a continuous gradient thickness or porous structure along the lateral direction via a gradient concentration of salt stamping. At relatively low concentrations of gradient salt stamping (0 - 0.6 - 0.9 M of NaCl or 0 - 0.1 - 0.2 M of $CaCl_2$), the swollen thickness was varied depending on the patterned regions. The continuous thickness gradient thin film would be helpful to modulate tissue cell adhesion of physicochemical characteristics.[129] Gradient porous transitions were also created with agarose stamps that had been soaked in 0 - 1 - 2 M of NaCl or 0 - 0.5 - 1 M of $CaCl_2$ concentration gradient salt column. These porous structures with a gradient in porosity and pore size are expected to find great potential for generating defect-free scaffolds in tissue engineering applications [130] as well as useful for tangential flow membrane to separate colloids from aquatic solutions and to allow for the fabrication of particles by size.

CHAPTER IV

FILM STABILITY DURING POST-ASSEMBLY MORPHOLOGICAL CHANGES IN POLYELECTROLYTE MULTILAYER DUE TO ACID AND BASE EXPOSURE*

4.1 INTRODUCTION

Polyelectrolyte multilayers (PEMs) fabricated by the layer-by-layer (LbL) method of directed self-assembly are a versatile and highly functional class of polymer coatings or thin films. Their use has been suggested in applications as varied as organic electronics, food packaging, and drug delivery devices.[131] Although extensive literature exists on PEMs, many fundamental questions about their nature and assembly remain. While polyelectrolyte complexes are thermodynamically stable, PEMs films are a competition between thermodynamics and kinetics,[132] making them more complicated structures. PEMs are dynamic and capable of reorganization and exchange processes, including loading and release of small molecules,[133] exchange between polymer chains in the films and in the environment,[134-136] and morphological changes such as porosity induced by exposure to a change in pH.

Although PEMs as assembled are permeable to small molecules and in some cases even to macromolecules, [137-139] they do not have micro- or even nanoscale pores.

---

*Reprinted with permission from "Film Stability During Post-Assembly Morphological Changes in Polyelectrolyte Multilayers due to Acid and Base Exposure" by Chungyeon Cho and Nicole S. Zacharia 2012. Langmuir, 28, 841-848, © 2012 ACS.

The creation of this type of porosity in PEMs was first reported by Rubner, *et al* using the weak polyelectrolyte system poly(allylamine hydrochloride)/poly(acrylic acid) (PAH/PAA).[140] Exposing pre-assembled PAH/PAA films to low pH solutions creates morphologies with either micro-scaled or nano-scaled pores, depending on the pH of both the assembly solutions and the post assembly treatment.[141,142] This same transition has also been reported for films of the weak polyelectrolyte pair linear polyethylene imine (LPEI) and PAA exposed to low pH,[143] films with dendrimers,[144] as well as hydrogen bonded films of PAA and poly(4-vinylpyridine) exposed to high pH solutions after assembly.[145-147] The basic mechanism for this morphology change is that the sharp change in pH protonates / deprotonates the chemical groups in the polymer chains, both breaking up existing ionic bonds as well as creating new bonds, creating a phase separation. This process is accompanied by swelling and then contraction as water is taken up and then ejected with the formation of new ionic crosslinks. The water is ejected in a non-uniform fashion, creating pores in the film structure.[60] This only occurs for weak polyelectrolyte systems; mixed strong and weak PEMs may undergo extreme changes in swelling with pH.[148]

While the literature reports a number of different types of porous structures being created depending on pH of assembly and post-assembly treatments, these structures are to some degree kinetically trapped. Our group has recently demonstrated the use of acid or base soaked hydrogel stamps to create patterns of porosity in weak LbL systems.[148] One advantage of our stamping technique is the ability to deliver the acid or base post-assembly treatment solution in a slow, controlled manner. We observed both nanoscale

and microscale pores for a variety of pH assembly conditions and post-assembly acidic treatment for both PAH/PAA and LPEI/PAA, in contrast to published reports.[140-143] For almost all sets of conditions we observe small pores that become larger, more organized, and eventually collapse. In our observations, nanopores created by exposure to low pH solution eventually will grow to micropores. We believe that the usual technique of completely immersing a film all at once in the post-assembly treatment creates a rapid rate of transformation, "hiding" certain structures from being readily viewed.

Here we present morphological film changes to LPEI/PAA systems created by post-base treatment, something that to the best of our knowledge is not elsewhere reported in the literature. We compare these morphological changes that occur due to exposure to base with the well known acid exposure case. There are some differences in the morphologies created as well as the mechanism of formation for acid and base treatments. In addition, we have used techniques such as quartz crystal microbalance (QCM) and FTIR spectroscopy to analyze these changes in morphology. We have discovered that the creation of pores is accompanied by a selective, partial dissolution of the PEMs in all cases, something that was not previously known.

4.2 EXPERIMENTAL METHODS

4.2.1 Materials

The polyelectrolytes, poly(acrylic acid) (PAA, MW=50 000 g/mol) and linear poly(ethylene imine) (LPEI, MW=40 000 g/mol) were obtained from Polysciences. Poly(allylamine hydrochloride) (PAH, MW = 56 000 g/mol) was purchased from Sigma-

Aldrich. Hydrogen peroxide (H_2O_2), sulfuric acid (H_2SO_4), hydrochloric acid (HCl), and sodium hydroxide (NaOH) were purchased from VWR. All chemicals were used as received. Ultrapure de-ionized (DI) water purified (> 18 MΩ) with a Milli-Q system (Millipore Co.) was used in all aqueous solutions and rinsing procedures. Glass slides used as substrates were cleaned using piranha solution (30% H_2O_2 / 98% H_2SO_4, 3:7 v/v) at 85℃ for 40 min. Solutions of all polyelectrolytes were prepared with a concentration of 20 mM with respect to the repeat unit. The pH of each solution was adjusted using 0.1 and 1M HCl or NaOH solutions.

4.2.2 Build-up of Multilayers

The layer-by-layer deposition of polyelectrolytes was done by alternately dipping substrates in polyelectrolyte solutions using either a programmable dipping machine (HMS programmable slide stainer from Zeiss Inc.) or a Nano Strata Sequence VI at room temperature, as described elsewhere.[21] In brief, multilayer assembly takes place by sequential exposure of the substrate to alternately charged solutions, with rinse steps in between.

4.2.3 Porosity Transformation

The assembled polyelectrolyte multilayer films were exposed into a series of high or low pH solutions for various immersion times. After immersing into these solutions, the LbL films were rinsed with neutral water for 30s or less, blown dry with a N_2 stream, and then kept under ambient conditions prior to measurement.

4.2.4 Characterization

Attenuated total reflection Fourier transform infrared spectroscopy (ATR-FTIR) as well as transmission mode spectra of polyelectrolyte films were collected on a Bruker optics spectrophotometer Alpha FTIR. In the case of transmission spectra, films were assembled on an IR transparent substrate, ZnSe. Thickness measurements were performed with a profilometer (KLA - Tencor Instruments P-6) using a 2 µm radius stylus with 1 mg stylus force. Atomic force microscopy (AFM) images were taken with a Digital Instruments Nanoscope using the tapping mode (scan rate 1 Hz) under ambient conditions. Root-mean-square (rms) surface roughness of LbL films was averaged from 5 different AFM images with a size of 60 × 60 μm^2. Optical microscopy was performed with a Carl Zeiss optical microscope (model no. 430014-9902) equipped with an Axiocam imaging system (AXIO M2m). Mass changes of LbL films were measured with a Maxtek Research Quartz Crystal Microbalance (RQCM) (Inficon, East Syracuse, NY) with a frequency range of 3.8-6 MHz. For the QCM experiment, the 5 MHz quartz crystal was inserted into a holder and dipped alternately into the polycations (LPEI or PAH) and polyanion (PAA) solution. After assembling the LbL films, the crystal was blown with nitrogen gas and then immersed into various pH solution for various time periods (2, 5, 10, 20, 30 min, and 1 h), prior to being left on the microbalance to stabilize for 5 min at each. Porous surface morphology was captured with scanning electron microscopy (SEM, JEOL JSM-7500F). For imaging a cross-section in SEM, the post-assembly treated LbL films were immersed in liquid nitrogen.

4.3 RESULTS AND DISCUSSION

The creation of pores by exposing PAH/PAA and LPEI/PAA films to low pH solutions post-assembly has been previously reported,[140-143] caused by the charging of amine groups, neutralization of carboxylic acid groups, and breaking and reforming of ionic crosslinks. During this redistribution of crosslinks, the film swells and then contracts, expelling water unevenly throughout its structure, creating pores. However, the effect of exposure to high pH solutions post-assembly is not as well documented. The effect of high pH post-assembly treatments on the structure of pH sensitive, electrostatically bound multilayers was investigated here. The immersion into basic solution will be referred to as post-base treatment (short for post-assembly base treatment) as distinguished from post-acid treatment (post-assembly acid treatment) in acidic solutions.

4.3.1 Morphologies Transitions in PAH/PAA Films

Figure 4.1 shows AFM images of changes in morphology to 4(LPEI/PAA) LbL films created by post-base treatments. Surface morphology changes occur as a function of immersion time for post-base treatments above pH 10. Prior to the immersion of the 4(LPEI/PAA) films into the high pH solution, the film surfaces are relatively smooth and have a featureless surface morphology, with rms roughness of 1~2 nm, as measured by stylus profilometer (Figure 4.3 (b)). Post-base treatment induces porosity, accompanied by a variety of structural transitions. A range of resultant surface morphologies from different pH treatments at various immersion times are observed, including pores, pitting, and localized swelling. An initial immersion for 2 min in pH 10 solution was not

sufficient to create a porous transition or a clear morphological change. However, after 5 min, the surface became rough and pores appeared. Isolated mirco-scale porous structures with discrete, round pores (2 ~ 3 μm in diameter) penetrating the film surface form and the density of these pores becomes higher until 20 min of treatment time. After 30 min, the surface became rougher and the pores appear to have collapsed between 30 min and 1 h of treatment. Similar morphological transitions in the 4(LPEI/PAA) films were observed at pH 10.5 post-base treatment, but more quickly. In the case of exposure to higher pH solutions, post-base treatment also created porous structures. Of note, both at pH 11 post-base treatment for prolonged exposure time (≥ 30 min) and/or at higher pH solutions (pH ≥ 11.5) for shorter immersion, the thin films were nonporous and partially dissolved (see below).

Besides LPEI/PAA multilayers, morphological transitions in 9.5PAH/3.5PAA LbL films were investigated at low (pH 2 to 4) and high pH (11.5) post-assembly treatment by prolonging the immersion time to 1h (Figure 4.2). When treated with either low or high pH solution, however, AFM images of the top surface of 9.5PAH/3.5PAA showed a microporous structure (post-assembly treatment pH 2 and 11.5), with pore sizes ranging from 2 to 5 microns, and a honey-combed structure over large length scales with an immersion time (pH 2.5, 3, and 4).

The morphological changes described here can be explained as a pH-induced ionic-bond-breaking and reformation. The initial, internal cross-links present in the LbL films undergo changes during the structural reorganization of the film components upon exposure to new environments. The significant morphological transitions observed at

high pH solution are attributed to the ionization of PAA and the neutralization of the polyamine (LPEI or PAH), resulting in bond breaking and reforming.

Figure 4.3 (a) shows optical micrographs of 4(LPEI/PAA) films that had been treated with various post-base treatments for 2 min of exposure time. The fact that micro-scaled features are formed on the film surfaces is observed, and this is unique to high pH treatments. The root-mean-square (rms) surface roughness of films are shown in figure 4.3 (b), on the left are values for different pH treatments all at 2 minutes and on the right are values for films treated at pH 10.5 for varying times. The surface roughness values reported were obtained from AFM analysis of at least 5 separate measurements on each film. The rms surface roughness of 4(LPEI/PAA) films post-assembly treated at pH 10 for 2 min or less immersion time was almost the same as that of untreated thin films, showing a featureless and uniformly smooth surface with a surface roughness of 2 - 3 nm. In contrast, as soon as the treatment pH increased to 10.5 or higher, the surface roughness after only 2 min of treatment are as high as 150 nm. Roughness measurements taken at various immersion times for pH 10.5 post-base treatment range from 50 to 200 nm, indicating that post-base treatment allows for a great deal of tailoring of the surface morphology. The roughness of 9.5PAH/3.5PAA films after exposure to pH 11.5 solution shows similar evolution (Figure 4.4).

The morphology of 4(LPEI/PAA) films treated in high pH solution was further examined with SEM to look at cross-sectional and top down views of the films. Figure 4.5 shows SEM images of 4(LPEI/PAA) films that were treated for 5 min in various high pH solutions, both top down views and cross sectional views. In addition, figure 4.5

shows a few representative cross-sectional views of 4(LPEI/PAA) treated at low pH. The top-view SEM images reveal that pores with 1µm diameters were observed on the surface of thin films treated at pH 10 and that the pore size increased to 2 – 3 microns with a pH value of 10 to 11.5. At pH 12 post-base treatment, nearly the entire film delaminated and dissolved. Cross-sectional SEM micrographs of a 4(LPEI/PAA) film show a porous structure, with pore sizes ranging from hundreds of nanometers to 2 micrometers in size, throughout the entire film, but not interconnected. This is in contrast to the cross-sectional images of acid treated LPEI/PAA films, which show an interconnected porous morphology.

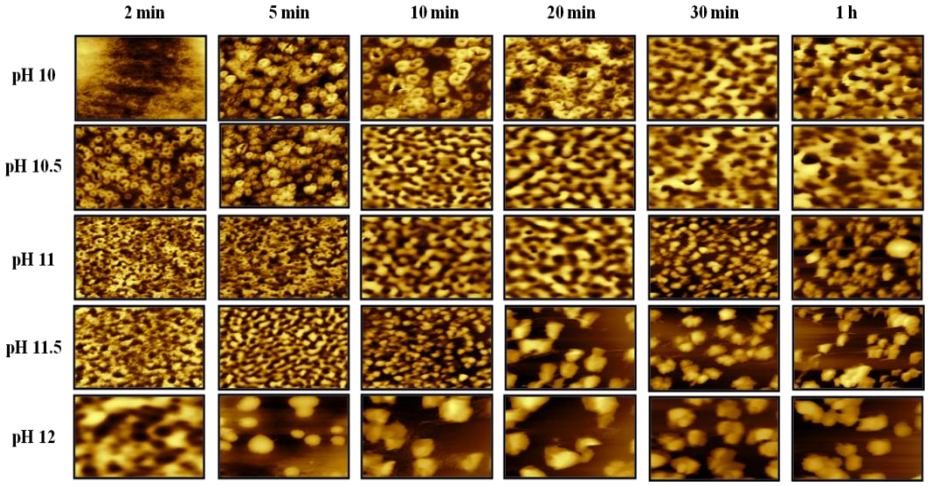

Figure 4.1: Representative AFM images of a 4(LPEI/PAA) LbL films treated at varying pH conditions as a function of immersion time. All images are in height mode with dimensions of 60 X 60 μm^2. Generally speaking, larger features are formed at higher pH values and for longer treatment times.

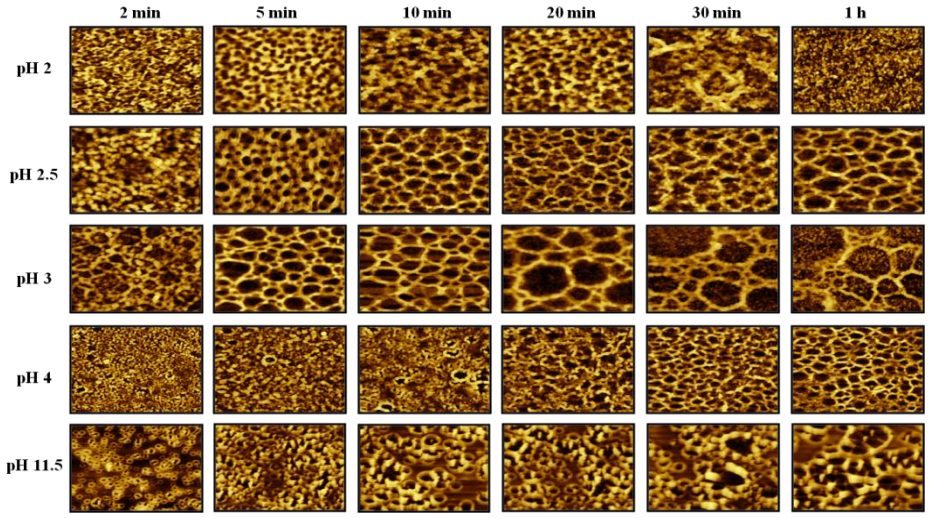

Figure 4.2: AFM images of 9.5(PAH/PAA)$_{12}$ LbL films post-assebly treated at different immersion time under various pH values. All images are in height mode with dimensions of 120 X 120 μm^2.

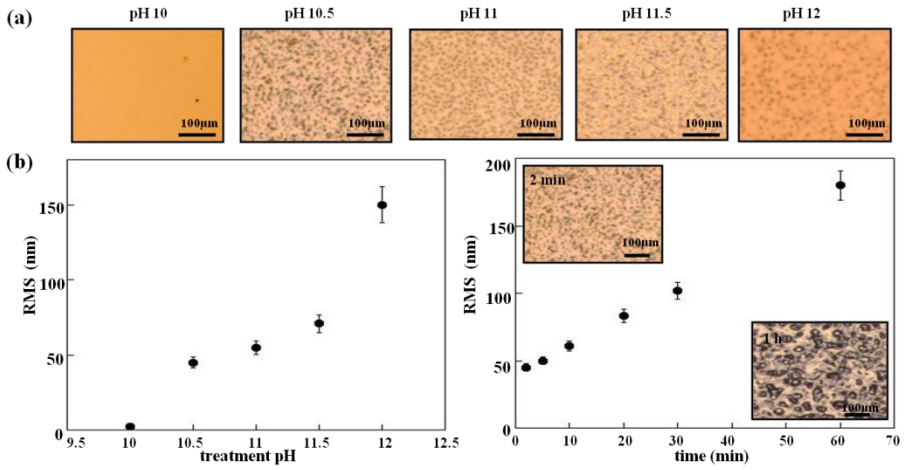

Figure 4.3: Optical microscopy images (a) of 4(LPEI/PAA) prepared at various post-base treatment and (b) rms surface roughness of the film with varying pH at 2 min immersion time (left) and different exposure time (right) at pH 10.5 post-base treatment. Inserted figure is the optical microscopy of pH 10.5 exposure with 2 min (top) and 1h (bottom).

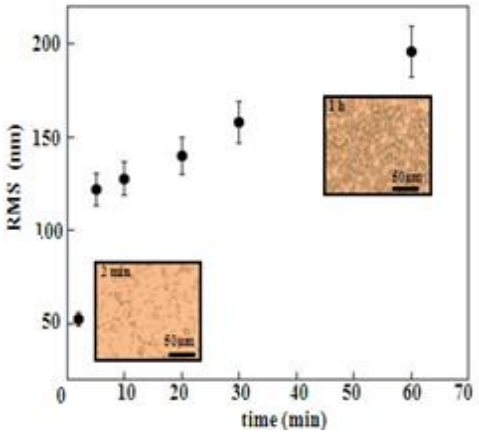

Figure 4.4: rms surface roughness of the 9.5PAH/3.5PAA film with time at pH 11.5 post-base assembly treatment. Inserted figure is the optical microscopy of pH 11.5 exposure with 2 min (bottom left) and 1h (top right).

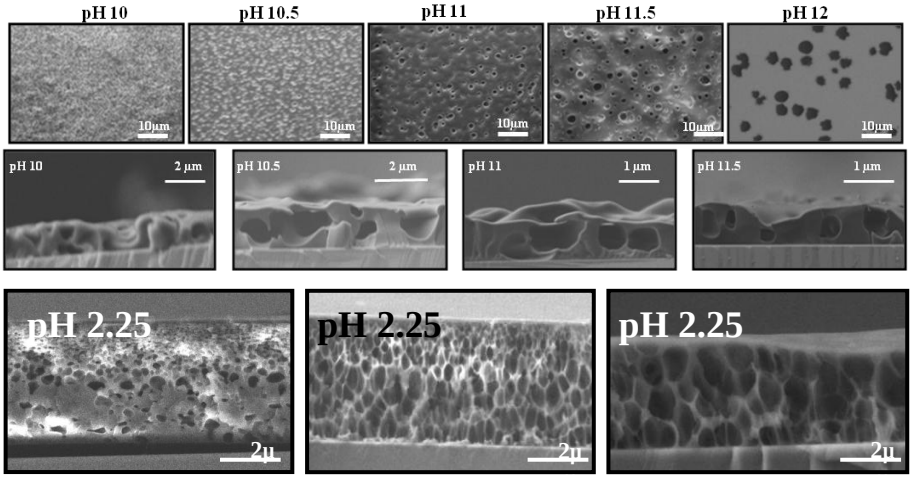

Figure 4.5: SEM top-view (top row) and cross-sectional (middle row) images of 4(LPEI/PAA) LbL films treated at different pH values for 5 min of immersion time. The bottom row shows cross sectional images of LPEI/PAA treated at pH = 2.25 of different time (10 min (left), 20 min (middle), and 30 min (right)). The difference in morphologies created by acidic and basic treatments can be seen.

4.3.2 Ionization within LbL Films under Post-Assembly Treatment

FTIR was used to study the ionization of polyelectrolytes and charge density variation. For FTIR data of 4(LPEI/PAA) films, two peaks at at1710 and 1550 cm^{-1}, as shown in Figure 4.6 (a) can be assigned to the C=O stretching of COOH groups and the symmetric stretching of ionized COO^- of PAA polyelectrolytes, respectively.[149,150] As treatment pH increases, the peak intensity of neutral carboxylic acid groups decreases in the spectra of LbL films. In a complementary fashion, with increasing treatment pH, the peak intensity at 1550 cm^{-1} increases, corresponding to an increase in the amount of ionized acid groups. Assuming that the extinction coefficient for both bands are about the same,[151-15] the degree of ionization of PAA within 4(LPEI/PAA) films under post-assembly treatment was calculated by using the ratio of the peak intensity of $v(COO^-)$ to the intensity sum of $v(COO^-)$ and v(COOH).[72]

Figure 4.6 (b) shows the fraction of charged carboxylic acid groups according to pH treatment. From pH 4 to pH 10 the fraction of charged carboxylic acid groups stays roughly the same, about 62 %, which was almost the same as that of untreated 4(LPEI/PAA) films. The environment of the multilayer is able to act as a buffer over this pH range. When exposed to solutions at $pH \leq 4$, the amount of charged carboxylic acid groups drops and for $pH \geq 10$ the proportion increases. As reported by others,[154-157] the degree of ionization, and pKa, of PAA in solution tends to be higher than the value measured in the LbL films. The pKa of PAA in solution is reported in the range of 5.5 - 6.5.[94] Electrostatic effects are mainly responsible for this change in pKa values as carboxylic acid groups are fairly labile and sensitive to their environment.[158] In this

study, the pKa of PAA in 4(LPEI/PAA) was estimated to be between 2.3 and 2.5, agreeing with literature reports that have PAA's pKa = 2.2 in a multilayer with PAH and about 3 in a multilayer with poly(diallyldimethyl ammonium chloride).[94] The pH ranges over which there are observed changes in the fraction of charged carboxylic acid coincide with observations of morphological change. This reinforces the idea that changes in ionic crosslink density after post-assembly treatment are responsible for changes in morphology.

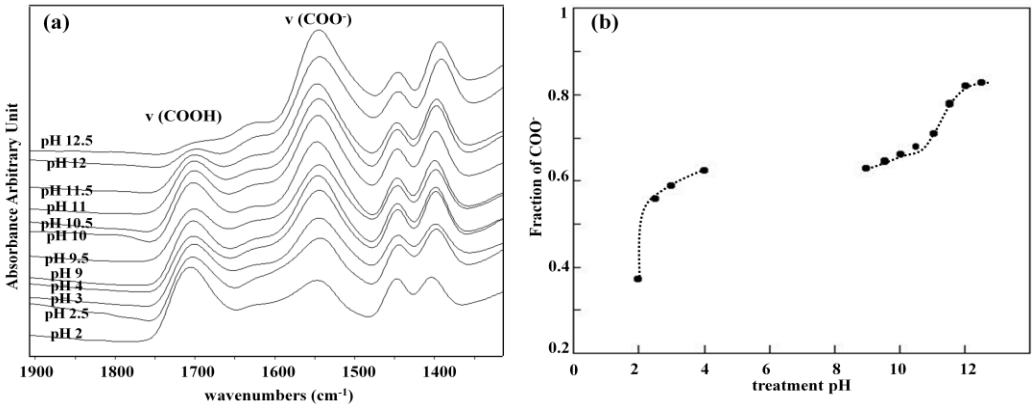

Figure 4.6: ATR-FTIR spectra (a) of LPEI/PAA films treated at varying post-assembly treatment pH and the degree of charged carboxylic acid groups (b).

4.3.3 QCM and FT-IR Analysis after Post-Assembly Treatment

There are some reports in which the partial release or deconstruction of the PEMs in response to pH variations is identified, but no quantitative measurements of this phenomenon have been reported. Kharlampieva, *et al*,[158] demonstrate selective release of polyelectrolytes from weak multilayers with an increase of pH, but not with a morphological change or in response to low pH. To gain insight into the morphological

transformation process, both QCM measurements and FTIR spectroscopy were employed to analyze the partial loss of polyelectrolyte in the 4(LPEI/PAA) and 9.5PAH/PAA LbL films at low and high pH values.

Figure 4.7 shows QCM data for LPEI/PAA films exposed to both acidic (a) and basic (b) post-assembly treatments as a function of immersion time. This was not an in situ experiment, but rather the crystal was removed from the instrument, exposed to whichever solution required, and then returned to the instrument. This explains the step-like nature of the data. The mass change of PAH/PAA films upon the immersion into low or high pH solution is shown in Figure 4.8. The QCM experiment after the low or high pH solution treatment showed a small initial increase in mass due to the uptake of water, followed by the stepwise, significant decrease in mass corresponding to each immersion event. In some cases the pH treatment did not produce an increase in mass at 2 min of immersion time, as the film was already swollen. Upon exposure to a wide range of pH conditions ($2 \leq pH \leq 11$), after some time the mass decrease due to the release of polyelectrolytes levels off, reaching a plateau. In more extreme cases, however, when the post-assembly treatment is at a pH of 11.5 or higher, the multilayers were dissolved or removed entirely from the substrate. This is in good agreement with our finding that the thin film thickness at these pH values was almost 0 nm using profilometer, as shown in Figure 4.9.

From these experiments we can see that LPEI/PAA and PAH/PAA multilayers lose mass during the course of post-assembly treatments. This means that the morphological rearrangements are not only a result of expulsion of water from the

increasingly cross-linked films, but also due to their partial dissolution. Exposure to high pH has the effect of deprotonating all acid and amine functional groups. This will disrupt some of the pre-existing ionic bonds, and also create an excess of charge by changing the neutral carboxylic acid groups to charged COO^- groups. The excess negative charge will cause the PAA chains to extend themselves as the charges self-repel. For low pH the opposite is true; the excess charge is positive charge of the polyamine.

QCM shows that mass is released from the films, and by taking the soaking solution, drying it, and taking FTIR spectrum of the resultant film it is possible to observe the chemical nature of the material released from the LbL films. Figure 4.10 shows the FTIR spectra of the released material from the 4(LPEI/PAA) thin films after various post-assembly pH treatments (at 1 h). In the acidic regime at pH 2 and 2.5, the COOH acid peak at 1718 cm^{-1} was detected, indicating that PAA was released from the LbL films in the non-ionized form during post-acid treatment. At post-base treatment of pH $\geq$ 10.5, COO^- peaks are observed. Characteristic peaks for LPEI are expected at 1605 and 1450 cm^{-1},[94] but were not observed in either the acid treatment or the base treatment case. The spectrum observed correspond to PAA at different pH values. From this it can be concluded that either that LPEI was not released during the observed immersion times or that it was released in quantities much less than PAA. Even in the cases of total film dissolution the PAA chains seem to be released first. It is difficult to make an absolute statement regarding this as both characteristic LPEI peaks overlap with PAA peaks. The FTIR spectra of released polyelectrolytes from the PAH/PAA thin films under post-assembly treatment is also shown in the Figure 4.11. In the case of PAH/PAA

multilayers the amine peaks are clearly seen (~1605 cm^{-1}), and it can be concluded that both polyelectrolytes are observed in the released material.

As the porous transition is reported in the literature to be reversible for some specific systems,[159] we also examined the reversibility of both LPEI/PAA and PAH/PAA thin films under post-base treatment. The mass change was investigated by alternatively immersing pre-assembled films into low or high pH solution and then exposing the resultant porous films to DI water (pH ~ 5.5) in between drying with compressed nitrogen gas. Alternating immersion steps of post-base treatment (pH 10.5 solution for 4(LPEI/PAA) and pH 11.5 solution for 9.5PAH/3.5PAA) and DI water treatment showed that the post-base transitions are not reversible and showed the film did not revert back to its untreated state.

The mass change of both LPEI/PAA and PAH/PAA thin films exposed to either low pH or high pH solution immersion and then DI water exposure were analyzed as shown in Figure 4.12 and 4.13. These results from the QCM analysis indicated that both thin films went through the increase and decrease of the mass according to the immersion into low pH solution for 1 min and subsequently DI water (pH ~ 5.5) for 15s, respectively. Mass increases during exposure to DI water can clearly not be due to uptake of polyelectrolyte, and we explain this by swelling of the film with water and a change in film stiffness which can look like a change in mass during QCM experiments. However, in the case of alternating immersion steps between high pH solution treatment and D.I water exposure, there was only a continuous decrease. These differences show clearly that post-acid and post-base treatments result in different changes within the

PEM films. When these porous thin films are immersed into deionized water (pH ~ 5.5), the ionic cross-links cleaved by previous pH treatment can be reformed as carboxylate-based ionic linkages are regenerated. This results in the rejection of water from the highly swollen thin films formed by osmotic forces and charge repulsion under post-acid treatment. When porosity created by exposure to basic pH values is re-exposed to DI water the original film structures cannot be reformed. Possible explanations include that the moderate pH of DI water is not enough of a change to regenerate previous ionic links or break newly formed ones, and that lost material precludes the reorganization of the film to its initial state.

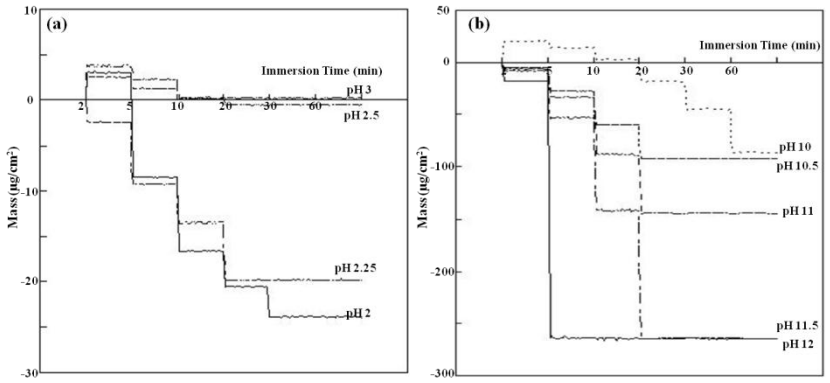

Figure 4.7: QCM data for (a) post-acid treatment and (b) post-base treatment of LPEI/PAA multilayers. Films assembled onto the quartz crystal substrate were immersed in either acid or base solutions for certain time intervals (2 min, 5 min, and 10 min) and then returned to the QCM instrument for the measurement. That the experiment was not performed *in situ* explains the step-like shape of the data.

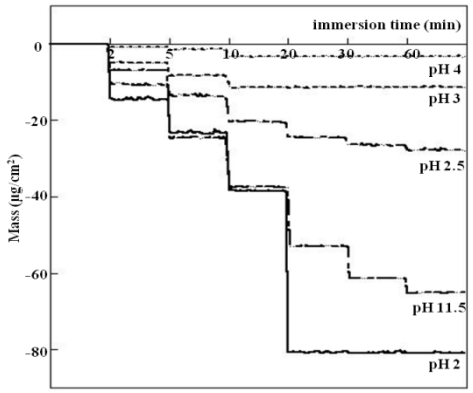

Figure 4.8: QCM data of 9.5PAH/PAA at various pH conditions as a function of immersion time.

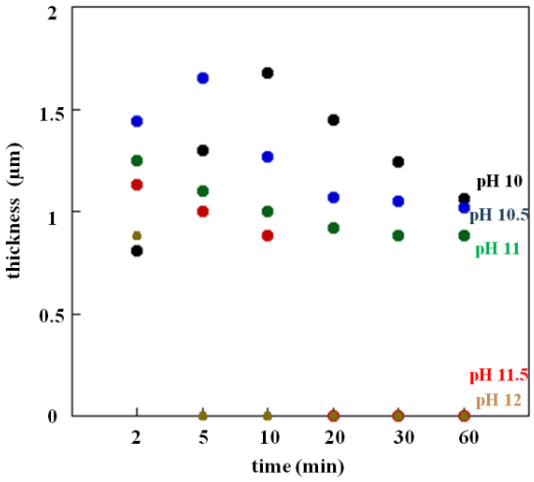

Figure 4.9: Thickness change of 4(LPLEI/PAA)$_{20}$ LbL films at different pH post-base treatments as a function of immersion time. Untreated multilayer is 800nm thick.

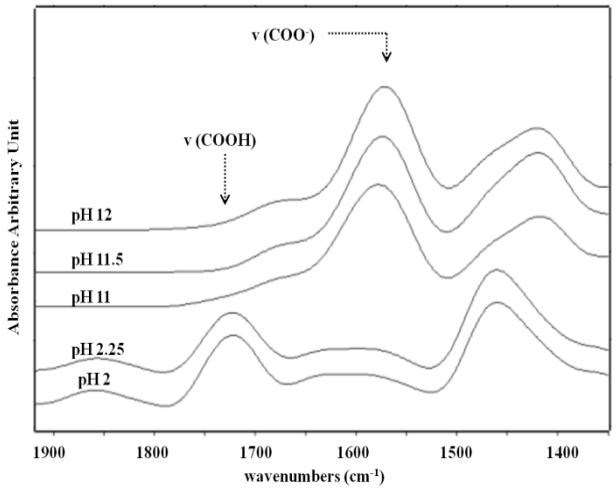

Figure 4.10: FTIR of the material released from LPEI/PAA films during post-assembly treatment over one hour. Peaks for neutralized and charged carboxylic acid groups can be seen depending on the pH. These spectra correspond to that of PAA, indicating that PAA leaves first, or leaves in a much greater proportion than LPEI does over the observation time.

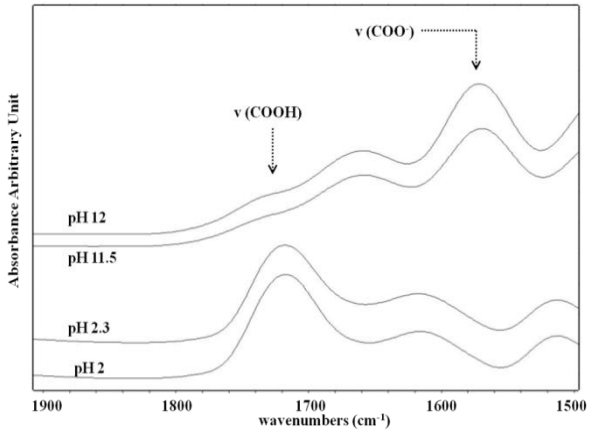

Figure 4.11: FTIR spectra of the materials released from PAH/PAA films during post-assembly treatment.

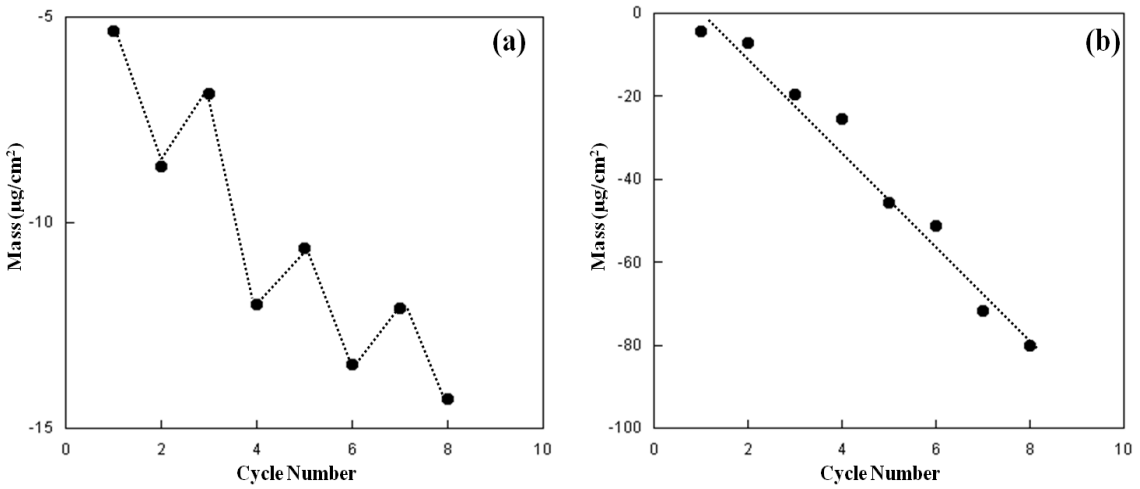

Figure 4.12: Mass change of 4(LPEI/PAA); Data for cycles 1, 3, 5, and 7 were obtained from the film that had immersed into pH 2.25 solution (a) and pH 10.5 solution (b) for 1min, respectively, followed by drying with nitrogen gas. The data for cycles 2, 4, 6, and 8 of both (a) and (b) were obtained by exposing the film of cycles 1, 3, 5, and 7 into D.I water (pH ~ 5.5) for 20s.

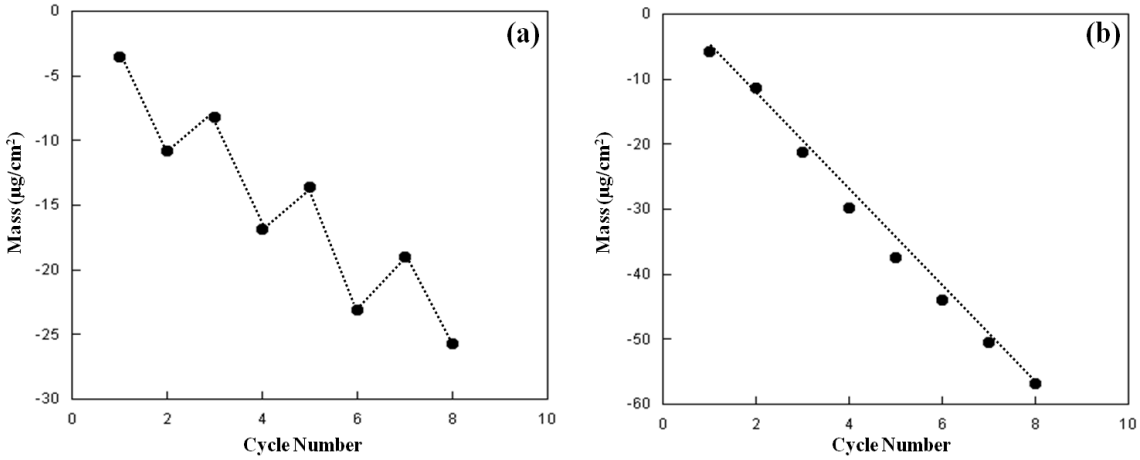

Figure 4.13: Mass change of 9.5PAH/3.5PAA; Data for cycles 1, 3, 5, and 7 were obtained from the film that had immersed into pH 2.0 solution (a) and pH 11.5 solution (b) for 1min, respectively, followed by drying with nitrogen gas. The data for cycles 2, 4, 6, and 8 of both (a) and (b) were obtained by exposing the film of cycles 1, 3, 5, and 7 into D.I water (pH ~ 5.5) for 20s.

4.3.4 Porosity within LbL Films

With the development of porosity in the films during post-base treatment, the overall pore volume in the film is closely related to the treatment pH. Pore volume was calculated by measuring the film thickness before and after pH treatment, as reported previously. However, previous calculations of pore volume assumed conservation of mass. The results here demonstrate that partial (or even complete) dissolution of film occurs during post-assembly treatments (Figure 4.14), so this assumption is not accurate. For a more accurate calculation of pore volume considering the lost mass, the fraction of decreased mass was first calculated by dividing the weight of the final structure after the exposure to high pH solution by the total weight of 4(LPEI/PAA) films before post-assembly treatment. The pore volume equation was defined as follows:

$$\text{Volume fraction} = \left(\frac{h-ho}{h}\right) \text{ X } (1 + \text{fraction of dcreased mass}) \text{ X } 100\%,$$

where h_0 and h are the film thickness before and after the post-assembly treatment, respectively. Upon exposure to pH 10 post-base treatment, 4(LPEI/PAA) films were observed to increase in thickness by nearly 100 %. Using the above equation, this corresponds to about 52% pore volume in the material. The greatest change in pore volume (56%) occurred when films were treated at pH 10.5. PEMs exposed to pH 12 solution exhibited complete delamination of the film from the substrate and a calculated pore volume of 0%.

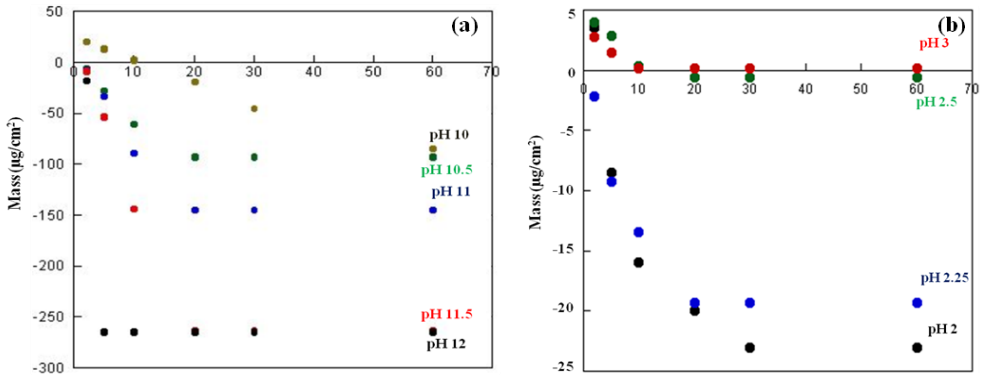

Figure 4.14. Amount of mass loss at different (a) high pH treatments with time and (b) low pH treatments. The x axis is number of minutes of acid/base treatment. It can be seen that although mass loss occurs in both cases, a much greater deal of polymer mass is lost in the high pH case. In fact, the highest pH treatments, 11.5 and 12, result in complete film delamination. However, even in the cases where a stable film is reached, larger absolute changes in mass occur under high pH treatment.

4.3.5 Mechanism of the Morphology Transition for Post-Base Treatment

On the basis of the above data, we propose a morphological transformation that includes the swelling of the thin films, the creation of porosity, and finally deconstruction of the LbL films under post-base treatment, closely related with releasing polyelectrolytes from the PEMs. When the as-assembled 4(LPEI/PAA) films are treated at high pH (≥ 10), the films undergoes a dramatic swelling with no pore formation due to a combination of water uptake and increased charge repulsion. Since both polyelectrolytes are only partially ionized in this system, LPEI (pKa ~ 6) and PAA (pKa ~ 5.5 – 6.5) chains both adsorb in coiled, loop-rich conformations, yielding thick layers. Therefore, when the charge densities of the chains change it is possible for the chain end-to-end distances to change greatly.

The expulsion of water due to the formation of new ionic cross-links has also been thought to be a driving force for the molecular rearrangements. Of particular interest is the finding reported here that during this step both neutral LPEI and ionized PAA components of the multilayer film appear to be released gradually, as revealed from QCM and FTIR analysis. When the LbL film is immersed in basic solution for prolonged times, the released amount of both polyelectrolytes increases with time and the pore structure of the thin film continually evolves, eventually collapsing.

4.4 CONCLUSIONS

Reported here is an investigation into the origin and mechanism of the porous transition in LPEI/PAA and PAH/PAA PEMs under both post-acid and post-base treatments. Although porous morphologies are seen in both acidic and basic cases, there are differences between the two. Basic treatment conditions create non-interconnected pores within the materials, while acidic treatment creates interconnected structures. In both cases the surface roughness of the PEMs can be hundreds of nanometers. For both cases, under certain pH conditions a single polyion is released from the film structure, and under harsher conditions both polyions are released. However basic conditions release a greater portion of the PE chains. As pH is increased above 11 films will irreversibly dissolve. Partial dissolution happens in the low pH case, but there is not total dissolution for as low as pH 2 treatment.

That the porous transformation in electrostatically bound multilayers is accompanied by a mass loss has not been previously reported. This new information

about the process of pore formation in polyelectrolyte based materials will help design porous materials for specific applications (such as cell scaffolds or filtration membranes). Varying treatment pH value and immersion time, especially with our hydrogel stamping technique that gives a very slow rate of delivery of acid or base solution, results in a number of different morphological transformations, ranging from the creation of pores to collapsed structures and finally, partially or completely dissolved films under high pH solution. Results obtained from QCM and FTIR suggest that a selective or partial dissolution of polyelectrolytes occurs as a function of pH treatment or exposure time. For extreme changes in pH or very long immersion times both polyelectrolytes are released from the PEM. We are able to provide new physical insight into the morphological changes as well as create greater control over pore formation than previously reported.

CHAPTER V

ELECTRIC FIELD-INDUCED MORPHOLOGICAL TRANSITIONS IN POLYELECTROLYTE MULTILAYERS

5.1 INTRODUCTION

There are a number of applications for porous polymer films and coatings including cell scaffolds,[160-162] drug delivery materials,[163-165] filtration media,[166,167] separators in electrochemical devices,[168] and antireflection (AR) coatings.[169-172] In each case the required pore sizes and design are somewhat different. For example, cell scaffold materials need pores that are tens of microns large whereas AR coatings require small pores that will not scatter light. The ability to tune in pore density, size, or even their shape or orientation could represent a breakthrough for the fabrication of materials for any of the aforementioned applications.

Polyelectrolyte multilayers (PEMs) assembled using the layer-by-layer (LbL) technique [70] are versatile films and coatings based on the complexation of oppositely charged polyelectrolytes (PEs), and they have been proposed for use in all of the aforementioned applications. They are typically fabricated by the sequential adsorption of oppositely charged polyelectrolytes from solution onto a charged substrate. The charged functional groups of each polymer chain associates with oppositely charged groups on another chain, building up the assembly. It has been demonstrated that porous structures can be spontaneously formed from weak polyelectrolyte containing PEMs.[81]

These films are built up at moderate pH so that the weak polyelectrolytes within the film are partially charged.

When that film is exposed to a sharp change in pH, the weak polyelectrolytes' functional groups become charged or charge-neutralized, ion pairs are broken and reformed, and pores are formed. During this rearrangement of the polymer chains, the thin film swells and then contracts, causing it to reject water unevenly during the contraction, which is the source of the pore formation.[148] This process is sometimes discussed in terms of a phase separation. Stable LbL films are generally formed under conditions where the corresponding polyelectrolyte complex would result in a stable solid phase. Changing the charge densities of the polyelectrolyte changes may change this balance, creating a reorganization of the film. There is a partial dissolution of the film during this process potentially as a result of this phase separation. The resultant structure can be either a nano- or microporous structure, depending on both film assembly conditions and the pH to which the film was exposed. Porosity transitions in weak PE films, including hydrogen bonded systems, induced by immersion into low-pH[123, 144] or high-pH solution[109-111], referred to as "post-assembly treatment," are well reported in the literature. There have been many studies both about their fundamental nature as well as their potential applications.

Recently, our group reported a method of using stamps to deliver acid or base to a polyelectrolyte multilayer in a more controlled manner, which can result in greater control over the porous structure. In this work the weak polyelectrolytes poly(acrylic acid) (PAA) and linear poly(ethylene imine) (LPEI) were used. For these

polyelectrolytes the charge density along the chain varies as a function of pH. In the case of PAA and LPEI the charge density follows an inverse relationship for the pair, shown in Figure 5.1. Our previous work also demonstrated that the change in morphology is accompanied by a loss in mass. Although the use of stamps brings about localized control, a greater degree of temporal control may be desired, especially in a manner that could be applied to larger areas. An electric field, or the application of a controlled potential, is an extremely promising means to control the porous transition via water electrolysis, which produces a sharp change in pH, and often used to manipulate pH for responsive polyelectrolyte based materials.[173] The application and amplitude of the field can be controlled precisely in order to command precision over the transition and the resulting morphology.

Here, we demonstrate a new platform for the controlled creation of porous structures within LbL films via electric fields. Only a few methods exist to create these porous structures in a controlled way, and to our knowledge there are no reports using this method. Electric fields have been used to influence the assembly of polyelectrolyte multilayers but not to affect post-assembly change in this manner.[174] We have applied an external electric field to the multilayers over a variety of time periods. The application of an electrical potential in an aqueous solution creates protons at the electrode-LbL film interface. The protons generated locally at the electrode can be used to create the same change in film morphology from continuous to porous within the LbL films that are reported elsewhere from exposure to acidic solutions. As it is possible to carefully

control the electrical field applied, it is then possible to control the formation of the porosity as well.

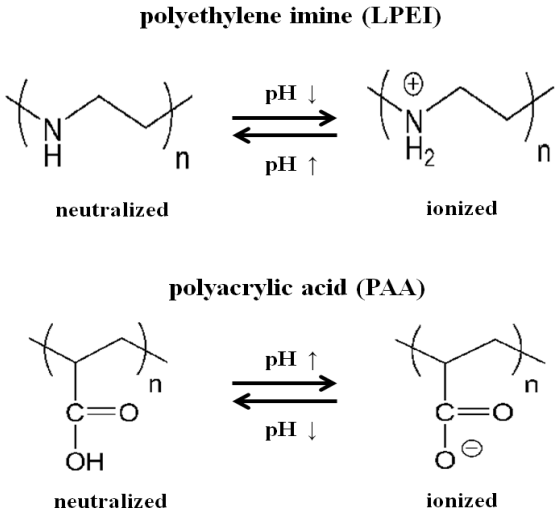

Figure 5.1: Molecular structures of polyelectrolytes (LPEI and PAA) used in this study.

5.2 EXPERIMENTAL METHODS

5.2.1 Materials

The molecular structures of the polyelectrolytes used in this study are described in Fig. 5.1. Poly(acrylic acid) (PAA, MW=50 000 g/mol, 25 % aqueous solution) and linear poly(ethylene imine) (LPEI, MW=40 000 g/mol) were obtained from Polysciences. Methylene blue chloride was purchased from EMD. All products were used as received without further purification. Ultra-pure water (Milli-Q, Millipore Co.) with a specific resistance greater than 18 MΩ was used. All of the aqueous solutions were adjusted to the appropriate pH using 0.1 and 1 M HCl or NaOH solutions,

respectively, as needed prior to multilayer assembly. Indium tin oxide-coated glass slides (ITO, Delta's Technologies) were used as substrates for the buildup of multilayers. Oxygen plasma treatment was performed to render the surface of ITO negatively charged.

5.2.2 Polyelectrolyte Multilayer Formation

The layer-by-layer deposition of LPEI and PAA was achieved by alternately dipping substrates in polyelectrolyte solutions using a Nano Strata Sequence VI at room temperature. Each polyelectrolyte was used without further purification to create polymer solutions of 0.02 M concentration based on the repeat-unit molecular weight in Milli-Q water. Plasma-treated-ITO substrates were first immersed in the polycation (LPEI) for 15 min and rinsed in three fresh water baths for 2, 1, and 1 min. The samples were then immersed in the polyanion (PAA) for 15min, followed again by three rinsing steps. This completed the deposition of one bilayer, which is defined as an adsorption step of polycation followed by an adsorption step of polyanion. This process was cycled until the desired number of bilayers was deposited. Unless otherwise stated, the outermost layer of the multilayers used in this experiment was the polyanion (PAA). For the remainder of this paper polyelectrolyte multilayers (PEMs) will be referred to as $X(LPEI/PAA)_Y$, where X is the pH value of the polycation and polyanion baths, and Y is the number of bilayers assembled. For example, $4(LPEI/PAA)_{20}$ refers to a sample constructed from 20 bilayers of LPEI and PAA, where the pH of both baths was adjusted to 4. Polyelectrolyte multilayers were dried using nitrogen gas for 2 min and further dried in ambient air for several hours before the measurements.

5.2.3 Electrical Field-Induced Post-Assembly Treatment

PEMs assembled on ITO substrates were used as the working electrode in a three electrode electrochemical cell. Ag/AgCl and Pt wire electrodes were used as reference and counter electrodes, respectively. The cell contained water pH-adjusted to 3.2; accordingly, the ionic strength of the Cl^- ion in pH 3.2 water was 0.59 mmol. A voltage of 4.0 V was applied for various time periods (10, 20, 30 min, and 1h), using a Solartron SI 1287 potentiostatat room temperature.

5.2.4 Release of Methylene Blue (MB) from LPEI/PAA Films by Applying Electric Potential

Some LbL samples were exposed to MB solutions prior to treatment with electrical potential. LbL films assembled on ITO were immersed for 1 h into a 0.05 M MB solution containing 0.1 M NaCl at pH 7 to load MB molecules into the multilayers. Then, the loaded samples were rinsed in pH 3.2 water several times to remove physically adsorbed excess MB molecules. The MB-loaded $4(LPEI/PAA)_{20}$ LbL films (1.4 cm^2 in area) were then exposed to 30 mL of pH 3.2 water. An electrical potential of 4.0 V was applied for varying times, and the amount of released MB molecules into the pH 3.2 water was measured using UV-vis absorption spectra.

5.2.5 Characterization

Atomic force microscopy (AFM) was conducted by using a Digital Instruments Nanoscope in tapping mode (scan rate 1 Hz) under ambient conditions. The thickness of the multilayer was analyzed before and after treatment with electric field using a profilometer (KLA – Tencor Instruments P-6) with 2 μm radius stylus and 1 mg stylus

force. Each sample was examined ten times at different locations. Scanning electron microscopy (SEM) images were obtained on a JEOL JSM-7500F field emission scanning electron microscope. Attenuated total reflection Fourier transform infrared spectroscopy (ATR-FTIR) spectra of polyelectrolyte films were collected on a Bruker Optics Alpha FT-IR spectrometer. UV-vis spectra were recorded on a Hitachi U-4100 UV-Vis-NIR spectrometer.

5.3 RESULTS AND DISCUSSION

5.3.1 Time Evolution of Morphological Transitions

First, 4(LPEI/PAA)$_{20}$ LbL films were immersed into pH 3.2 water for 1h without any applied potential. AFM images indicated that the film treated at pH 3.2 solution had a featureless and continuous surface morphology similar to the untreated films, as shown Figure 5.2. The RMS (root-mean-square) surface roughness of both films was also similar (1.5 ~ 2.0 nm), indicating that this pH condition has little effect on the surface morphology. However, below this pH value (pH $\leq$ 3.0), 4(LPEI/PAA)$_{20}$ LbL films underwent transitions in porosity, in agreement with previously reported results.

Next, we applied an electrical potential of 4.0 V vs. (Ag/AgCl) to multilayer-coated ITO substrates in pH 3.2 water. Figures 5.3 and 4 show top-view and cross-sectional SEM images of 4(LPEI/PAA)$_{20}$ LbL films treated under electric fields for various times. The films undergo different stages of morphological evolution with characteristically different pore sizes and pore distribution with increasing time. Prior to applying the electric potential, the thin films were relatively smooth and had a featureless morphology

at the surface and in the interior. However, after 10 min of treatment, pores about 100-200 nm in size were created near the multilayer-ITO interface, while the film's surface remained smooth and intact. With increasing treatment time, the films became increasingly more opaque to the eye, while those films treated for less than 10 min were optically transparent as shown in Fig. 5.5. After 20 min of treatment, SEM images (Figures 5.3 (c) and 5.4 (c)) show a nanoporous surface and asymmetrical morphology in the interior of the film. Cross-sectional SEM images show a dense, nanoporous top layer with pores ~ 100 nm in size and a microporous interior region at the film-ITO interface. At longer times (30 min), pore size and pore density increases, and the asymmetric structure remains. At 1 h of treatment the average pore size increases to several microns in diameter throughout the film, and the asymmetric structure vanishes.

The morphologies formed within the multilayers can be explained by considering the electrolysis of water, changes in local pH, and the breaking and reformation of ion-pair crosslinks. The LbL films in this experiment were assembled using weakly charged polyelectrolytes of LPEI and PAA both at pH 4, which is a pH at which both polymers are only partially charged. Both LPEI (pKa~ 6) and PAA (pKa ~ 5.5 – 6.5) [94] chains adsorb in loop-rich conformations with an ion-paired internal structure at this pH condition. However, when an anodic electric potential (4.0 V vs. Ag/AgCl) is applied, water electrolysis occurs, and the local pH at the film-ITO interface becomes markedly acidic by the following reaction:[175-177]

$$2H_2O \rightarrow 4H^+ + O_2 + 4e^- \qquad (1)$$

Therefore, the local pH at the film-ITO interface is much lower than that of the solution (pH = 3.2). Considering that LPEI/PAA films undergo post-assembly porous transitions at pH values less than 3.0, we can conclude that the local pH is less than 3.0. Thus, some of the ionic linkages between the NH_3^+ groups of LPEI layers and COO^- of PAA layers are dissociated and rearrangements of both LPEI and PAA chains lead to porosity transitions induced by the application of an electric field.

An interesting point during the evolution of the morphological structure is the creation of an asymmetric structure with smaller pores near the free surface and larger pores near the electrode/multilayer interface. This structure is similar to those reported elsewhere both by simply immersing a polyelectrolyte multilayer into an acidic solution and with stamping a film to slowly release acidic solution into it. At first thought, an explanation for the formation of this structure may be the diffusion of protons from the electrode through the film. Clearly, the process is diffusion mediated. In the electric field case pores are first seen at the electrode/film interface, later forming in portions of the film further away from that interface. In our previous work with stamping, pores are first observed near the interface of the film and the stamp, away from the substrate. We also observe in both cases that smaller pores grow to be larger, possibly matching the formation of the asymmetric structure. However, in all three cases the same asymmetric structure is observed, larger pores at the substrate, smaller ones at the free surface, regardless of the location of the source of protons. In this work the protons are being delivered from the substrate, in the other two cases the protons are delivered from the free surface, and yet the same ultimate structure is observed.

We have considered two other possible explanations for this observation. One possibility is that the substrate somehow confines the diffusion of chains within the film and their reorganization, causing smaller pores to coalesce with one another to form larger pores. We have shown previously that loss of polyelectrolyte chains accompanies this morphology transformation,[111] and perhaps this is frustrated near the substrate, causing different structures to be formed.

Another possibility is that the structure of the film is different away from the substrate and near the top, free surface.[178] It is generally observed that there are differences in the first few deposition steps when compared to later steps. Also, the LPEI/PAA system is one that grows exponentially;[179, 180] that is, each bilayer does not have the same thickness, but during later deposit steps much more material is deposited than during earlier steps. This is attributed at least in part to the ability of one or the other of the polyelectrolytes to diffuse through the growing film during deposition. It is therefore likely the case that the structure of the film is not uniform throughout. It is known both that polyelectrolyte charge density is extremely susceptible to the surrounding environment, and that different charge densities within weak polyelectrolyte films can result in different types of pores even with the same post-assembly treatment.[181] We hypothesize that either the non-uniform manner of film growth for this system or some kind of confinement of the chain rearrangement and diffusion near the substrate results in the asymmetric film structure regardless of the source of protons, although the exact mechanism is not known.

Figure 5.6 shows the film's thickness and corresponding swelling ratio for LbL films treated by electrical potential as a function of time. The thickness of each film was measured before (T_{before}) and after (T_{after}) the application of electrical potential and the swelling percentage was calculated as $100*(T_{after}-T_{before}) / T_{before}$. [124] After 1 h of treatment, the film thickness increased by nearly five times its original thickness, and the swelling percentage was calculated to be 400%, corroborating our prior SEM observations. As the charge density and therefore crosslink density in the film changes with application of the electric field the osmotic pressure in the film and therefore its swelling will change both because of a change in affinity to water and the changes in crosslink density.[182] Changing charge densities will change coil conformations as well, another potential source of thickness change, and finally the introduction of pores clearly requires an increase in film thickness. Although during this process there is loss of mass, the overall percentage of film mass lost is relatively small, necessitating the increase in film thickness.

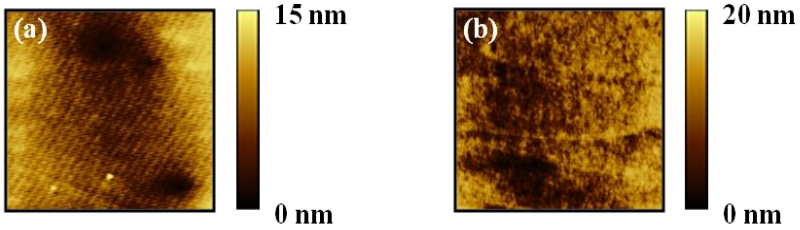

Figure 5.2: AFM images of 4(LPEI/PAA)$_{20}$ LbL films untreated (a) and post-treated in pH 3.2 solution for 1 h (b). All images are in height mode with dimensions of 20 X 20 μm^2.

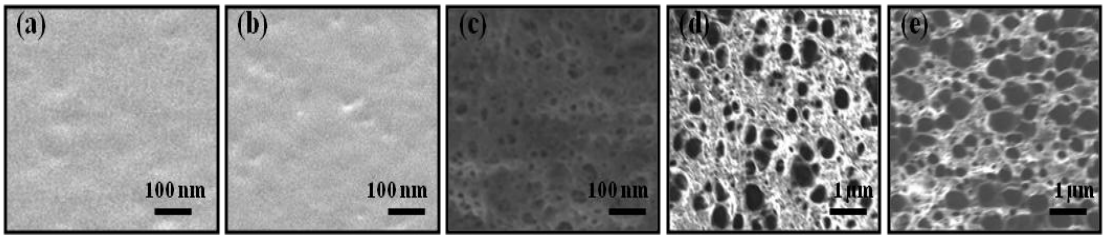

Figure 5.3: SEM images (top-view) of 4(LPEI/PAA)$_{20}$ LbL films after application of an electric field for various times. (a) Untreated films and those treated after (b) 10 min, (b) 20 min, (c) 30 min, and (d) 1 h of exposure to the electric field.

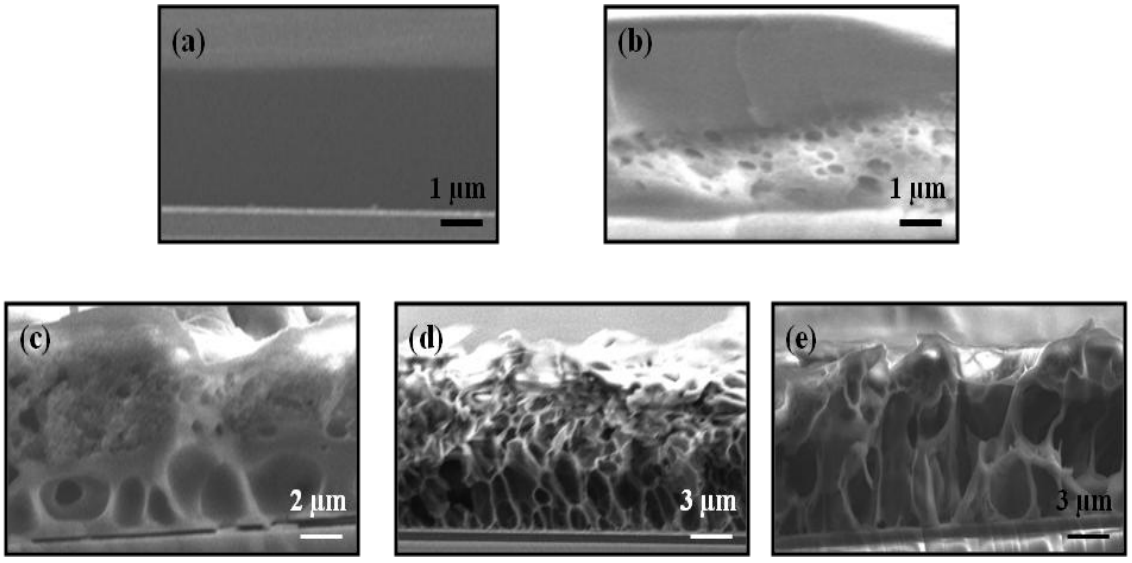

Figure 5.4: Cross-sectional SEM images of 4(LPEI/PAA)$_{20}$LbL films after application of an electric field for various times.(a) Untreated films and those treated after (b) 10 min, (b) 20 min, (c) 30 min, and (d) 1 h of exposure to the electric field.

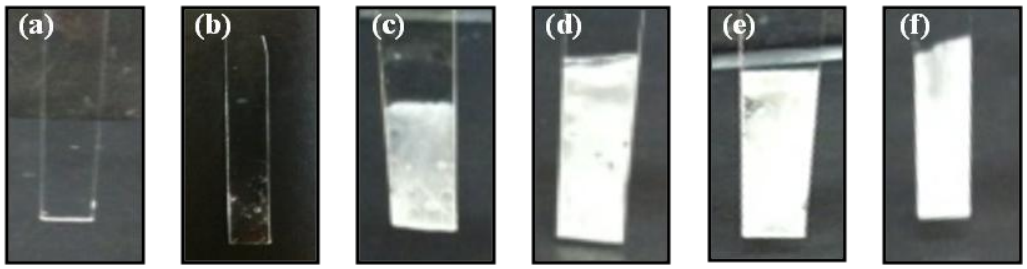

Figure 5.5: Optical microscopy images of 4(LPEI/PAA)$_{20}$ LbL films on ITO substrate after application of an electric field for various times.(a) Untreated films and those treated after (b) 5 min, (C) 10 min, (d) 20 min, (e) 30 min, and (f) 1 h of exposure to the electric field.

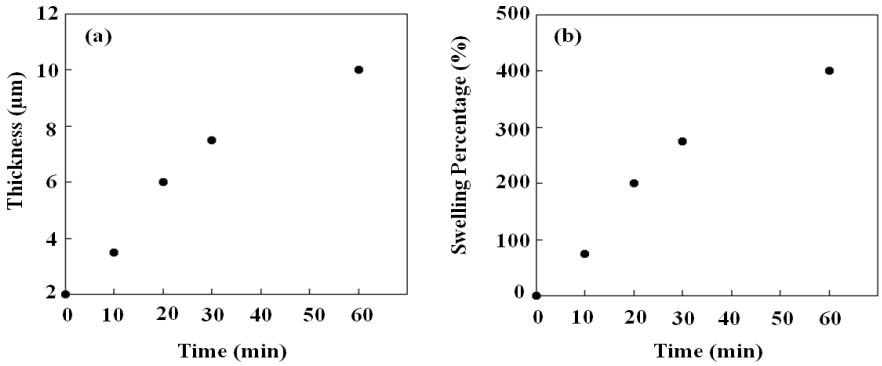

Figure 5.6: (a) Thickness and (b) swelling percentage of thin films after application of an electric field for various times.

5.3.2 Ionization in Multilayers under an Electric Potential

FT-IR spectroscopy of 4(LPEI/PAA)$_{20}$ LbL films was used to further investigate the influence of electrical potential on the ionization of PEs during the porous transition as a function of treatment time. Two pronounced peaks were observed at 1710 and 1550 cm^{-1} for the films, as shown in Fig. 5.7 (a); the former peak is assigned to neutralized carboxylic acid groups and the latter peak corresponds to ionized carboxylate acid groups in PAA.[149] As the electrical potential was applied over time, the peak intensity of

neutral COOH groups increased, and that of ionized COO^- groups decreased. Assuming that these two absorption bands have about the same extinction coefficient,[152] the percentage of charged COO^- groups was calculated using the ratio of the peak intensity of $v(COO^-)$ to the intensity sum of $v(COO^-)$ and v(COOH), Figure 5.7 (b). The amount of charged COO^- groups dropped from 55 % to 43 % in response to the application of the electrical potential for 1 h. The results of this analysis may be attributed to a change in charge density of PAA chains; upon the application of an electrical potential, partially ionized PAA become protonated due to the locally acidic environment.

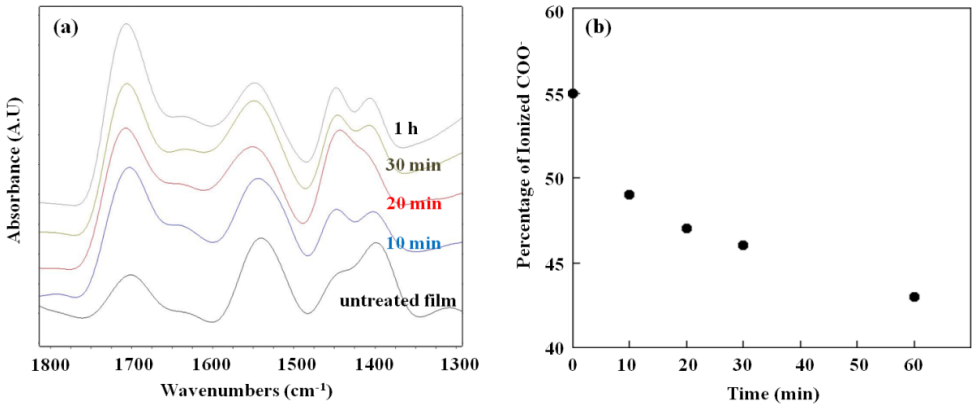

Figure 5.7: ATR FT-IR spectra (a) and the percentage of carboxylate group (COO^-) (b) of 4(LPEI/PAA) $_{20}$ films after application of an electric field for various times. The peaks of interest at 1710 and 1550 cm^{-1}, corresponding to neutralized and charged carboxylic acid groups, respectively, can be seen depending on the time period for which the electrical potential is applied.

5.3.3 Release of Methylene Blue from the Thin Films under Electric Potential

We also investigated the amount of methylene blue (MB) released during the electrical potential-induced porous transition. Positively charged MB molecules bind with free, unpaired carboxylate groups, as shown in Figure 5.8. If a carboxylate anion associated with an MB molecule becomes protonated, then the MB molecule is released. Thus, a measure of the MB released into solution using UV-Vis spectroscopy should correspond to the protonation of carboxylate groups.

First, $4(LPEI/PAA)_{20}$ LbL films were immersed into a 5 mM MB solution containing 0.1 M NaCl at pH 7 for 1h. The UV-Vis spectra of the as-immersed film is shown is Figure 5.9. Peaks ranging from 500 to 750 nm are present, which indicates loading of MB into the PEMs. Pristine LbL films before loading did not show any apparent peaks in visible range. At an assembly of pH of 4.0, both LPEI (pKa ~6) and PAA (pKa ~ 5.5 – 6.5) are partially ionized. At this condition, film formation produces thick layers and loop-rich conformations; the internal structure contains a mixture of ion-paired polyelectrolyte and unpaired free acid and amine groups. MB is known to have its maximum absorbance peak at 664 nm,[183] but the maximum peak of $4(LPEI/PAA)_{20}$–MB films was observed at 585 nm with the additional shoulder peak at around 664 nm. The ~ 664 (n-Π*) nm band is assigned to an isolated molecule (monomer) in dilute aqueous solution,[184] and the peak at 585 nm appears when MB molecules aggregate as trimers (face-to-face association, H-aggregates).[185-189] Based on this fact, the UV-Vis spectrum of thin films loaded with MB reveals that MB molecules exist as highly aggregated

molecular states with the strong Π-Π interaction among MB molecules in the 4(LPEI/PAA)$_{20}$ LbL films.

Next, the MB-loaded LbL films were subjected to 4.0 V for varying times. Direct UV-vis spectroscopic measurement of the films was challenging due to the scattering of light from the porosity; therefore, UV-vis measurements were performed on the electrochemical cell's solution to observe the release of MB, Figure 5.10 (a). As can be seen, the UV-Vis solution spectra of MB released were different from the spectrum of the original MB-loaded LbL films. UV-Vis spectra showed that the maximum peak was observed mainly at around 664 nm with a small shoulder at 615 nm, which indicates that MB molecules mainly exist as monomers and dimmers when released from the multilayers into solution. As expected, the absorbance of MB released in the solution increased with time that the electrical potential was applied. These results suggest that the amount of MB released can be controlled by applying an electrical potential for a certain time. As a control experiment, a MB-loaded 4(LPEI/PAA)$_{20}$ LbL films was immersed in the pH 3.2 water with no application of electrical potential for 1 h and the UV-Vis spectra of that solution was measured. Even though the peak at 664 nm corresponding to MB was observed as shown in Figure 5.10 (a), the amount of MB released passively without applying electrical potential was much smaller than those samples where an electrical potential had been applied.

The absorbance of the 664 nm peak was plotted as a function of the time that the potential was applied, Figure 5.10 (b). The amount of MB released from the multilayers increases with time, coinciding with our observations of a decrease in COO^- groups from

FTIR spectra and the increase in swelling percentage. It is quite evident that the amount of MB released from the films under electrical potential is directly related to the number of COOH groups remaining in the multilayers. As electrical potential is applied, COO^- groups become protonated, and fewer carboxylate groups are available for binding with MB molecules. In addition to the protonation of COO^-groups, the nano- and micro-porous structure created during the application of electrical potential can also expedite the diffusion of MB out of the $4(LPEI/PAA)_{20}$ LbL films.

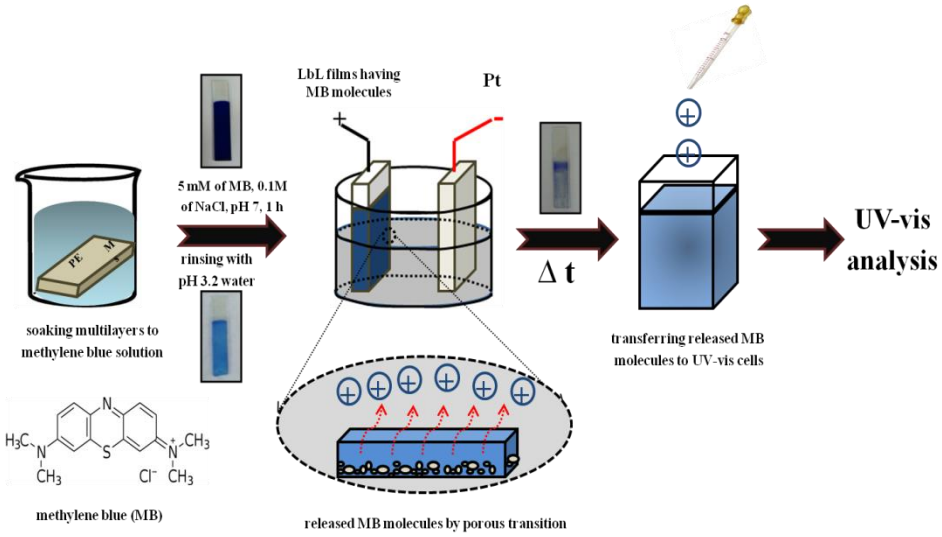

Figure 5.8: Loading methyle blue (MB) molecules into the multilayers and measuring the absorbance of released MB from the multialyers after applying the electric potential using UV-vis spectra.

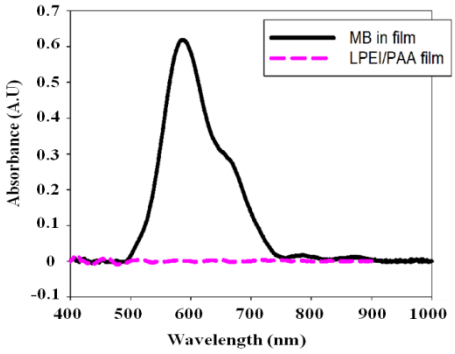

Figure 5.9: UV-vis spectrum of 4(LPEI/PAA)$_{20}$ LbL films after immersing into methylene blue solutions for 1 h.

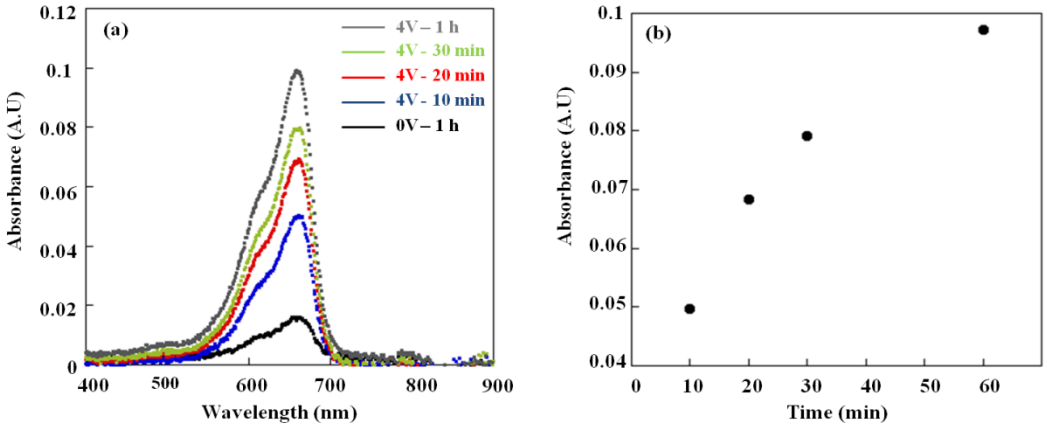

Figure 5.10: UV-vis spectra of released MB molecules from the 4(LPEI/PAA) $_{20}$LbL films (a) and absorbance change (b) after application of an electric field for various times. The maximum absorbance at 664 nm of the solution in which MB-loaded LbL films were soaked with no application of electrical potential in pH 3.2 water for 1 h was 0.012. After electrical potential is applied, the maximum absorbance of the same sample increases from 0.051 at 10 min to 0.1 at 1 h treatment.

5.3.4 The Number of Protons Generated by Electrical Potential

The amount of Coulombs generated by the application of 4.0 V was recorded with time in Figure 5.11 (left). Based on the amount of Coulomb produced, the number of moles of protons generated was calculated. At positive voltage (theoretically higher

than1.0 V vs Ag/AgCl),[190] water is decomposed into protons and oxygen gas, and electrons are generated. While electric potential is applied, the number of moles of protons generated is equal to that of electron produced according to the above reaction. The amount of protons generated during the application of electrical potential to the coated ITO substrate was higher than that of bare ITO substrate, as shown in Figure 5.11 (right). This can be explained by considering that the electrolysis of water is pushed forward to the product (protons and oxygen) side of the reaction by Le Chatelier's principal because protons are consumed to protonate the COO^-groups of PAA. This hypothesis is in good agreement with FTIR results of $4(LPEI/PAA)_{20}$ LbL films that show protonation taking place with time. As can be seen in Figure 5.7 (b), the degree of ionization of PAA decreased while the reaction of water electrolysis occurred, which means that the COO^-groups of PAA were neutralized by protons produced. Therefore, the continuous consumption of protons can move the reaction forward (towards the H^+ product side of the electrolysis reaction) compared to the case of bare ITO.

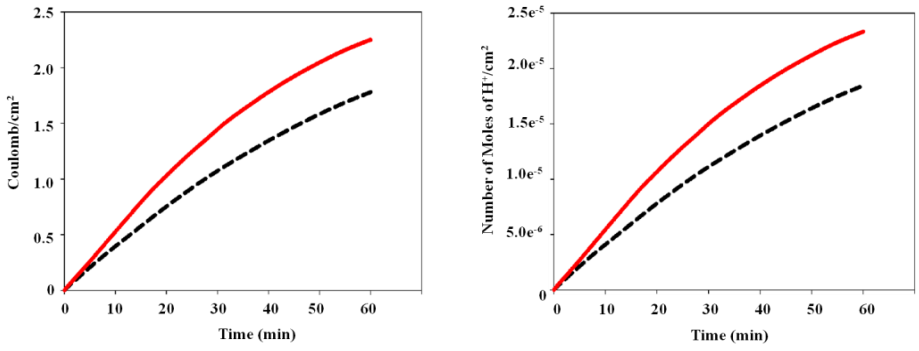

Figure 5.11: The amount of Coulomb (left) and the number of protons (right) generated after an application of an electric field for various times. Red solid line and black dotted line are LPEI/PAA films on ITO and bare ITO, respectively.

5.4 CONCLUSIONS

In this report, we use an electric field to manipulate polyelectrolyte multilayers post assembly. Application of an electric field locally lowers the pH in an aqueous solution at the electrode due to the hydrolysis of water. When that electrode is coated with a polyelectrolyte multilayer this local drop in pH can be used to induce a morphological change in the film yielding a porous structure. Depending on the time duration of the application of electric potential, the multilayers exhibited a range of morphologies. This began with the formation of separate nano-scale pores at the electrode/multilayer interface, then an asymmetric porous structure, and finally micro-sized pores throughout the films. The ability to precisely control the application of potential therefore allows us to control pore structure. This includes formation of nano or microscaled features, and closed or open celled morphologies. The variation of pore structure is closely related to the reorganization of polymer chains, resulting from changes in the chains' charge density. It was also shown that this method can be used to control binding and release of small molecules (methylene blue in this case) within the multilayer environment based on charge density with application of electric field.

CHAPTER VI

POLYELECTROLYTE MULTILAYERS STABILIZED PLATINUM NANOPARTICLES FOR PROTON EXCHANGE MEMBRANE FUEL CELLS

6.1 INTRODUCTION

Creating energy conversion and storage devices are some of the most pressing problems we currently face. Fuel cells are electrochemical devices that transform hydrogen, natural gas, and alcohols, such as methanol, into energy without the emission of greenhouse gases. A number of different types of fuel cells exist, such as molten carbonate (MCFC) and solid oxide fuel cells (SOFC), but among the various fuel cell types proton exchange membrane fuel cells (PEMFC) have been identified as the most likely candidate to provide energy for applications from vehicle transportation to conventionally batter driven devices due to their high power density, low operating temperature, and relatively quick startup.[191, 192] In addition to this, other likely PEMFC markets include stationary power and electronic portable devices. Metal nanoparticles (NPs) such as platinum (Pt), Ruthenium (Ru) or other precious metals are attractive catalytic materials due to their large surface-area-to-volume ratios, quantum confinement effects and tunable electronic properties.[193] So far, of numerous catalysts, Pt NPs have still served as the most dominant and widely used electrocatalyst material because of their superior catalytic activity and long term operation stability.[194] However, the catalyst is the most expensive component in current fuel cells. One problem with these nanoparticles is that with time they lose electrochemically active surface area through a

number of mechanisms. These include corrosion of the carbon support, dissolution of the Pt NPs, Ostwald ripening of the particles, detachment of the particles from the carbon support, or diffusion of particles along the carbon support and then their aggregation. [195-201] In light of this fact, two of the main challenges to the use of PEMFC for stationary and automotive power applications are cost and durability. Therefore, as the catalytic particles are the most expensive component of the fuel cell, increase their ability and lifetime is critical to making PEMFCs commercially viable.

Polyelectrolyte multilayer (PEMs) are polymer thin films assembled by the sequential exposure of a charged substrate to oppositely charged solutions of polyelectrolytes, or polymer salts (a technique known as layer-by-layer or LbL).[202] The process is to expose the substrate to polyelectrolyte, rinse off the excess material, and then expose the film to polyelectrolyte of the opposite charge. This deposition technique has the advantage that it can conformally coat nearly any type and geometry of substrate. Using PEMs it is possible both to create ultra-thin coating of tens of nanometers, and also films that are many microns thick, and they can be made as free-standing assemblies. One of the strongest points about LbL method is the incorporation of functionality, and PEMs have been proposed as being useful in applications ranging from anti-reflection [203] and surface-enhanced Raman spectroscopy,[204] to electronics (LEDs,[205] solar cells [206]) for membranes [207] and drug delivery platforms [208].

Recently, PEMs have been used as nanoreactors in which many nanoparticles are synthesized within PEMs by use of the binding of available functional groups with metal ions.[209-211] For example, in carboxylic acid-containing PEMs, metal cations can bind

with the acid groups, and then in the presence of a reducing environment (either in solution such as aqueous $NaBH_4$ or a gaseous environment such as H_2 gas) be reduced to particles.[212] Particles are therefore synthesized without organic capping groups or ligands, which can inhibit catalytic activity. The literature contains reports of PEMs used as nanoreactors for a number of different metal NPs (Ag, [213] Au, [214] Pd, [215] Cu [216]) and demonstrations that these particles are catalytically active. Particle density and size can be controlled by loading of metal ion into the film, and particles less than 10 nm are routinely reported. [217]

In this study, polyelectrolyte multilayers were used to stabilize catalytic Pt NPs and increase the useful lifetime of catalyst materials suitable for use in PEMFC, consequently lowering the costs associated with PEMFC. The polymer thin film would be a template for the synthesis and growth of Pt NPs, and act to immobilize the particles. PEMs with available carboxylic acid groups were formed to bind Pt complexes and subsequently, the complexes were reduced to form metal Pt NPs. The resulting structure will be in effect a mesh of Pt NPs surrounded by but not encapsulated by PE molecules. The polyelectrolytes will serve to both bind the Pt NPs to the support and to prevent their mobility along the surface of the support, thus preventing the loss of active Pt surface area by agglomeration. Because the particles will be embedded in the polymer film, this may also reduce corrosion the carbon support.

6.2 Experimental Methods

6.2.1 Materials

Poly(allylamine hydrochloride) (PAH, MW = 56 000 g/mol) and Chloroplatinic acid hexahydrate (H2PtCl6·6H2O) were purchased from Sigma-Aldrich. Poly(acrylic acid) (PAA, MW=50 000 g/mol, 25% aqueous solution) and linear poly(ethylene imine) (LPEI, MW=40 000 g/mol) were obtained from Polysciences. The structures of the polyelectrolytes examined in this work are shown in Figure 1. Sodium borohydride was purchased from EMD. All chemicals were used as received without further purification. Ultra-pure water (Milli-Q, Millipore Co.) with a specific resistance greater than 18 MΩ was used in all aqueous solutions and rinsing procedures. All of the aqueous solutions were adjusted to the appropriate pH using 0.1 and 1 M HCl or NaOH solutions, respectively, as needed prior to multilayer assembly. Glass slides used as substrates were cleaned using piranha solution (30% H_2O_2 / 98% H_2SO_4, 3:7 v/v) at 85 ℃ for 30 min.

6.2.2 Layer-by-Layer Assembly

Polyelectrolyte multilayers thin films were assembled by the layer-by-layer deposition of polyelectrolytes in which either of glass slides or Si-wafer substrates were alternatively dipped into polyelectrolyte solutions using a Nano Strata Sequence VI at room temperature. In this study, five different LbL thin films were made as follows; first, PAH/PAA or LPEI/PAA films were obtained by submerging the substrates in polycation solution (PAH or LPEI) for 10 - 15 min and then in a series of three rinsing steps of D.I water. This was followed by polyanion solution (PAA) for 10 - 15 min and three rinsing

steps again. The outermost layer of the PEMs in this experiment was the polyanion (PAA) unless otherwise stated.

6.2.3 Porous Polyelectrolyte Multilayers

The assembled polyelectrolyte multilayer films were exposed into low-pH solutions for different immersion times; PAH/PAA LbL thin films were immersed into pH 2.3 water for 5 min, and LPEI/PAA LbL thin films were exposed to pH 2.25 water for 20 min. After immersing into these solutions, the films were rinsed with D.I water for 20 s or less, dried under a smooth stream of N_2 stream, and then kept under ambient conditions prior to measurement.

6.2.4 Electrochemical Characterization of Pt-Loaded Multilayers

Cyclic voltammetry (CV) were measured in both Ar and O_2-saturated 0.1 M sulfuric acid (96.3%, Veritas VYCOR) electrolyte solution using a CHI 660A electrochemical workstation (CH Instruments, Inc.). A glassy carbon electrode (GCE) ((Pine Instruments Co., geometric area: 0.196 cm^2) coated with PEMs-loaded Pt NPs was used as the working electrode. A Twisted gold wire was used as the counter electrode and Hg/Hg_2SO_4 electrode with a filling solution of 0.5 M H_2SO_4 as the reference electrode, respectively. Both Ar and O_2 gases used ultrahigh purity (99.999% Ar, 99.99 O_2, Linde). All potentials reported here refer to the reversible hydrogen electrode (RHE). All electrochemical experiments were performed at room temperature. The GC electrode was polished with 0.5 and 0.3 μm Al_2O_3 powders successively and sonicated in water for about 10 min after each polishing step. The electrolyte solution was purged with high purity Ar for deaeration before CV experiments.

6.2.5 Characterization

Atomic Force Microscopy (AFM) was conducted by using Digital Instruments Nanoscope in the tapping mode (scan rate 1 Hz) under ambient conditions. Scanning electron microscopy (SEM) images were obtained on a JEOL JSM-7500F field emission scanning electron microscope. In order to capture the cross-sectional SEM image, the LbL films were immersed in liquid nitrogen and cut with a diamond cutter. The Attenuated Total Reflection Fourier Transform Infrared spectroscopy (ATR-FTIR) spectra of polyelectrolyte films were collected on a Bruker Optics Alpha FT-IR spectrometer. UV-vis spectra were recorded on a Hitachi U-4100 UV-Vis-NIR spectrometer. The TEM images of LbL thin films containing platinum nanoparticles were obtained using a JEOL JEM-2010 microscope at 200kv. The Theremogravimetric Analysis (TGA) analysis of the Pt NPs was done on a Q50 (TA Instruments, New Castle, DE). Each sample was run under N_2 stream from room temperature to 900 ℃, at the scan rate of 10 ℃ /min.

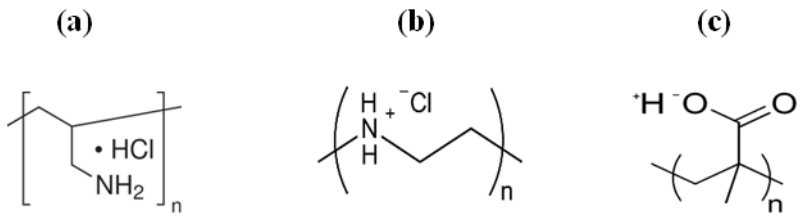

Figure 6.1: Chemical structures of polyelectrolytes used in this study; (a) polyallyamine hydrochloride (PAH), (b) polyethyleneimine (LPEI), and (c) polyacrylic acid (PAA).

6.3 RESULTS AND DISCUSSION

In this study, polyelectrolyte multilayers containing polyacrylic acid were fabricated. Two different multilayer systems were studied including PAH/PAA and LPEI/PAA thin films. These systems were chosen because PAH, LPEI and PAA are frequently used in the literature for metal NP synthesis. For the synthesis of Pt NPs within the thin films, PEMs were dipped into H_2PtCl_6 solution (1 mM) for 10 min, where $PtCl_6^{2-}$ anions were incorporated into the PEMs via the ion exchange method with COOH groups of PAA polyelectrolytes, and then treated with $NaBH_4$ (5 mM) for 10 to 15 sec, reducing $PtCl_6^{2-}$ salt to Pt NPs inside the LbL thin films (Figure 2).

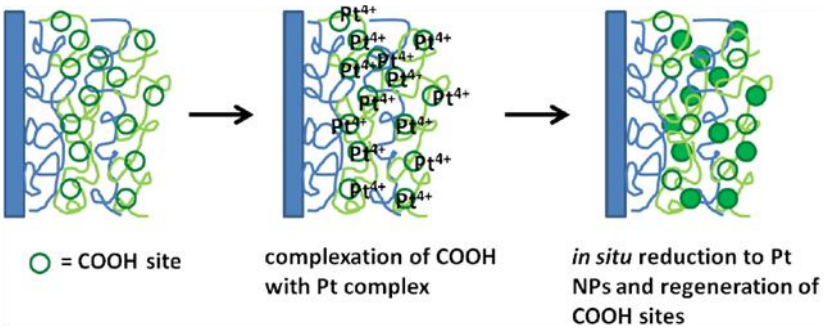

Figure 6.2: Schematic diagram of the formation of Pt NPs in polyelectrolyte multilayers. First, polymer thin film containing chemically available COOH sites is formed. Metal complexes are loaded into the film by soaking in aqueous solution, and these complexes bind to the carboxylic acid sites. Finally, the complexes are reduced to metal NPs, regenerating the original acid sites.

6.3.1 UV-vis Spectroscopy

The formation of Pt NPs in the PEMs was monitored with UV-vis spectrometer, by observing the surface Plasmon resonance frequency. As seen in Fig. 3 (a) and (b),

both as-assembled PAH / PAA and LPEI / PAA LbL thin films possessed no observable absorption peak in the UV region. However, after immersing in H_2PtCl_6 solution, a new absorption band at 272 nm appeared. For the H_2PtCl_6 solution, the characteristic absorbance of $PtCl_6^{2-}$ ions is known to appear at 260 nm. This peak arises from the ligand-to-metal charge-transfer transition.[218] When the LbL thin films were placed in contact with the H_2PtCl_6 solution, $PtCl_6^{2-}$ anions were incorporated into the multilayers via ion exchange and the absorbance peak for the Pt ions bound to the thin films shifted to 272 nm, indicating a change in the ligand field when the Pt ions were incorporated into the multilayers from the aqueous solution. For the film treated with $NaBH_4$ solution, the UV spectrum was reverted to that of the as-assembled multilayers, and the new absorption peak disappeared, indicating that $PtCl_6^{2-}$ ions were completely reduced and Pt NPs were formed in the PEMs.

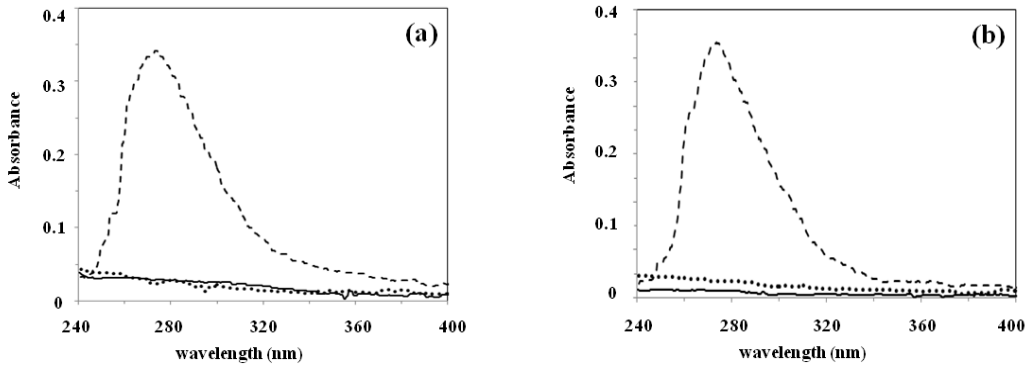

Figure 6.3: UV-vis spectra of LbL thin films of (a) PAH/PAA and (b) LPEI/PAA LbL thin films.

6.3.2 Electrochemical Properties of Pt-Loaded Multilayers

In order to assess the charge for hydrogen adsorption and desorption and the activity of the thin films for the oxygen reduction reaction (ORR), 12 bilayers of PAH/PAA and LPEI/PAA thin films were assembled onto the GCE and then, CV experiments were performed. Different scan rates from 10 to 100mV/s were used, but 50mV/s gave the most pronounced CV features. Figure 4 shows the voltammetric responses of PAH/PAA and LPEI/PAA LbL films-modified electrodes in the potential range of -0.69 to 0.9V in an Ar-saturated 0.5 M H_2SO_4 solution at a potential scan rate of 50 mV/s. The CV results show that a pair of well-defined redox peaks was observed at the electrode, corresponding to hydrogen adsorption-desorption at -0.69 to -0.45 V and Pt-oxide formation of a broad anoidic peak at 0.4 to 0.6 V well before the oxygen evolution peak at 0.8 to 0.9 V versus RHE. The strong cathodic peak at 0 V is produced due to the reduction of Pt (II) into Pt (0).

The Pt content in the supporting films is crucial to its performance as a catalyst. It has been demonstrated that metal NPs loading in the PEMs can be manipulated by repeating the exchange / reduction cycles multiple times or by increasing the number of LbL assembly layers. [219] The catalytic activity toward oxygen reduction as well as H adsorption/desorption was increased gradually by simply repeating load and reduction cycles of Pt NPs, as shown in Fig. 5. Aside from the two ways above, the loading of metal NPs in the PEMs is also controlled and improved with post-assembly treatment in which as-assembled PEMs are immersed into low pH [220] or high pH [111] solutions. Fig. 6 shows that the redox peak currents increase after post-assembly treatment.

This increased catalytic activity from the post-assembly treatment is closely related to the ionization of PEs since polymer chains used in this study are weak polyelectrolytes, and their charge densities are very sensitive to pH variations.[22] ATR FT-IR data in Fig. 7 showed that the peak intensity at 1703 nm, corresponding to neutralized carboxylic acid groups, increased after the thin films were immersed in low pH solutions. On the contrary, the peak at 1540 cm^{-1}, which is assigned to ionized carboxylate, decreased. This observation reinforces the idea that an increase of COOH groups of PAA in the multilayers after post-acid treatment offers more availability for binding Pt complexes, which results in an enhanced-electrochemical activity.

As is already well-known,[63] both PAH/PAA and LPEI/PAA LbL thin films had spinodal decomposition and pore formation due to phase separation of the neutralized PAA and protonation of positively charged PEs (PAH or LPEI) when exposed to low pH solutions after assembly. AFM in Fig. 8 and SEM images in Fig. 9 showed the morphology changes on the surface and internal structure of each film. Both pure PAH/PAA and LPEI/PAA LbL films had a featureless and continuous surface, but they showed porosity structures after post-assembly treatment. The internal structure of LPEI/PAA films also showed organized-porosity structure with a high degree of swelling while PAH/PAA was observed to swell with no pores. We consider this porous morphology of the PEMs to be beneficial to dispersion of Pt NPs due to its high surface area, and therefore increases the density of active sites on the electrode.

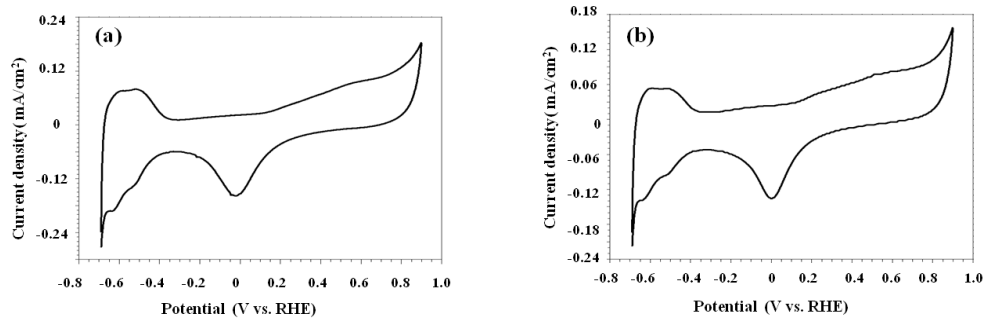

Figure 6.4: Cyclic voltammetric of (a) PAH/PAA and (b) LPEI/PAA LbL thin films at a scan rate of 50 mV/s in 0.5 M H_2SO_4.

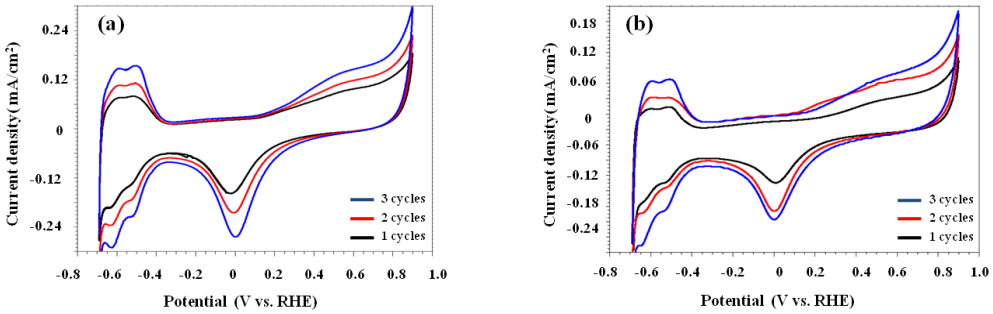

Figure 6.5: Cyclic voltammetric of (a) PAH/PAA and (b) LPEI/PAA LbL thin films under different exchange / reduction cycles; 1 cycle (black), 2 cycle (red), and 3cycle (blue).

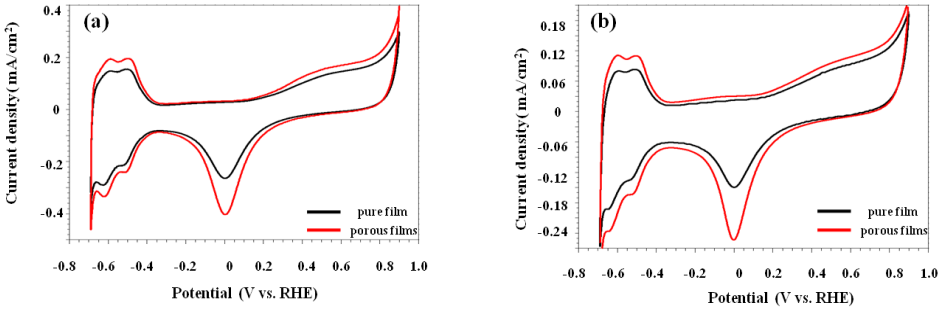

Figure 6.6: Cyclic voltammetric of pure film (black) and porous film (red) for (a) PAH/PAA and (b) LPEI/PAA LbL thin films. Each CV data was taken from the LbL films that had 3 cycles of load / reduction.

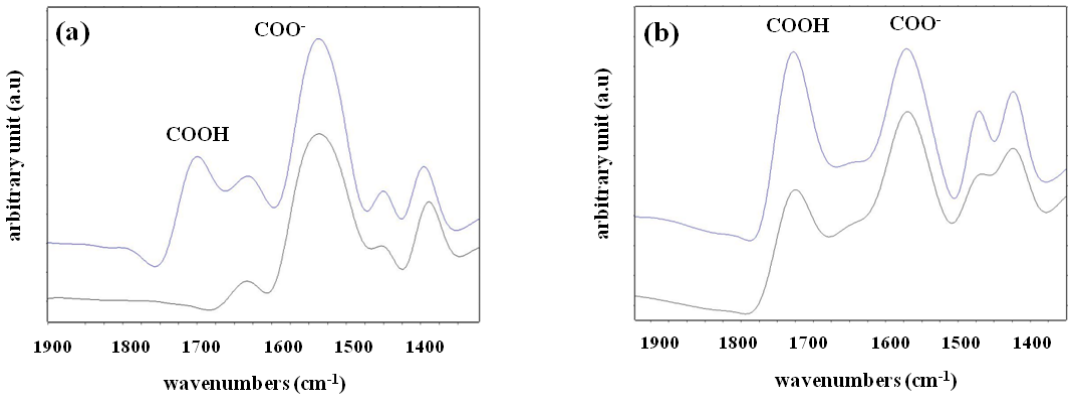

Figure 6.7: ATR FT-IR of (a) PAH/PAA and (b) LPEI/PAA LbL thin films before (below) film and after (above) post-acid treatment. In each post-assembly treatment, PAH/PAA films were immersed into pH 2.3 for5 min and LPEI/PAA LbL thin films were exposed in pH 2.25 for 20 min.

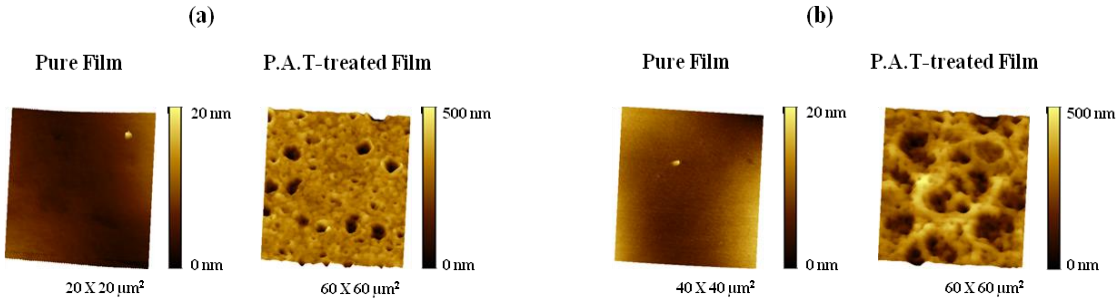

Figure 6.8: 3-dimensional AFM images of pure film and post-assembly treatment (P.A.T)-treated film for (a) PAH/PAA and (b) LPEI/PAA LbL thin films. For the post-assembly treatment, PAH/PAA film was immersed in pH 2.3 solutions for 5 min and LPEI/PAA film was dip into pH 2.25 solutions for 20 min.

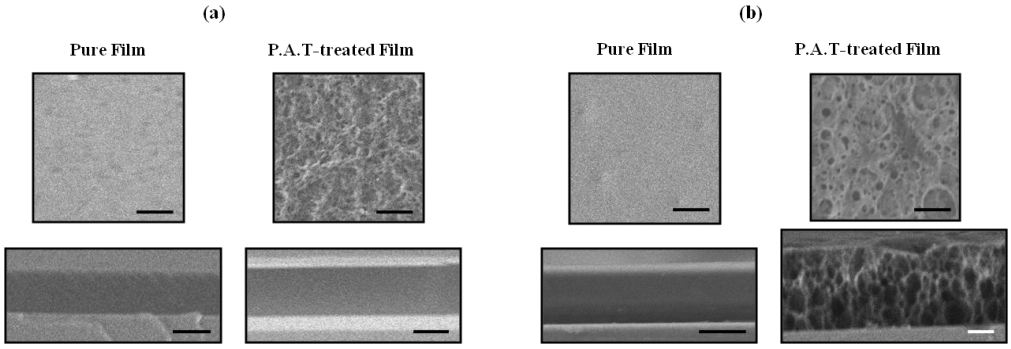

Figure 6.9: Top view and cross-sectional SEM images of pure film and post-assembly treatment (P.A.T)-treated film for (a) PAH/PAA and (b) LPEI/PAA LbL thin films. The scale bar indicates 1µm.

6.3.3 Stability of the Multilayers Containing Pt NPs

In addition to the study of electrochemical activity, the stability (durability) of the Pt NPs against electrochemical active surface area was also evaluated with periodic measurement of the surface area. In order to investigate the stability of the electrochemically active surface area (EASA) in each LbL thin film, the CV of Pt-loaded multilayers on the GCE was performed with 100 potential cycles between -0.69 and 0.4 V at a potential scan rate of 50mV/s in an Ar-saturated 0.5 M H_2SO_4 solution. Fig. 10 shows the CV of post-assembly treatment treated-PAH/PAA and LPEI/PAA films under multiple cycles, and the inserted figure represents CV of the first cycle and the 100^{th} cycle. The EASA of PAH/PAA films was decreased with periodic cycles, while there were negligible changes in the shape and height of the current of H-adsorption/desorption in LPEI/PAA LbL thin films, indicating the better stability of this film as compared with that of PAH/PAA film.

The exact reason for the difference in durability of two LbL thin films is not clear at this stage, but one of the reasons could be attributed to different p-orbital character of the amine group. This group is basic and nucleophilic due to a lone pair on the nitrogen of the amine. Both PAH/PAA and LPEI/PAA LbL thin films have nitrogen groups in polymer chains (PAH and LPEI). The difference between two PEs is that PAH has sp^2 hybridized nitrogens, whereas LPEI has sp^3 hybridized nitrogens. Since the lone pair on the nitrogen of the amine allows the nitrogen to act like a Lewis Base, it has electrons that can be donated to the electron deficient species. Considering that a greater p-orbital character of the amine shows a greater basicity, the lone pair of the amines in LPEI/PAA films could have a stronger interaction with Pt ions than that of PAH/PAA. As a result, the dissolution of Pt could be decreased in the LPEI/PAA films, showing more stability under multiple cycle measurements.

Another possible explanation includes that PAH/PAA and LPEI/PAA film may have different structural stability during extended cycles, as conventional C black supports undergo morphological changes and induce catalyst aggregation.[222] To compare the film's stability between two PEMs, we investigated the thickness changes by exposing the multilayers in a variety of concentrations of NaCl solution. The results in Fig. 11 indicated that in every case the thickness of PAH/PAA film was decreased with NaCl concentrations, while the thickness of LPEI/PAA film remained almost the same. The film's stability was further examined by using optical microscopy and AFM in Fig. 12 and Fig. 13. With increasing ionic strength solutions, the morphology of PAH/PAA film was dramatically collapsed and deconstructed, but the morphology of LPEI/PAA

film remained intact. The morphological changes under NaCl solutions confirmed that LPEI/PAA films are more stable than PAH/PAA films.

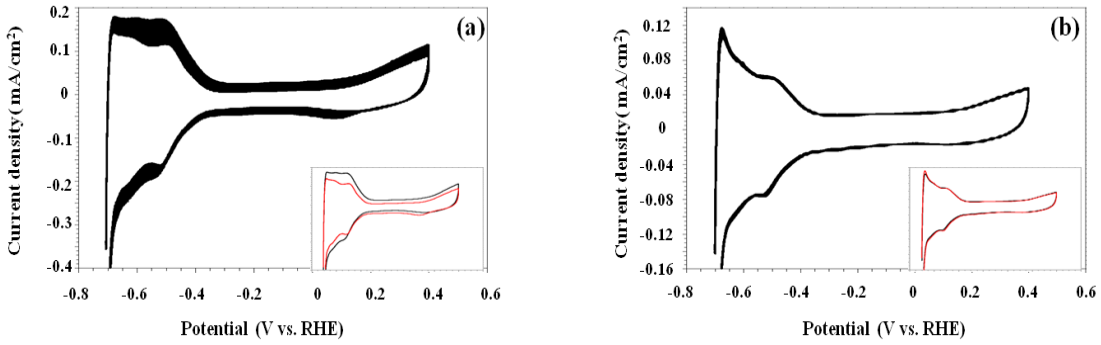

Figure 6.10: Cyclic voltammetry of post-assembly treatment treated-(a) PAH/PAA and (b) LPEI/PAA LbL thin films recorded in an Ar-purged 0.5 M H_2SO_4 solution at 50 mV/s with 100 potential cycles. Insert figure shows the CV of the first cycle (black) and 100th cycle (red).

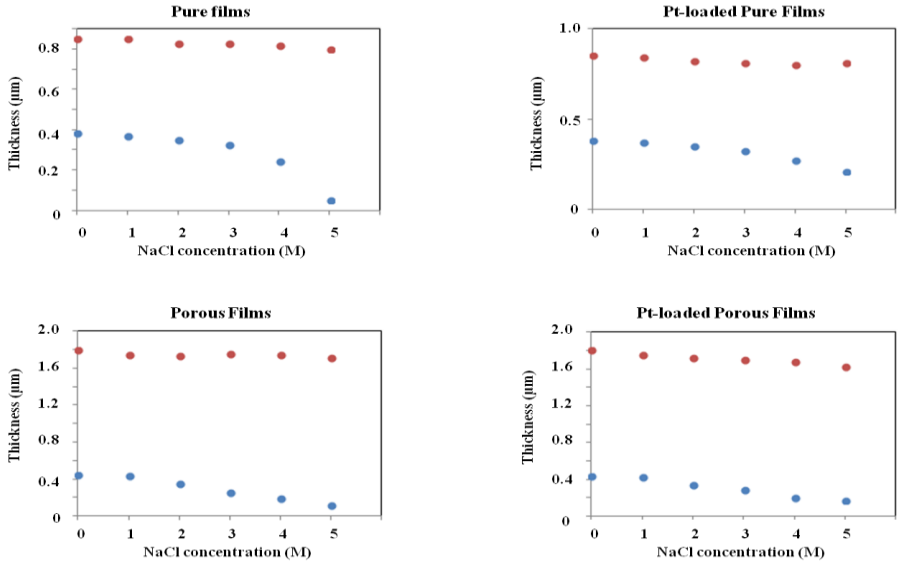

Figure 6.11: Thickness change of PAH/PAA (blue) and LPEI/PAA (red) LbL thin films under a variety of NaCl solutions. The multilayers were immersed into NaCl solutions for 30 min and then, rinsed with D.I water for 10 to 15 sec. Porous films are LbL thin films that were treated with post-assembly treatment.

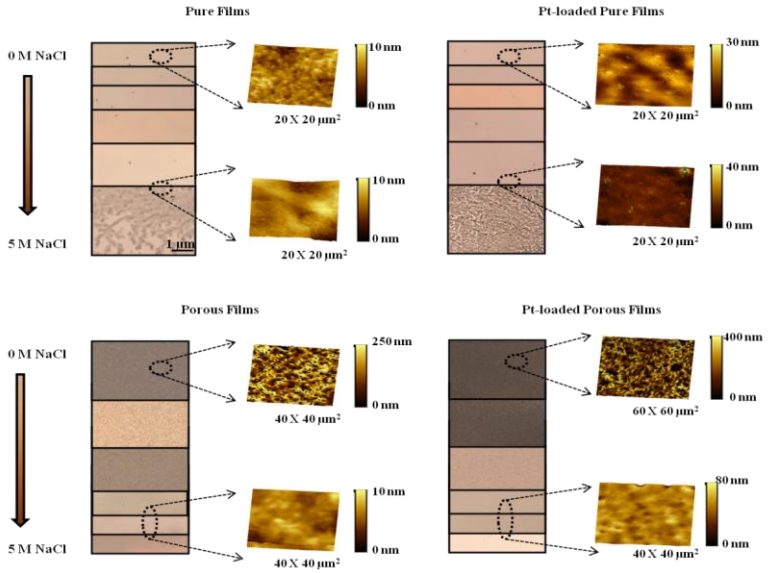

Figure 6.12: Optical Microscopy image and AFM images of PAH/PAA LbL thin films under various NaCl solutions.

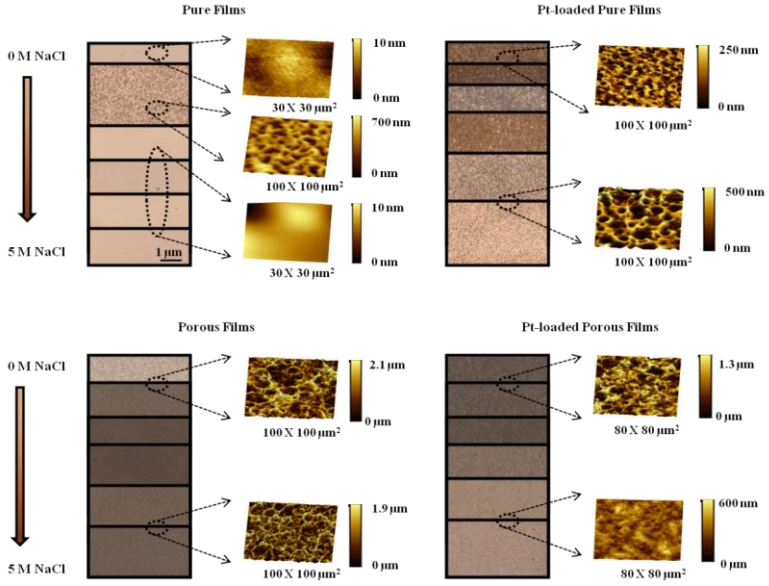

Figure 6.13: Optical Microscopy image and AFM images of LPEI/PAA LbL thin films under various NaCl solutions.

6.3.4 Microstructure of Pt NPs in the PEMs

The distribution and the size of Pt NPs in the PEMs were investigated using the high-resolution TEM. Well-dispersed Pt NPs were visualized as dark contrast and became homogeneously distributed, as shown in Fig. 14. TEM images of the multilayers clearly exhibited the presence of numerous small particles with fairy even distribution, although a few aggregates were observed. Pt NPs were typically bound on the multilayers, which further confirmed that Pt NPs could firmly were adsorbed onto the composite by electrostatic interactions. The histogram of the particle size distribution was determined by measuring the sizes of more than 200 Pt NPs (particle agglomerates are excluded). A narrow particle size distribution of the Pt NPs was found, with sizes mostly falling between 2 and 5 nm. The particle size of Pt NPs, nearly spherical in shape, in the multilayers from the size histogram is estimated to be between 3.5 and 4 nm for both LbL thin films, which is comparable to the typical size of commercial Pt catalysts used in fuel cells.

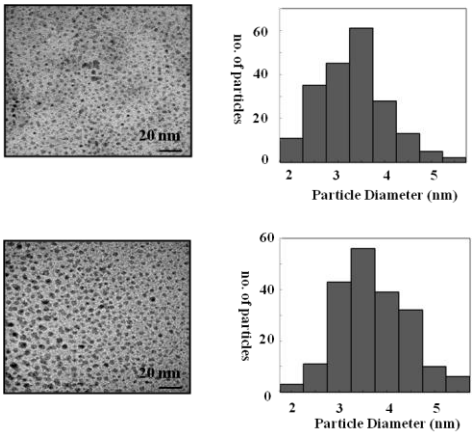

Figure 6.14: TEM images (left) and size histogram (right) films of PAH/PAA (above) and LPEI/PAA (bottom) LbL thin films.

6.3.5 TGA Analysis

In order to determine the loading of Pt NPs in the multilayers TGA analysis was carried out under a nitrogen atmosphere. The TGA results of pure film, Pt-loaded film, and Pt-loaded porous films in PAH/PAA and LPEI/PAA LbL thin films are shown in Fig. 15, in which the temperature was ramped from 25 to 900 ℃ at 10 ℃/min. The degradation temperature of Pt-loaded LbL thin films was decreased by 10 ℃ in each film. The immobilization of Pt NPs in the PEMs affects the thermal stability, as the decomposition of pure films occurs at the lower temperature owing to the catalytic effect of Pt NPs.

The Pt content in the multilayers was calculated as a differential weight loss between pure film and Pt-loaded film. It was found that the Pt content was 16 % for PAH/PAA film and 12 % for LPEI/PAA film. As was expected, the wt % of Pt NPs in the porous films increased up to 19 and 17 % for PAH/PAAA and LPEI/PAA LbL thin films, respectively, which is most likely due to an increase of COOH groups by post-assembly treatment.

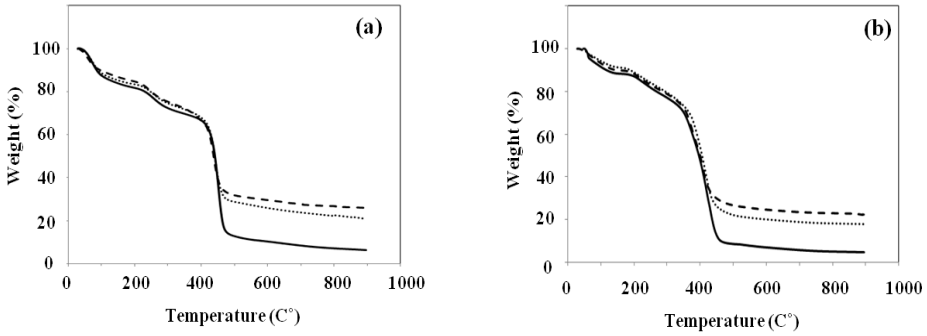

Figure 6.15: TGA results of (a) PAH/PAA and (b) LPEI/PAA LbL thin films under a nitrogen atmosphere.

6.3.6 Electrochemical Active Surface Area (EASA)

The electrocatalytic activity of the Pt NPs is closely related to the electrochemically active surface are (EASA) of the Pt NPs on the supporting materials. EASA provides important information regarding how much of electrochemically active surface area is available during an electrochemical reaction and at the same time accounts for the access of a conductive path available to transfer electrons to and from the electrode surface.[223]

Table 6.1 summarizes the EASA, theoretical surface area (TSA), and utilization of the PAH/PAA and LPEI/PAA LbL thin films. The EASA of Pt was calculated from the following equation;[224, 225]

$$\text{EASA} = \frac{Q_H}{([\text{Pt}] \times q_H)}$$

Q_H is columbic charges accumulated during hydrogen adsorption and desorption after correcting for the double-layer charging current from the CV and q_H ($210\mu/cm^2$) is the charge required for the adsorption of a monolayer of hydrogen on a Pt surface.[224] [Pt] (mg/cm^2) is the amount of Pt loaded in the LbL films, which was obtained from the TGA. TSA was determined using the following equation; [226]

$$\text{TSA} = \frac{6 \times 10^4}{(\rho_{Pt} \times d)}$$

where d and ρ_{Pt} stand for the diameter measured by TEM and the density of bulk Pt (21.45×10^6 g/cm^3). This equation was based on assumption that Pt NPs have spherical geometry.

The Pt utilization efficiency was obtained; [227]

$$\text{Utilization} = \frac{\text{EASA}}{\text{TSA}}$$

On the basis of equations above, PAH/PAA films had a higher EASA value of 15.3 m^2/g compared to that of 14.3 m^2/g for the LPEI/PAA film. From the TSA, Pt utilization was 19.7 % and 19.4 % for PAH/PAA and LPEI/PAA films, respectively. The utilization efficiency for both LbL thin films is lower than that of a commercial Pt/CB catalyst that has an EASA of 50.6 m^2/g and Pt utilization of 49 %.

One of the reasons for low EASA is that the Pt content obtained from the TGA to calculate EASA may result in smaller EASA. The Pt loading from TGA analysis was measured with 100 bilayers of free-standing films, but for the CV measurements 12 bilayer of LbL film was used. As well reported, [87] both PAH/PAA (assembly pH of 7.5 and 3.5 for PAH and PAA, respectively) and LPEI/PAA system grows exponentially; that is, many more polymer chains are deposited during later steps than the initial layers. Therefore, the Pt content calculated above from TGA could be higher than that actually loaded in the films used for electrochemical analysis.

A possible explanation for the lower Pt efficiency is that the particle size of the Pt NPs obtained from TEM to calculate TSA was calculated to be a bit smaller than actual Pt particle size deposited within the PEMs. The average Pt NP size from TEM analysis was based on 3 bilayers of the LbL thin films, but for the CV measurement 12 bilayers of the multilayers were assembled. Considering that PEMs are interdigitated, where layers overlap and interpenetrate to form fuzzy boundaries, [228] Pt NPs could be somehow aggregated into larger size of particles in the thicker films. With this reasoning,

the actual Pt NPs loaded in the 12 bilayers of thin films could be bigger than those in 3 bilayers of thin films.

Table 6.1. The EASA, TSA, and utilization for PAH/PAA and LPEI/PAA LbL thin films containing Pt NPs.

	EASA (m^2/g)	TSA (m^2/g)	Utilization (%)
PAH/PAA	15.3	77.7	19.7
LPEI/PAA	14.3	73.6	19.4

6.4 CONCLUSIONS

This study demonstrates the use of the polyelectrolyte multilayer thin films as a microreactor for Pt NP synthesis for the application of fuel cells. The characterization of the Pt-loaded PEMs and the evaluation of electrocatalytic performance presented in this study provide an insight into the utilization of PEMs as Pt NP support in fuel cells. The polymer matrix assembled with LbL method is shown to act as a stabilizing layer for the Pt NPs and provide a sufficiently homogeneous distribution as well as chemically stable immobilization of Pt NPs in the PEMs. Both PAH/PAA and LPEI/PAA LbL thin films showed good electrochemical activities and catalytic properties could be enhanced by simply using post-assembly treatment to increase diffusion to the surface of the particles. EASA results show that PAH/PAA films provide for more active platinum sites than LPEI/PAA films, but the electrocatalytic activity of the latter system was more stable.

CHAPTER VII

SUMMARY AND FUTURE WORK

7.1 THESIS SUMMARY

The main objective of this thesis is to investigate the origin of the mechanism of the structural rearrangements leading to the porous transitions and swelling behavior in weak PEMs under external stimuli such as low/high pH or salt solutions and electric field. By using hydrogel stamps soaked into various pH values of water or high ionic strength solutions and then, applying to the film's surface, these solutions can be delivered locally at controlled rates, enabling to give a deeper understanding and more detailed information about the surface morphology transitions. For weak PEMs, the polymer thin films were used to stabilize catalytic Pt NPs and increase the useful lifetime of catalyst materials suitable for use in PEMFC, consequently lowering the costs associated with PEMFC.

Chapter 2 presented here the use of a modified microcontact printing method, reactive wet stamping (r-WETs), using a hydrogel stamp soaked in aqueous solution to create patterns in PEMs. By using r-WETS technique, we are able to locally control the porous transition, phase transformation and physical properties such as pore size, pore morphologies, and swelling as a function of stamping time. This technique has the potential to locally control chemical functionality, film thickness, and mechanical properties, leading to a new ability to control film architectures both at the film surface and within the bulk of the film.

Chapter 3 dealt with another use of r-WETS to weak PEMs in order to investigate morphological / physical / mechanical changes from the salt stamping. Upon salt stamping of the thin film, these thin films underwent a variety of molecular reorganizations depending on the ionic strength of salt solution; swelling transition with no change in morphology at low concentration, porous transitions with deswelling behavior at specific concentration (1 M of NaCl or 0.3 M of $CaCl_2$), spinodal with more deswelling at higher concentrations, and finally complete dissociation of polymer chains at NaCl > 3 M or $CaCl_2$ > 1M. This paper also presents a novel strategy to create a continuous gradient structure with thickness or porosity along the later direction of thin films by simply tuning the concentration of salt solutions.

Chapter 4 presented the mechanism of the transition from a continuous morphology to a porous morphology within LPEI / PAA and PAH/PAA LbL thin films. These morphological changes were created by both acidic and basic postassembly treatments. The results obtained in this work confirmed that polyelectrolytes are partially released from the PEM in response to the pH treatment as a function of exposure time. This information about the structural reorganization will be useful in designing functional materials based on polyelectrolytes.

In Chapter 5, the morphological transitions in weak PEMs assembled with LPEI and PAA were investigated by applying an electric field. Exposure to an electric field resulted in the creation of a porous structure, which can be ascribed to local changes in pH and subsequent structural rearrangements of weak polyelectrolyte constituents. It was discovered that the morphological variation of the LbL films starts at the multilayer-

electrode interface and propagates through the film. Eventually, an asymmetrical structure consisting of nano-sized pores at the upper layers and micro-sized pores layer at the bottom region forms. The results found in this study not only demonstrate experimental feasibility for controlling variation in pore size and porosity of multilayer films, but also deepen the understanding of the mechanism of the porous transition.

Chapter 6 describes the *in situ* synthesis of metallic nanoparticles in PEMs for the application of PEMFCs. Carboxylic acid groups in the PEMs bind Pt complexes by ion exchange method with the acid protons. The complexes are reduced to metal NPs, regenerating the original acid sites. Pt NPs with diameters of 3 to 4 nm were uniformly distributed in the PEMs. The PEMs loaded with Pt NPs showed high catalytic activity for H-adsorption/desorption and Pt oxide reduction. Porous thin films were created by post-assembly treatment with low pH water and therefore more carboxylic acid groups available for binding catalytic NPs were shown to be higher electrocatalytic activity than untreated films. The use of PEMs as nanoreactors can decrease the loss of Pt NPs and also minimize the aggregation of them in a polymer matrix, the multilayers containing Pt NPs will be a promising candidate for an efficient electrode material in the fuel cells.

7.2 FUTURE RESEARCH DIRECTIONS

Owing to the functionality and versatility of the LbL method, there are many avenues which can be pursued with regards to external stimuli-responsive weak PEMs. Also, the r-WETS technique is an effective way to locally perform chemistry in thin hydrogel films in a controlled manner, leading to a deeper understanding of the

relationship between structural rearrangements and post-assembly treatments. Additional experiments will explore the possibility of applying these materials to various applications.

Future research will focus on generating membranes with porosity gradients of sizes relevant to nanoparticles separation in PEMs using the r-WETS technique. Hydrogel stamping with different pH solutions or salt solutions of various concentrations can be used to produce depth-wise porosity gradients, demonstrating that patterned PEMs can be used as tangential-flow filtration membranes to separate nanoparticles. Tangential-flow filtration is a process in which the solution passes across the surface of the membrane and pressure is applied from above. Due to this pressure, solvent and particulate matter smaller than the pore size of the membrane will pass through the membrane while larger particles are retained. To achieve the creation of porosity gradients and further precise control of pore size, the density and placement of these pores must be controllably tailored. In previous research in our lab, we have developed a method to control the phase separation induced porosity transitions within PEMs assembled with the LbL method. Also, porosity gradients on the surface of the PEMs were created by using an agarose stamp having a gradient of salt concentration.

To precisely control both pore size and density in this process, experiments will be performed investigating the following parameters; 1) salt content of the dipping baths for the polyelectrolyte, 2) stamping time, and 3) type of salt used to swell the stamp. Secondly, our work aims to form depth-wise porosity gradients with pore sizes varying from the film's surface to the bottom of the film. The porosity gradient in the direction

of the film thickness will be achieved by both salt stamping PEMs and stamping with acidic or basic solution, depending on the rate of the flow of low/high pH solutions or salt solution into the PEMs. To control the diffusion rate into the PEMs, several parameters including varying the crosslink density of the hydrogel stamp will be manipulated.

Another area rich for future research is to increase the utilization efficiency of Pt NPs in fuel cells by using other catalyst support such as carbon nanotubes (CNTs) [229] and carbon nanofibers (CNFs) [226], and by using electronically conductive polymers, such as polyaniline (PANI), polypyrrole (PPy) and polythiophene (PTh). [230] The addition of an electronically conducting polymer such as PANI would be able to enhance the relatively low EASA found in our system. PANI has been one of the most studied conducting polymers because of (i) easy preparation under reproducible conditions by electropolymerization of aniline, (ii) good stability in a relatively wide potential window (from 0.0 V to 1.1 V vs. RHE), (iii) reversible acid doping / base de-doping properties, and (iv) sufficient electronic conductivity (10 to 10^2 S/cm) to minimize any ohmic drop limitation.[231] One of the limitations in our LbL system is that the nonconductive polymer matrix in which the Pt NPs are dispersed limits the electrochemical activity. Therefore, introducing PANI into the multilayers to make complex PEMs will offer a possibility of further increasing the electrochemical activity as well as Pt utilization efficiency. Currently, studies of the electrocatalytic performance regarding complex LbL thin films containing polyaniline are underway.

REFERENCES

1. Zhang, J.; Senger, B.; Vautier, D.; Picart, C.; Schaaf, P.; Voegel, JC.; Lavalle, P. *Biomaterials* 2005, 26, 3353-3361.
2. Hammond, P. T. *Colloid Interface Sci*. 2000, 4, 430-442.
3. Wood, K. C.; Boedicker, J. Q.; Lynn, D. M.; Hammond, P. T. *Langmuir* 2005, 21, 1603-1609.
4. Dautzenberg, H.; Jaeger, W.; Kotx, J.; Philipp. B.; Seidel, C.; Stscherbina, D. "Polyelectrolytes Formation, Characterization and Application" Carl Hanser Verlag, Munich, 1994.
5. Sharp, K. A. *Biopolymers* 195, 36, 227-243.
6. Blacklock, J.; Maoc, G.; Oupickýd, D.; Möhwald, H. *Langmuir* 2010, 26, 9597-8605.
7. Dobrynin, A. V.; Rubinstein, M. *Prog. Polym. Sci.* 2005, 30, 1049-1118.
8. Dodoo, S. " Structure and Swelling Behavior of Polyelectrolyte Multilayers" 2011, Berlin Institute of Technology, Berlin, Germany.
9. Van der Schee, H. A.; Lyklema, *J. J. Phys. Chem.* 1984, 88, 6661-6667.
10. Bohmer, M. R.; Evers, O. A.; Scheutjens, J. M. *Macromolecules* 1990, 23, 2288-2301.
11. Yoo, D. "Functional Material Organic Thin Films Fabricated by Layer-by-Layer Sequential Adsorption Technique" 1997, M.I.T, Boston, U.S.A.

12. Rmaile, H. H. “Structural-Property Relationships in the Design, Assembly and Applications of Polyelectrolyte Multilayer Thin Films” 2004, FSU, Florida, U.S.A.
13. Kharlampieva, E.; Sukhishvili, S. A. *Langmuir* 2003, 19, 1235-1241.
14. Dubas, S. T.; Schlenoff, J. B. *Langmuir* 2001, 17, 7725-7727.
15. Kohler, K.; Biesheuvel, P.M.; Weinkamer, R. *Phys. Rew. Lett.* 2006, 97, 188301-188308.
16. Dubas, S.; Schlenoff, J. *Macromolecules* 1999, 32, 8153-8160.
17. Young, T.S.; Fu, E. *Tappi. J*. 1991, 74, 197-207.
18. Natarajan, R.; Deshpande, K.V. *Corr. Maint*. 1985, 8, 205-211.
19. Radoiu, M. T.; Martin, D.I.; Calinescu, I; Iovu, H. *J. Harzad. Mater*. 2004, 106, 27-34.
20. Von H, A.; Krentz, D.O.; Kulick, W.M.; Lerche, D. *Coll. Polym. Sci.* 1999, 277, 637-644.
21. Amuda, O. S.; Amoo, I. A. *J. Harzad. Mater*. 2007, 141, 778-783.
22. Macdonald, M. L.; Samuel, R. E.; Shah, N. J.; Padera R, F.; Beben, Y. M.; Hammond, P. T. *Biomatrials* 2012, 32, 1446-1453.
23. Bakeev, K. N.; Izumrudov, V. A.; Kuchanov, S. I.; Zezin, A. B.; Kabanov, V. A. *Macromolecules* 1992, 25, 4249-4254.
24. Bucur, C. B.; Sui, Z.; Schlenoff, J. B. *J. Am. Chem. Soc.* 2006, 128, 13690-13691.
25. Kabanov, A. V.; Kabanov, V. A. *Bioconjugate Chem.* 1995, 6, 7-20.

26. Dubas, S. T.; Schlenoff, J. B. *Macromolecules* 2001, 34, 3736-3740.

27. Iler, R. *J. Colloid & Interface Sci.* 1966, 21, 569-594.

28. Decher, G.; Hong, J-D. *Macromol. Chem. Macromol. Chem. Macromol. Symp*. 1991, 46, 321-327.

29. Choy, K. L. *Progress in Materials Science* 2003, 48, 57-170.

30. Ariga, K.; Mori, T.; Hill, J. P. *Soft Matter* 2012, 8, 15-20.

31. Decher, G. *Science* 1997, 277, 1232-1237.

32. Boudou, T.; Crouzier, T.; Ren, K.; Blin, G.; Picart, C. *Adv. Mater.* 2009, 21, 1-27.

33. Klitzing, R, V. *Phys. Chem. Chem. Phys.* 2006, 8, 5012-5033.

34. Bruening, M. L.;Dotzauer, D. M.; Jain, P.; Puyang, L.; Baker, G. L. *Langmuir* 2008, 24, 7663-7673.

35. Schlenoff, J, B. *Langmuir* 2009, 25, 14007-14010.

36. Decher, G.; Schmitt, *J. Prog. Colloid Polym. Sci.* 1992, 89, 160-164.

37. Srivastava, S.; Kotov, N, A. *Accounts of Chemical Research* 2008, 41, 1831-1841.

38. Stockton, W. B.; Rubner, M. F. *Macromolecules* 1997, 30, 2717-2725.

39. Shimazaki, Y.; Mitsuishi, M.; Ito, S.; Yamamoto, M. *Langmuir* 1997, 13, 1385-1387.

40. Tagliazucchi, M.; Calvo, E. J. *Chemphyschem.* 2010, 11, 2957-2968.

41. Lojou, E.; Bianco, P. *Langmuir* 2004, 20, 748-755.

42. Seo, J.; Lutkenhaus, J, L.; Kim, J.; Hammond, P. T.; Char, K. *Langmuir* 2008,

24, 7995-8000.

43. Kato, S.; Pac, C. *J. Phys. Chem. B* 2004, 108, 19932-19939.

44. Qi, Z.; Saito, T.; Fan, Y.; Isogai, A. *BioMacromolecules* 2012, 13, 553-558.

45. Du, Y.; Luna, L, E.; Tan, W, T.; Rubner, M. F.; Cohen, R. E. *ACS Nano* 2010, 4, 4308-4316.

46. Fou, A. C.; Onitsuka, O.; Ferreira, M.; Rubner, M. F.; Hsieh, B. R. *J. Appl. Phys.* 1996, 79, 7501-7509.

47. Lvov, Y.; Ariga, K.; Ichinose, I.; Kunitake, T. *J. Chem. Soc. Chem. Commun.* 1995, 33, 2313-2314.

48. Lee, S.; Hong, J. *Macromolecules* 2001, 34, 5358-5360.

49. Chiarelli, P. A.; Johal, M. S.; Casson, J. L.; Roberts, J. B.; Robinson, J. M.; Wang, H. L. *Adv. Mater.* 2001, 13, 1167-1171.

50. Cho, J.; Char, K.; Hong, J. D.; Lee, K. B *Adv. Mater.* 2001, 13, 1076-1078.

51. Schlenoff, J. B.; Dubas, S. T.; Farhat, T. *Langmuir* 2000, 16, 9968-9969.

52. Bruening, M.; Dotzauer, D. *Nature Materials* 2009 449-450.

53. Tang H.; Zhang, G.; Ji, S. *Alche Journal* 2013, 59,250-257.

54. Estillore, N. C.; Advincula, R. C. *Langmuir* 2011, 27, 5997-6008.

55. Buscher, K.; Graf, K.; Ahrens, H.; Helm, C. A. *Langmuir* 2002, 18, 3585-3591.

56. Sui, Z.; Salloum, D.; Schlenoff, J. B. *Langmuir* 2003, 19, 2491-2495.

57. Kozlovskaya, V.; Kharlampieva, E.; Khanal, B. P.; Manna, P.; Zubarev, E. R.; Tsukruk, V. V. *Chem. Mater.* 2008, 20, 7474-7485.

58. Peng, C.; Thio Y. S.; Gerhardt,R. A.; Ambaye, H.; Lauter, V. *Chem. Mater.*

2011, 23, 4548-4556.

59. Serpe, M. J.; Lyon, L. A. *Chem. Mater.* 2004, 16, 4373-4380.

60. Chia, K.; Rubner, M. F.; Cohen, R. E. *Langmuir* 2009, 25, 14044-14052.

61. Choi, J.; Rubner, M. F. *Macromolecules* 2005, 38, 116-124.

62. Decher, G.; Schlenoff, J. B. "Multilayer Thin Films : Sequential Assembly of Nanocomposite Materials" Wiley-VCH, Weinheim, 2003.

63. Mendelsohn, J. D.; Yang, S. Y.; Hiller, J.; Hochbaum, A. I.; Rubner, M. F. *Biomacromolecules* 2003, 4, 96-106.

64. Shiratori , S. S.; Rubner, M. F. *Macromolecules* 2000, 33, 4213-4219.

65. Healy, K.E.; Thomas, C.H.; Rezania, A.; Kim, J.E.; McKeown, P.J.; Lom, B.; Hockberger, P. E. *Biomaterials* 1996, 17, 195-208.

66. Jackman, R.J.; Wilbur, J.L.; Whitesides, G.M. *Science* 1995, 269, 664-666.

67. Folch, A.; Ayon, A.; Hurtado, O.; Schmidt, M.A.; Toner, M. J *Biomech Eng-T Asme* 1999, 121, 28-34.

68. Chou, S. Y.; Krauss, P. R.; Renstrom, P. J. *Appl. Phys. Lett.* 1995, 67, 3114.

69. Sotomayor Torres, C. M.; Zankovych, S.; Seekamp, J.; Kam, A. P.; Cedeño, C. C.; Hoffmann, T.; Ahopelto, J.; Reuther, F.; Pfeiffer, K.; Bleidiessel, G.; Gruetzner, G.; Maximov, M. V.; Heidari, B. *Mater. Sci. Eng. C* 2003, 23, 2301-2308.

70. Decher, G. *Science* 1997, 277, 1232-1237.

71. Hammond, P. T. *Adv. Mater.* 2004, 16, 1271-1293.

72. Shiratori, S. S.; Rubner, M. F. *Macromolecules* 2000, 33, 4213-4219.

73. Sukhishvili, S. A.; Granick, S. *Macromolecules* 2002, 25, 301-310.

74. Doron-Mor, I.; Cohen, H.; Cohen, S. R.; Popovitz-Biro, R.; Shanzer, A.; Vaskevich, A.; Rubinstein, I. *Langmuir* 2004, 20, 10727-10733.

75. Zhang, Y. J.; Yang, S. G.; Guan, Y.; Cao, W. X.; Xu, J. *Macromolecules* 2003, 36, 4238-4240.

76. Park, J.; Fouche, L. D.; Hammond, P. T. *Adv. Mater.* 2005, 17, 2575.

77. Kidambi, S.; Chan, C.; Lee, I. S. J. *Am. Chem. Soc.* 2004, 126, 4697-4703.

78. Lit, Y. V. X.; Hit, W.; Ma, Y.; Zhang, L. B.; Sun, J. Q.; Lu, N.; Shen, L. C. *Macromol. Rapid Commun.* 2006, 27, 505-510.

79. Zhang, C.; Hirt, D. E. *Polymer* 2007, 48, 6748-6754.

80. Park, J.; Hammond, P. T. *Adv. Mater.* 2004, 16, 520-527.

81. Mendelsohn, J. D.; Barrett, C. J.; Chan, V. V.; Pal, A. J.; Mayes, A. M.; Rubner, M. F. *Langmuir* 2000, 16, 5017-5023.

82. Nolte, A. J.; Takane, N.; Hindman, E.; Gaynor, W.; Rubner, M. F.; Cohen, R. E. *Macromolecules* 2007, 40, 5479-5486.

83. Campbell, C. J.; Smoukov, S. K.; Bishop, K. J. M.; Grzybowski, B. A. *Langmuir* 2005, 21, 2637-2640.

84. Smoukov, S. K.; Bishop, K. J. M.; Klajn, R.; Campbell, C. J.; Grzybowski, B. A. *Adv. Mater.* 2005, 17, 1361-1365.

85. Campbell, C. J.; Fialkoski, M.; Bishop, K. J. M.; Grzybowski, B. A. *Langmuir* 2009, 25, 9-12.

86. Decher, G.; Lehr, B.; Lowack, k.; Lvov, Y.; Schmtt, J. *Biosens.*

*Bioelectron.*1994, 9, 677-684.

87. Park, J.; Park, J.; Kim, S. H.; Cho, J.; Bang, J. *J. Mater. Chem.* 2010, 20, 2085-2091.

88. Lutkenhaus, J.L.; McEnnis, K.; Hammond, P.T. *Macromolecules* 2008, 41, 6047-6054.

89. Jiang, B.; Barnett, J, B.; Li, B. *Nano. Tech. App.* 2009, 2. 21-27.

90. Zhang, H.; Fu,Y.; Wang, D.; Wang, L.; Wange, Z.; Zhang, X. *Langmuir* 2003, 19, 8497-8502.

91. Mendelsohn, J. D.; Yang, S.Y.; Hiller, J.A.; Hochbaum, A.I,; Rubner, M.F. *Biomacromolecules* 2003, 4, 96-106.

92. Chia K.; Rubner, M. F, Cohen, R. E. *Langmuir*. 2009, 25, 14044-14052.

93. Hiller, J.A.; Mendelsohn, J. D.; Rubner, M.F. *Nat. Mater.* 2002, 1, 59-64.

94. Choi, J.; Rubner, M. F. *Macromolecules* 2005, 38, 116-124.

95. Zhai, L.; Nolte, A.J.; Cohen, R. E.; Rubner, M.F. *Macromolecules* 2004, 37, 6113-6123.

96. Olugebefola, S. C.; Ryu, S. W.; Nolte, A. J.; Rubner, M. F.; Mayes, A. M. *Langmuir* 2006, 22, 5958-5962.

97. Thompson, M. T.; Berg, M. C.; Tobias, I. S.; Rubner, M. F.; Van Vliet, K. J. *Biomacromolecules* 2005, 26, 6836-6845.

98. Nemir, S.; Hayenga, H.N.; West, J.L. *Biotechnol Bioeng.* 2010, 105, 636-644.

99. Decher, G.; Hong, J-D. *Macromol. Chem. Macromol. Symp*. 1991, 46, 321-327.

100. Krogman, K. C.; Zacharia, N. S.; Schroeder, S.; Hammond, P. T. *Langmuir* 2007,

23, 3137-3141.

101. Priya, D. N.; Modak, J. M.; Raichur, A. M. *ACS Appl. Mater. Inter.* 2009, 1, 2684-2693.

102. Park, M. S.; Lee, Y.; Kim, J. K. *Chem. Mater.* 2005, 17, 3944-3950.

103. Bertrand, P.; Jonas, A.; Laschewsky, A.; Legras, R. *Macromol. Rapid Commun.* 2000, 21, 319-348.

104. Quinn, J. F.; Caruso, F. *Langmuir* 2004, 20, 20-27.

105. Mauser, T.; Dejugnat, C.; Sukhorukov, G. B. *Macromol. Rapid Commun.* 2004, 25, 1781-1785.

106. Kugler, R.; Schmitt, J.; Knoll, W. *Macromol. Chem. Phys.* 2002, 203, 413-419.

107. Kim B.; Gao, H.; Argun, A. A.; Matyjaszewski, K.; Hammond, P. T. *Macromolecules* 2009, 42, 368-375.

108. Berg, M. C.; Zhai, L. Cohen, R. E.; Rubner, M. F. *Biomacromolecules* 2006, 7, 357-364.

109. Bai, S.; Wang, Z.; Gao, J.; Zhang, X. *European Polymer Journal* 2006, 42, 900-907.

110. Radi, H.; Hamzeh, Y.; Ebrahimi, G.; Behrooz, R.; Nazhad, M, M. *Ind, Eng. Chem. Res.* 2012, 51, 11054-11058.

111. Cho, C.; Zacharia N. S. *Langmuir* 2012, 28, 841-848.

112. Wood K. C.; Zacharia, N. S.; Schmidt, D. J.; Wrightman, S. N.; Andaya, B. J.; Hammond, P. T. *Proc. Nat. Acad. Sci. U.S.A*. 2008, 105, 2280-2285.

113. Cho, C.; Valverde, L; Ozin, G. A.; Zacharia, N. S. *Langmuir* 2010, 26, 13637-

13643.

114. Cambell, C. J.; Smoukov, S. K.; Bishop, K. J. M.; Grzybowski, B. A. *Langmuir* 2005, 21, 2637-2640.

115. Bishop, K. J. M.; Fialkowski, M.; Grzybowski, B. A. *J. Am. Chem. Soc.* 2005, 127, 15493-15948.

116. Nolte, A. J. D.; Takane, N.; Hindman, E.; Gaynor, W.; Rubner, M. F.; Cohen, R. E. *Macromolecules* 2007, 40, 5479-5486.

117. Heuvingh, J.; Zappa, M.; Fery, A. *Langmuir* 2005, 21, 3165-3171.

118. Han, L.; Mao, Z.; Wu, J.; Gong, X.; Yang, Y.; Gao, C. *Langmuir* 2012, 28, 193-199

119. Cambell, C. J.; Fialkoski, M.; Bishop, K. J. M.; Grzybowski, B. A. *Langmuir* 2009, 25, 9-12.

120. McAloney, R.; Dudnik, V.; Goh, M. C. *Langmuir* 2003, 19, 3947-3952.

121. Porcel, C. H.; Schlenoff, J. B. *Biomacromolecules* 2009, 10, 2968-2975.

122. Fery, A.; Scholer, B.; Cassagneau, T.; Caruso, F. *Langmuir*, 17, 3779-3783.

123. Lowman, G. M.; Tokuhisa, H.; Lutkenhaus, J. L.; Hammond, P. T. *Langmuir* 2000, 20, 9791-9795.

124. Itano, K. Choi, J.; Rubner, M. F. *Macromolecules* 2005, 38, 3450-3460.

125. Caruso, F.; Li, Q.; Quinn, F. *Adv. Mater.* 2005, 17, 2058-2062.

126. Einaga, Y.; Kim, G.S.; Ohnishi, K.; Park, S. G.; Fujishima, A. *Mater. Sci. Eng. B* 2001, 83, 19-23.

127. Plummer, S. T.; Bohn, P. W. *Langmuir* 2002, 18, 4142-4149.

128. Jung, H.; Yook, S.; Kim, H. Koh, Y. *Materials Letters* 2009, 63, 1545-1547.

129. Nemir, S.; Hayenga, H. N.; West, J. L. *Biotechnol. Bioeng.*2010, 105, 636-644.

130. Hammond, P. T. *Adv. Matter.*2004, 16, 1271-1293.

131. Zhang, H.Y.; Wang, Y. F.; Wang, L.; Wang, Z.; Zhang, X. *Langmuir* 2003, *19*, 8497-8502.

132. Schlenoff, J.B.; Dubas, S.T. *Macromolecules* 2001, 34, 592-598.

133. Caruso, F.; Yang, W.; Trau, D.; Renneberg, R. *Langmuir* 2000, 16, 8932-8936.

134. Jomaa, H.W.; Schlenoff, J.B. *Langmuir* 2005, 21, 8081-8084.

135. Zacharia, N.S.; DeLongchamp, D. M.; Modestino, M.; Hammond, P. T. *Macromolecules* 2007, 40, 1598-1603.

136. Zacharia, N.S.; Modestino M.; Hammond, P. T. *Macromolecules* 2007, 40, 9523-9528.

137. Antipov, A. A.; Sukhorukov, G. B.; Leporatti, S.; Radtchenko, I. L.; Donath, E.; Möhwald, H. *Coll. Surf. A* 2002, 198, 535-541.

138. Sukhorukov, G. B.; Antipov, A. A.; Voigt, A.; Donath, E.; Möhwald, H. *Macromol. Rapid Commun*. 2001, 22, 44-46.

139. Sukhorukov, G. B.; Brumen, M.; Donath, E.; Möhwald, H. *J. Phys. Chem. B* 1999, 103, 6434-6440.

140. Mendelsohn, J.D.; Barrett, C. J.; Chan, V. V.; Pal, A. J.; Mayes, A. M.; M. Rubner, F.; *Langmuir* 2000, 16, 5017-5023.

141. Hiller, J. A.; Mendelsohn, J. D.; Rubner,M. F. *Nature Mater.* 2002, 1, 59-64.

142. Lowman G. M.; Tokuhisa, H.; Lutkenhaus, J. L.; Hammond, P. T. *Langmuir* 2004,

20, 9791-9795.

143. Lutkenhaus, J.L.; McEnnis, K.; Hammond, P. T. *Macromolecules* 2008, 41, 6047-6054.

144. Guo, Z.; Chen, X.; Xin, J.; Wu, D.; Li, J.; Xu, C. *Macromolecules* 2010, 43, 9087-9093.

145. Tian, Y.; Qiang, H.; Cui, Y.; Tao, C.; Li., J. *Chem – Eur J.* 2006, 12, 4808-4812.

146. Fue, Y.; Bai, S.; Cui, S.; Qiu, D.; Wang, Z.; Zhang, X. *Macromolecules* 2002, 35, 9451-9458.

147. Bai, S.; Wang, Z.; Zhang X.; Wang B. *Langmuir* 2004, 20, 11828-11832.

148. Lichter, J. A.; Rubner M. F. *Langmuir* 2009, 25, 7686-7694.

149. Lee, J. Y.; Painter, P. C.; Coleman, M. M. *Macromolecules* 1988, 21, 346-364.

150. Elvira, T.; Quinn, J. F.; Caruso, F. *Langmuir* 2005, 21, 8785-8792.

151. Lu, X.; Weiss, R. A. *Macromolecules* 1995, 28, 3022-3029.

152. Xie, A. F.; Granick, S. *Macromolecules* 2002, 35, 1805-1813.

153. Li, Q.; Quinn, J. F.; Caruso, F. *Adv. Mater.* 2005, 17, 2058-2065.

154. Rmaile, H.H.; Schlenoff, j. B. *Langmuir* 2002, 18, 8263-8265.

155. Vonklitzing, R.; Mohwald, H. *Langmuir* 1995, 11, 3554-3559.

156. Burke, S. E.; Barrett, C. J. *Langmuir* 2003, *19*, 3297-3003.

157. Kharlampieva, E.; Shkhishvili, S. A. *Langmuir* 2003, 19, 1235-1243.

158. Kharlampieva, E., Ankner J. F.; Rubinstein M.; Sukhishvili S.A. *Physical Review Letters* 2008, 100, 12803-12809.

159. Zhai, L.; Nolte, A. J.; Cohen, R. E.; Rubner, M. F. *Macromolecules* 2004, 37,

6113-6123.

160. Zhu, H.; Ji, J.; Shen, J. *Biomacromolecules* 2004, 5, 1933-1939.

161. Watanabe, J.; Eriguchi, T.; Ishihara, K. *Biomacromolecules* 2002, 3, 1375-1383.

162. Furbert, P.; Lu, F.; Winograd, N.; DeLouise, L. *Langmuir* 2008, 24, 2908-2915.

163. Salehi, P.; Sarazin, P.; Ravis, B.D. *Biomacromolecules*2008, 9, 1131-1138.

164. Xiang, Z.; Sarazin, P.; Favis, B. D. *Biomacromolecules* 2009, 10, 2053-2066.

165. Lecomte, F.; Siepmann, J.; Walther, M.; MacRae, R. J.; Bodmeier, R. *Biomacromolecules* 2005, 6, 2074-2083.

166. Wang, C.; Wang, Q.; Wang T. *Langmuir* 2010, 26, 18357-183361.

167. Watanabe, K.; Yuasa, M.; Kida, T; Shimanoe, K.; Teraoka, Y.; Yamazoe, N. *Chem. Mater.* 2008. 20, 6965-6973.

168. Hess, K.C.; Epting, W.K.; Litster, S. *Anal. Chem.* 2011, 83, 9492-9498.

169. Kuo, C.; Chen, Y.; Lu, S. *ACS Appl. Mater. Interfaces* 2009, 1, 72-75.

170. Joo, W. Park, M.S.; Kim, J. K. *Langmuir* 2006, 22, 7960-7963.

171. Park, M.S.; Kim J. K. *Langmuir* 2005, 21, 11404-11408.

172. Shimomura, H.; Gemici, Z.; Cohen, R.E.; Rubner, M.F. *ACS Appl. Mater. Interfaces* 2010, 2, 813-820.

173. Glazer, P.J.; van Erp, M.; Embrechts, A.; Lemay, S.G.; Mendes, E. *Soft Matter* 2012, 8, 4421-4426.

174. Van Tassel, P.R. *Curr. Opin. Colloid. In*. 2012, 17, 106-113.

175. Guillaume-Gentil, O.; Graf, N.; Boulmedais, F.; Schaaf, P.; Voros, J.; Zambelli, T. *Soft Matter* 2010, 6, 4246.

176. Ko, Y. H.; Kim, Y. H.; Park, J.; Nam, K. T.; Park, J. H.; Yoo, P. J. *Macromolecules* 2011, 44, 2866-2872 .

177. Schmidt, D.; Min, Y.; Hammond, P. T. *Soft Matter* 2011, 7, 6637.

178. Ladam, G.; Schaad, P.; Voegel, J. C.; Schaaf, P.; Decher, G.; Cuisinier, F. *Langmuir* 2000, 16, 1249-1255.

179. Zacharia, N. S.; DeLongchamp, D. M.; Modestino, M.; Hammond, P. T. *Macromolecules* 2007, 40, 1598-1603.

180. Zacharia, N. S.; Modestino, M.; Hammond, P. T. *Macromolecules* 2007, 40, 9523-9528.

181. Geoffrey M. L.; Tokuhisa, H.; Lutkenhaus, J. L.; Hammond, P. T. *Langmuir* 2004, 20, 9791-9795.

182. Sui, Z.; Schlenoff, J. B. *Langmuir* 2004, 20, 6026-6031.

183. Heger, D.; Jirkovsky, J.; Klan, P. J. *Phys. Chem. A* 2005, 109, 6702-6709.

184. Parkanyi, C.; Boniface, C.; Aaron, J. J.; Maafi, M. *Spectrochim. Acta, Part A* 1993, 49, 1715.

185. Chung, A.J. and Rubner, M. F. *Langmuir* 2002, 18, 1176-1183.

186. Ding, C.; Xu, S.; Wang, J.; Liu, Y.; Hu, X.; Chen, P.; Feng, S. *Polym. Adv. Technol.* 2011

187. Kittredge, M.C.; Durst, T.S.; Kittredge, K.W. *Thin Solid Films* 2010. 518, 3949-3953.

188. Bergmann, K.; O'Konshk, C.T. *J. Phys. Chem.* 1963, 67, 6169-6176.

189. Braswell, E. J. *Phys. Chem.* 1968, 72, 2477-2484.

190. Ngankam, A.P.; Van Tassel, P. R. *Proc. Natl. Acad. Sci. U.S.A.* 2007, 104, 1140-1146.

191. Zhong, C.J.; Luo, J.; Fang, B.; Wanjala, B. N.; Njoki, P. N.; Loukrakpam, R.; Yin, J. *Nanotechnology* 2010, 21, 062001-062021.

192. Sopian, K.; Daud, W. R. W. *Renewable Energy* 2006, 31, 719-727.

193. Li, Y.; Boone, E.; El-Sayed, M. A. *Langmuir* 2002, 18, 4921-4925.

194. Qiao, Y.; Li, C. M. J, *Mater. Chem.* 2011, 21, 4027-4036.

195. Honji, A.; Mori, T.; Tamura, K.; Hishinuma, Y. *J. Electochem. Soc.* 1988, 135, 355-359.

196. Bett, J. A. S.; Kinoshita, K.; Stonehart, P. *Journal of Catalysis* 1976, 41, 124-133.

197. Wilson, M. S.; Garzon, F. H.; Sickafus, K. E.; Gottesfeld, S. *J. Electochem. Soc.*1993, 140, 2872-2877.

198. Makharia, R.; Kocha, S.; Yu, P. Sweikart, M. A.; Gu, W.; Wagner, F.; Gasteriger, H.A *ECS Trasactions* 2006, 1, 3-18.

199. Stevens, D. A.; Hicks, M. T.; Haugen, G. M.; Dahn, J. R. *J. Electochem. Soc.* 2005, 152, A2309-A2315.

200. Yasuda, K.; Taniguchi, A.; Akita. T.; Ioroi, T.; Siroma, Z *Phys. Chem. Chem. Phys.* 2006, 8, 746-752.

201. Yasuda, K.; Taniguchi, A.; Akita. T.; Ioroi, T.; Siroma *J. Electochem. Soc.* 2006, 153, A1599-A1603.

202. Decher, G.; Hong, J. D.; Schmitt, J. *Thin Solid Films* 1992, 210, 831-835.

203. Fujita, S.; Shiratori, S. *Jpn. J. Appl. Phys., Part 1* 2004, 43, 2346-2351.

204. Wang, X.; Wang, C.; Cheng. L.; Lee, S.; Liu, Z. *J. Am. Chem. Soc*. 2012, 134, 7414-7422.

205. Baur, J. W.; Kim S.; Balanda, P. B.; Reynolds, J. R.; Rubner, M. F. *Adv. Mater*. 1998, 19, 1452-1455.

206. Kang, H.; Lee, C.; Yoon, S. C.; Cho, C.; Cho J.; Kim, B. J. *Langmuir* 2010, 26, 17589-17595.

207. Tokuhisa, H.; Hammond, P. T. *Adv. Funct. Mater*. 2003, 13, 831-838.

208. Wood, K. C.; Zacharia, N. S.; Schmidt, D. J.; Wrightman, S. N.; Andaya, B. J.; Hammond, P. T. *Proc. Natl. Acad. Sci. U.S.A.* 2008, 105, 2280-2287.

209. Zhang, X.; Wang, H.; Su, Zhaohui. *Langmuir* 2012, 28, 15705-15712.

210. Zan, X.; Su, Z. *Thin Solid Films* 2010, 518, 5478-5482.

211. Lee, D.; Cohen, R. E.; Rubner, M. F. *Langmuir* 2005, 21, 9651-9659.

212. Joly, S.; Kane, R.; Radzilowski, L.; Wang, T.; Wu, A.; Cohen, R. E.; Thomas, E. L.; Rubner, M. F. *Langmuir* 2000, 16, 1354-1359.

213. Dai, J.; Bruening, M. L. *Nano Letters* 2002, 2, 497-501.

214. Chia, K.; Cohen, R. E.; Rubner, M. F. *Chem. Mater*. 2008, 20, 6756-6763.

215. Miyazaki, Y.; Shiratori, S. *Thin Solid Films* 2006, 499, 29-34.

216. Yang, G.; Yu, L.; Chen, X.; Zhang, P. *Applied Surface Science* 2009, 255, 4097-4101.

217. Wang, T. C.; Rubner, M. F.; Cohen, R. E. *Langmuir* 2002, 18, 3370-3375.

218. Teranishi, T.; Hosoe, M.; Tanaka, T.; Miyake, M. *J. Phys. Chem, B.* 1999, 103, 3818-3827.

219. Huang, M.; Shao, Y.; Sun, X.; Chen, H.; Liu, B.; Dong, S. *Langmuir* 2005, 21, 323-329.

220. Lutkenhaus, J. L.; McEnnis, K.; Hammond, P. T. *Macromolecules* 2008, 41, 6047-6054.

221. Shiratori S. S.; Rubner, M. F. *Macromolecules* 2000, 33, 4213-4219.

222. Segar, B.; Kamat, P. V. *J. Phys. Chem. C* 2009, 113, 7990-7995.

223. Sharma, S.; Ganguly, A.; Papakonstantinou, P.; Miao, X. P.; Li, M. X.; Hutchison, J. L.; Delichatsios, M.; Ukleja, S. *J. Phys. Chem. C* 2010, 114, 19459-19466.

224. Schmidt, T. J.; Gasteiger, H. A.; Stab, G. D.; Urban, P. M.; Kolb, D. M.; Behm, R. J. *J. Electrochem. Soc.*1998, 145, 2354-2358.

225. Colombi Ciacchi, L.; Pompe, W.; De Vita, A. *J. Phys. Chem. B* 2003, 107, 1755-1764.

226. Knupp, S. L.; Li, W.; Paschos, O.; Murray, T. M.; Snyder, J.; Haldar. P. *Carbon* 2008, 1276-1284.

227. Li, W.; Zhou, W.; Li H.; Zhou, Z.; Zhou, B.; Sun, G.; Xin, Q. *Electrochemica Acta* 2004, 49, 1045-1055.

228. Shao, Lin.; Lutkenhaus, J. L. *Soft Matter* 2010, 6, 3363-3369.

229. He, D.; Zeng, C.; Xu, C.; Cheng, N.; Li, H.; Mu, S.; Pan, M. *Langmuir* 2011, 27, 5582-5588.

230. Croissant, M. J.; Napporn, T.; Leger, J. M.; Lamy, C. *Electrochimica Acta* 1998, 43, 2447-2457.

231. Shi, L.; Liang, R.; Qiu, J. *J. Mater. Chem.* 2012, 22, 17196-17203.